

Copyright
By
Jennifer Elizabeth Ridd
2004

Fatigue Performance of Stay Cables

by

Jennifer Elizabeth Ridd, B.S.C.E.

Thesis

Presented to the Faculty of the Graduate School of

The University of Texas at Austin

in Partial Fulfillment

of the Requirements

for the Degree of

Master of Science in Engineering

The University of Texas at Austin

August 2004

Fatigue Performance of Stay Cables

**APPROVED BY
SUPERVISING COMMITTEE:**

Sharon L. Wood, Supervisor

Karl H. Frank

Dedication

To my wonderful parents whose unfailing love and support have driven me in all my endeavors. Without them, I would not be where I am.

Acknowledgements

I would first like to acknowledge the Texas Department of Transportation for funding this research and making my education at the University of Texas at Austin possible.

I would also like to express gratitude to Dr. Sharon Wood and Dr. Karl Frank for kindly sharing their knowledge, experience, and wisdom throughout my graduate education and for their unfailing support in my academic and professional endeavors. I would especially like to thank them in their patience and dedication as I completed the research process.

I also wish to thank Blake Stasney, Dennis Phillip, and Mike Bell, the staff of the Ferguson Structural Engineering Laboratory. Without the laboratory instruction and assistance of these three individuals, completion of this project would not have been possible. Their assistance, from fabricating the necessary parts to helping with equipment use, is a great help to all students at the lab.

I also express appreciation to John Eggers and Tammer Botros, as well as others who have previously worked on this research project, for paving the way for me and making my portion of the research much easier.

I would like to express my deepest gratitude to Dylan Freytag for always going above and beyond the call of duty on all aspects of this project. His resourcefulness in the laboratory and engineering expertise were invaluable to the research project and to me personally.

Similarly, I would like to express deepest thanks to Margaret (Meg) Warpinski, for her tremendous work on this research project, both in the lab and out. I would like to thank her especially for keeping me motivated these two years and for convincing me that I could, indeed, accomplish my goals.

I wish to thank my family. To my grandparents, for helping fund my undergraduate education and for their constant support, I express sincere thanks and love. And I wish to thank my parents for always believing in me and teaching me to work hard, but always find the fun in life. The opportunities they have created for me are limitless, and for that I express my deepest love and appreciation.

August, 2004

Fatigue Performance of Stay Cables

Jennifer Elizabeth Ridd, M.S.E.

The University of Texas at Austin, 2004

SUPERVISOR: Sharon L. Wood

The cables of the Fred Hartman Bridge have experienced large-amplitude vibrations under light wind and rain conditions, a problem with cable-stayed bridges around the world. This thesis presents observations from ten full-scale bending fatigue tests performed on 32-ft. specimens modeled after the cables on the bridge. The strand used to construct the cables is evaluated in axial fatigue and compared with published specifications. The goal of the project is to relate the cable vibrations to fatigue damage and estimate the fatigue damage to the stay cables on the bridge.

Table of Contents

CHAPTER 1 INTRODUCTION.....	1
1.1 The Fred Hartman Bridge	1
1.2 Cable Vibration Problems on the Fred Hartman Bridge	4
1.3 Previous Research and Solutions	5
1.3.1 Whitlock, Dalrymple, Poston and Associates (WDP).....	5
1.3.2 Johns Hopkins University (JHU)	6
1.3.3 Texas Tech University (TTU).....	6
1.3.4 University of Texas at Austin (UT).....	7
1.3.4.1 Field Measurements	7
1.3.4.2 Full-Scale Bending Fatigue Tests	7
1.3.4.3 Computational Models	8
1.3.4.4 Characterization of Vibration Data	8
1.4 Topics Presented in This Thesis.....	8
1.4.1 Full Scale Bending Fatigue Tests.....	8
1.4.2 Single-Strand Tension Fatigue Tests.....	9
CHAPTER 2 OVERVIEW OF CABLE FATIGUE TESTS	10
2.1 Test Setup	10
2.2 Cable Stay Test Specimens	12
2.2.1 Material Properties of Prestressing Strand	17
2.2.2 General Assembly of Cable Stay Test Specimens	18
2.2.3 Grouting of Cable Stay Specimens	25
2.2.3.1 Grouted Specimens	25
2.2.3.2 UngROUTED Specimens	26
2.2.4 Details of Cable Stay Test Specimens.....	27

2.2.4.1	Details of Specimen 5	28
2.2.4.2	Details of Specimen 6	31
2.2.4.3	Details of Specimen 7	32
2.2.4.4	Details of Specimen 8	32
2.2.4.5	Details of Specimen 9	33
2.2.4.6	Details of Specimen 10	34
2.3	Testing of Specimens	34
2.3.1	Free-Vibration Testing	34
2.3.2	Static Testing	35
2.3.3	Fatigue Testing	36
2.4	Fatigue Test Monitoring	36
CHAPTER 3 SINGLE-STRAND TENSION FATIGUE TESTS		39
3.1	Introduction	39
3.2	Test program	39
3.2.1	Test Set-up	40
3.2.2	Aluminum Grips	43
3.3	Results	45
3.3.1	Comparison with Published Fatigue Standards	46
3.3.2	Comparison with Previous Fatigue Testing	48
CHAPTER 4 BENDING FATIGUE TEST RESULTS		50
4.1	Methods of analysis	50
4.1.1	Method of Autopsy Investigation	50
4.1.2	Types of Fatigue Fractures	50
4.1.3	Nomenclature	54
4.2	Fatigue test results	55
4.2.1	Specimen 5	56

4.2.1.1	Grout Condition.....	57
4.2.1.2	Corrosion.....	57
4.2.1.3	Wire Breaks.....	58
4.2.1.4	Lateral Stiffness.....	59
4.2.1.5	Stress Range Near End of Stay	62
4.2.2	Specimen 6	67
4.2.2.1	Grout Condition.....	67
4.2.2.2	Corrosion.....	70
4.2.2.3	Location of Wire Breaks	72
4.2.2.4	Characteristics of Wire Breaks.....	78
4.2.2.5	Lateral Stiffness.....	80
4.2.3	Specimen 7	82
4.2.3.1	Grout Condition.....	83
4.2.3.2	Corrosion.....	85
4.2.3.3	Location of Wire Breaks	87
4.2.3.4	Wire Break Characteristics.....	96
4.2.3.5	Lateral Stiffness.....	99
4.2.4	Specimen 8	100
4.2.4.1	Grout Condition.....	101
4.2.4.2	Corrosion.....	101
4.2.4.3	Location of Wire Breaks	104
4.2.4.4	Wire Break Characteristics.....	110
4.2.4.5	Lateral Stiffness.....	113
4.2.5	Specimen 9	115
4.2.5.1	Grout Condition.....	116
4.2.5.2	Corrosion.....	118
4.2.5.3	Location of Wire Breaks	119
4.2.5.4	Wire Break Characteristics.....	128
4.2.5.5	Lateral Stiffness.....	130

4.2.6 Specimen 10	132
4.2.6.1 Grout Condition.....	133
4.2.6.2 Corrosion.....	134
4.2.6.3 Location of Wire Breaks	136
4.2.6.4 Wire Break Characteristics.....	142
4.2.6.5 Lateral Stiffness.....	144
CHAPTER 5 ANALYSIS OF RESULTS	146
5.1 Effect of Testing Variables	146
5.1.1 Type of Strand.....	147
5.1.2 Presence of Grout.....	148
5.1.3 Amplitude of Imposed Displacements	149
5.1.4 Orientation of Stressing End	151
5.1.5 Number of Strands in the Cross-Section	151
5.2 Stiffness Comparison	153
5.3 Location of Wire Breaks	155
5.3.1 Location of Wire Breaks	156
5.3.2 Wire Breaks at Wedges	159
5.3.3 Soundprint Comparison.....	159
CHAPTER 6 CONCLUSIONS.....	162
6.1 Summary....	162
APPENDIX A MODULUS AND TENSILE TESTING OF STRAND.....	167
A.1 Modulus Testing.....	167
A.1.1 Test Program	167
A.1.1.1 Test Setup	168
A.1.1.2 Extensometer Details.....	170
A.1.2 Test Results	173

A.2 Direct Tension Tests.....	175
A.2.1 Test Setup.....	175
A.2.2 Test Results.....	176
A.2.2.1 Strand A.....	176
A.2.2.2 Strand B.....	176
APPENDIX B GROUT STRENGTH	181
B.1 Summary	181
REFERENCES	182
VITA..	184

List of Tables

Table 2-1: Test parameters of all cable-stay test specimens	13
Table 2-2: Mechanical properties of prestressing strand	18
Table 2-3: Measured material properties for prestressing strand	18
Table 2-4: Stressing increments	23
Table 2-5: Distance of strain gages from deck anchor head – Specimen 5	30
Table 3-1: Test frequency for axial fatigue testing	42
Table 3-2: Axial fatigue test results	46
Table 3-3: PTI Specifications for Strand Fatigue Life	47
Table 3-4: Maximum Stress During Axial Fatigue Testing	47
Table 4-1: Summary of Fatigue Test Results	56
Table 4-2: Wire break distribution on Specimen 6	72
Table 4-3: Wire break distribution on Specimen 7	87
Table 4-4: Wire break distribution on Specimen 8	104
Table 4-5: Wire break distribution on Specimen 9	120
Table 4-6: Wire break distribution on Specimen 10	136
Table 5-1: Comparison of strand type	148
Table 5-2: Comparison between Specimen 2 and Specimen 5	149
Table 5-3: Comparison between Specimen 7 and Specimen 8	149
Table 5-4: Comparison of displacement amplitude	149
Table 5-5: Number of cycles to first wire break	150
Table 5-6: Comparison of stressing end	151
Table 5-7: Comparison of number of strands	152
Table 5-8: Comparison of cable stiffness	154
Table A-1: Measured modulus of elasticity for prestressing strand	174
Table A-2: Results of direct tension tests	176
Table B-1: Grout cube breaking strength	181

List of Figures

Figure 1-1: The Fred Hartman Bridge.....	2
Figure 1-2: Two independent decks of the Fred Hartman Bridge.....	3
Figure 1-3: Point at which bridge towers are joined	3
Figure 1-4: Cable restrainers on bridge.....	5
Figure 1-5: Dampers installed by WDP	6
Figure 2-1: Test setup.....	11
Figure 2-2: Geometry of loading clamp	11
Figure 2-3: Loading clamp.....	12
Figure 2-4: Longitudinal geometry of grouted test specimen	15
Figure 2-5: Longitudinal geometry of ungrouted test specimen	15
Figure 2-6: Geometry of anchorage regions.....	16
Figure 2-7: Exploded view of anchorage elements	17
Figure 2-8: Tension ring (left) and smooth end sleeve (right) attached to transition pipe.....	19
Figure 2-9: Wood shelf used to separate strands during construction	19
Figure 2-10: Helical spacer wire inside PE pipe (Poser, 2001)	20
Figure 2-11: PE pipe and white PVC end caps used on ungrouted specimens	20
Figure 2-12: Wedges supplied by VSL (Poser, 2001)	21
Figure 2-13: Setup for mono-strand stressing	22
Figure 2-14: Tapered adapter used for mono-strand stressing.....	22
Figure 2-15: Setup for stressing	24
Figure 2-16: Spring plate used during stressing.....	24
Figure 2-17: Inclination of stay for grouting.....	26
Figure 2-18: Grouting setup for Specimen 8.....	27
Figure 2-19: Grout mixing using electric drill and paddle mixer	27
Figure 2-20: Orientation of Specimen 5.....	28
Figure 2-21: Center section of Specimen 5	29
Figure 2-22: Placement of strain gages – Specimen 5	30
Figure 2-23: Strand layout - Specimen 6	31
Figure 2-24: Orientation of Specimen 6.....	32
Figure 2-25: Filling of grout void near tower anchor head.....	33
Figure 2-26: Setup for free-vibration test.....	35
Figure 2-27: Soundprint acoustic sensors	37
Figure 2-28: Placement of Soundprint sensors on a grouted specimen	38
Figure 2-29: Placement of Soundprint sensors on an ungrouted specimen	38
Figure 3-1: 220-kip MTS load frame	41
Figure 3-2: Grips in position during testing	42
Figure 3-3: Aluminum grip design.....	43
Figure 3-4: New aluminum grips used for axial fatigue testing.....	44

Figure 3-5: Strand wrapped with copper wire before fatigue testing.....	45
Figure 3-6: Grips after use in multiple axial fatigue tests.....	45
Figure 3-7: Results of Tensile Fatigue Tests.....	48
Figure 3-8: Fatigue Test Results of Strand B vs. Strand A.....	49
Figure 4-1: Fretting between the center wire and an outer wire.....	51
Figure 4-2: Fretting fatigue of center and outer wires.....	51
Figure 4-3: Fretting between adjacent outer wires.....	52
Figure 4-4: Fretting fatigue between outer wires.....	52
Figure 4-5: Isolated fatigue failure at wedge.....	53
Figure 4-6: Fatigue caused by external source.....	54
Figure 4-7: Nomenclature of strands looking from tower end to deck end.....	55
Figure 4-8: Nomenclature for wires in a strand.....	55
Figure 4-9: Grout condition - Specimen 5.....	57
Figure 4-10: Interface between caulk and grout – Specimen 5.....	58
Figure 4-11: Simulated wire break – Specimen 5.....	59
Figure 4-12: Peak loads during fatigue test - Specimen 5.....	60
Figure 4-13: Load - displacement response from static tests - Specimen 5.....	61
Figure 4-14: Strain data from static test - Specimen 5.....	64
Figure 4-15: Location of strain gages.....	65
Figure 4-16: Estimated stress range during fatigue test near deck anchorage - Specimen 5.....	66
Figure 4-17: Large grout crack at deck anchorage - Specimen 6.....	68
Figure 4-18: Grout cracking at tower end - Specimen 6.....	69
Figure 4-19: Grout cracking under the ram - Specimen 6.....	69
Figure 4-20: Corroded fretting product on Strand 19 – Specimen 6.....	71
Figure 4-21: Corrosion on Strand 19 near tower anchor head - Specimen 6.....	71
Figure 4-22: Corrosion product on grout from tower end - Specimen 6.....	71
Figure 4-23: Wire breaks based on Soundprint data - Specimen 6.....	73
Figure 4-24: Wire breaks at the tower end - Specimen 6.....	74
Figure 4-25: Location of wire breaks near tower anchorage of Specimen 6.....	75
Figure 4-26: Wire breaks on strand 1 near the tower anchor head - Specimen 6.....	76
Figure 4-27: Wire breaks on strand 17 at the face of the tower anchor head - Specimen 6.....	76
Figure 4-28: Wire breaks under the load point - Specimen 6.....	77
Figure 4-29: Location of wire breaks under load point - Specimen 6.....	78
Figure 4-30: Observed fretting fatigue mechanisms – Specimen 6.....	79
Figure 4-31: Distribution of fretting fatigue mechanisms - Specimen 6.....	80
Figure 4-32: Peak loads during fatigue tests - Specimen 6.....	81
Figure 4-33: Load – displacement response from static tests - Specimen 6.....	82
Figure 4-34: Grout condition at tower end - Specimen 7.....	83
Figure 4-35: Grout condition at deck anchor head immediately after removing polyethylene pipe - Specimen 7.....	84

Figure 4-36: Condition of grout at deck anchor head several minutes after removing polyethylene pipe - Specimen 7	84
Figure 4-37: Grout condition under load point - Specimen 7	85
Figure 4-38: Corrosion found near anchorage on strand 18 - Specimen 7	86
Figure 4-39: White substance on strand 17 at midspan - Specimen 7	86
Figure 4-40: Corrosion on strand 17 at midspan - Specimen 7	87
Figure 4-41: Wire breaks based on Soundprint data – Specimen 7	88
Figure 4-42: Wire breaks at tower anchorage - Specimen 7	89
Figure 4-43: Location of wire breaks near the tower anchorage - Specimen 7.....	90
Figure 4-44: Wire breaks at the deck anchorage - Specimen 7	91
Figure 4-45: Location of breaks near the deck anchorage - Specimen 7	92
Figure 4-46: Wire breaks under the load point - Specimen 7	93
Figure 4-47: Location of wire breaks under the load point - Specimen 7	94
Figure 4-48: Location of wire breaks under the load point - Specimen 7	95
Figure 4-49: Distribution of failure mechanisms - Specimen 7	97
Figure 4-50: Observed fretting fatigue mechanisms - Specimen 7	97
Figure 4-51: Multiple wire breaks on the same wire.....	98
Figure 4-52: Peak loads during fatigue tests - Specimen 7	99
Figure 4-53: Load - displacement response from static tests - Specimen 7	100
Figure 4-54: Grout condition at center of Specimen 8.....	101
Figure 4-55: Evidence of fretting fatigue at deck tension ring – Specimen 8.....	102
Figure 4-56: Wearing of the strands due to fretting - Specimen 8.....	103
Figure 4-57: Corrosion at interface between strand and caulk - Specimen 8.....	104
Figure 4-58: Wire breaks based on Soundprint data - Specimen 8	105
Figure 4-59: Wire breaks at the tower anchorage - Specimen 8	106
Figure 4-60: Wire breaks at deck anchorage - Specimen 8.....	107
Figure 4-61: Location of wire breaks near the tower anchorage - Specimen 8...	108
Figure 4-62: Location of wire breaks near the deck anchorage - Specimen 8	109
Figure 4-63: Wire break on strand 9 at deck end	110
Figure 4-64: Wire break on strand 11 at deck end	110
Figure 4-65: Wire break on strand 11 near wedge on the deck end - Specimen 8	111
Figure 4-66: Wire breaks on strand 9 at wedge on tower end - Specimen 8	112
Figure 4-67: Scraping of strand due to stressing at tower end	112
Figure 4-68: Observed fretting fatigue mechanisms - Specimen 8	113
Figure 4-69: Peak load during the fatigue tests - Specimen 8.....	114
Figure 4-70: Load – displacement response from static tests - Specimen 8	115
Figure 4-71: Grout lens at tower anchorage - Specimen 9.....	117
Figure 4-72: Grout void at tower anchorage - Specimen 9	117
Figure 4-73: Grout condition under the load point - Specimen 9	118
Figure 4-74: Corrosion near the tower anchorage - Specimen 9.....	118
Figure 4-75: Corrosion under the load point - Specimen 9.....	119

Figure 4-76: Wire breaks reported by Soundprint - Specimen 9	120
Figure 4-77: Wire breaks at tower anchorage - Specimen 9	122
Figure 4-78: Location of wire breaks near tower anchorage - Specimen 9	123
Figure 4-79: Wire breaks under the load point - Specimen 9	124
Figure 4-80: Location of wire breaks under the load point - Specimen 9	125
Figure 4-81: Location of wire breaks under the load point - Specimen 9	126
Figure 4-82: Wire breaks at deck anchorage - Specimen 9	127
Figure 4-83: Location of wire breaks near the deck anchorage - Specimen 9	128
Figure 4-84: Observed failure mechanisms - Specimen 9	129
Figure 4-85: Distribution of failure mechanisms - Specimen 9	130
Figure 4-86: Peak load during fatigue tests - Specimen 9	131
Figure 4-87: Load –displacement response from static tests - Specimen 9	132
Figure 4-88: Grout at tower end immediately after opening - Specimen 10	133
Figure 4-89: Grout at midspan immediately after opening - Specimen 10	134
Figure 4-90: Grout at deck end immediately after opening - Specimen 10	134
Figure 4-91: Corroded fretting product under the load point – Specimen 10	135
Figure 4-92: Corroded fretting product at the tower end - Specimen 10	135
Figure 4-93: Wire breaks reported by Soundprint - Specimen 10	136
Figure 4-94: Wire breaks at the tower anchorage - Specimen 10	137
Figure 4-95: Location of wire breaks near tower anchorage - Specimen 10	138
Figure 4-96: Wire breaks under the load point - Specimen 10	139
Figure 4-97: Location of wire breaks relative to the load point - Specimen 10..	140
Figure 4-98: Wire breaks near the deck anchorage - Specimen 10	141
Figure 4-99: Location of wire breaks relative to deck anchorage - Specimen 10	142
Figure 4-100: Observed fretting fatigue mechanisms - Specimen 10	143
Figure 4-101: Distribution of failure mechanisms - Specimen 10	143
Figure 4-102: Average load during the fatigue test - Specimen 10	144
Figure 4-103: Load - displacement response from static test data - Specimen 10	145
Figure 5-1: Comparison of specimens with different displacement amplitudes.	150
Figure 5-2: Cross-section of specimen	153
Figure 5-3: Location of wire breaks at ends of stay	157
Figure 5-4: Geometry at end of stay	157
Figure 5-5: Location of wire breaks at center of stay	158
Figure 5-6: Geometry at center of stay	158
Figure 5-7: Soundprint comparison at ends of stay specimens	161
Figure 5-8: Soundprint comparison at midspan of stay specimens	161
Figure A-1: Setup for modulus testing	169
Figure A-2: Full view of extensometer	170
Figure A-3: Bottom portion of extensometer with LVDTs	171
Figure A-4: Calibration curve for LVDT 1	172

Figure A-5: Calibration curve for LVDT 2	173
Figure A-6: Load vs. Displacement for Strand B, Specimen 1 modulus test	174
Figure A-7: Load vs. Displacement for Strand A Tensile Test 1	177
Figure A-8: Load vs. Displacement for Strand A Tensile Test 2	178
Figure A-9: Load vs. Displacement for Strand A Tensile Test 3	178
Figure A-10: Load vs. Displacement for Strand B Tensile Test 1	179
Figure A-11: Load vs. Displacement for Strand B Tensile Test 2	179
Figure A-12: Load vs. Displacement for Strand B Tensile Test 3	180

CHAPTER 1

Introduction

Upon completion in 1995, the Fred Hartman Bridge was among the premier cable-stayed bridges in the United States. Before construction was finished, large-amplitude cable vibrations were observed under light wind and rain conditions—a phenomenon seen on a number of cable-stayed bridges around the world, including the Veterans Memorial Bridge, which is also in Texas. These vibrations raised concerns regarding fatigue damage that may occur near the cable anchorages due to the large-amplitude events. In 1997, The Texas Department of Transportation (TxDOT) initiated a research effort among several universities and an engineering consulting firm to prevent further vibrations, repair damage already observed on the bridge, and estimate the extent of fatigue damage to the cables. This thesis documents the results of six, large-scale, bending fatigue tests of stay cables in the laboratory.

1.1 THE FRED HARTMAN BRIDGE

The Fred Hartman Bridge (Figure 1-1) spans the Houston Ship Channel from Baytown to LaPorte, Texas. Completed in September of 1995 after nine years of construction at a cost of \$100 million, it replaced the Baytown-LaPorte Tunnel as the primary means of crossing the Ship Channel on the east side of Houston. The bridge, which has a capacity of 200,000 vehicles per day, can accommodate almost ten times more traffic than could its tunnel predecessor and is much more efficient and aesthetically pleasing.



Figure 1-1: The Fred Hartman Bridge

The bridge is 2,475 ft long with a main span of 1250 ft. With an overall width of 160 ft, the Fred Hartman Bridge is one of the largest cable-stayed bridges in the world in terms of total deck area. The bridge comprises two independent decks, each 78 ft wide. Each deck accommodates four lanes of traffic and two emergency lanes (Figure 1-2). The decks are supported by 192 cables arranged in a fan pattern from the four diamond-shaped concrete towers. The towers are 436 ft tall and are connected at the deck level to provide stiffness against lateral loads (Figure 1-3). Where the double-diamond towers intersect are the only points along the bridge that the two decks are connected.



Figure 1-2: Two independent decks of the Fred Hartman Bridge



Figure 1-3: Point at which bridge towers are joined

The cables of the Fred Hartman Bridge are parallel-strand cables. A parallel-strand cable consists of a bundle of seven-wire steel prestressing strands surrounded by a polyethylene (PE) pipe. After the superstructure is complete, the cables are stressed and the pipe is filled with grout. A helical steel wire is wrapped on the inside of the PE pipe to ensure a grout barrier between the strands and the PE pipe at all points along the cable. This cable system is considered a two-barrier system because theoretically both the grout and the PE pipe act to protect the strand against corrosion.

1.2 CABLE VIBRATION PROBLEMS ON THE FRED HARTMAN BRIDGE

Since construction of the bridge, the cables have experienced wind-rain induced vibrations. This type of vibration occurs when a light wind causes rainwater to form rivulets on the cable. The rivulets change the aerodynamic cross section of the stay and make the stays more susceptible to vibration (Verwiebe, 1998).

The maximum deflections from the neutral position caused by wind-rain induced vibrations have been observed to be as large as ± 21 in. (Poston, 1998) These large-amplitude displacements caused 101 of 192 anchorage guide pipes to fracture before 1998. This damage indicates the large lateral forces generated when cables vibrate.

The damage to the guide pipes raised questions regarding the fatigue damage that may be occurring within the stay cables. To investigate this damage and propose solutions and repairs, TxDOT initiated a research effort involving Whitlock, Dalrymple, Poston, and Associates, Johns Hopkins University, Texas Tech University, and the University of Texas at Austin. This research effort was intended to:

- Design repair solutions for the existing damage caused by the vibrations

- Provide a structural solution to minimize and control cable vibrations
- Characterize the vibrations such that effective dampers can be designed
- Characterize the fatigue properties of the cable stays
- Estimate the extent of fatigue damage caused by the vibrations

1.3 PREVIOUS RESEARCH AND SOLUTIONS

1.3.1 Whitlock, Dalrymple, Poston and Associates (WDP)

The primary goal of the engineers at WDP was to design repairs for the existing damage on the bridge and to develop a solution to reduce the cable vibrations. Stiffeners designed to withstand the lateral forces produced during a vibration event were added to the guide pipes. To limit vibrations, cable restrainers were installed. When a cable begins to vibrate, these restrainers distribute the vibration among the adjacent cables. The restrainers also reduce the effective length of the cables, which reduces the deflection an excited cable will undergo. WDP also installed dampers to reduce the amplitude of the cable vibrations (Figure 1-5).



Figure 1-4: Cable restrainers on bridge



Figure 1-5: Dampers installed by WDP

1.3.2 Johns Hopkins University (JHU)

Researchers at JHU instrumented several cables of both the Fred Hartman Bridge and Veterans Memorial Bridge with accelerometers to collect vibration data in an attempt to model vibration characteristics. Knowing the characteristics of the cable vibration allows for the design of efficient dampers. The data collected by JHU is compiled in a statistical database with vibration characteristics and weather data for each event since October, 1997 (Eggers, 2003).

1.3.3 Texas Tech University (TTU)

Researchers at TTU developed an aerodynamic damping solution for the cables on the Fred Hartman Bridge. The system acts to prevent vibration by rings which are wrapped around the cable at frequent intervals. These rings were designed to prevent the rivulets that cause wind-rain induced vibration from forming. This aerodynamic damping solution did not work.

1.3.4 University of Texas at Austin (UT)

The primary goal for researchers at UT is to characterize the fatigue behavior of the stay cables. This has been done by instrumenting the cables, building full-scale fatigue test specimens, developing computational models of both the test specimens and cables on the Fred Hartman Bridge, and by characterizing the vibration data collected by JHU to estimate the displacement and number of cycles to which each cable has been subjected.

1.3.4.1 Field Measurements

The UT research team attempted to measure strains at various locations on the bridge to relate measured strains to accelerations during a vibration event. Strain gages were applied to the exterior PE pipe, the surface of the grout just under the pipe, and the anchorage guide pipes at the deck level. The attempt to take field measurements was unsuccessful because the strain gages did not function properly in the hostile environment on the bridge. No future attempts to instrument the cables are planned.

1.3.4.2 Full-Scale Bending Fatigue Tests

As of August 2004, ten full-scale bending fatigue tests have been completed. Each test specimen has a cross section based on the design drawings for the smallest cable on the Fred Hartman Bridge and a length of approximately 33 ft. The cables were displaced at a point in the center of the specimen; the displacement amplitude was different for each test. Other variables included the presence of grout and the number of strands. Specimens 1 and 2 are documented by Poser (2001). Specimens 3 and 4 were constructed and tested by Poser but were not documented. Specimens 5 through 10 are documented in this thesis. An overall summary of all specimens is presented in Chapter 4 of this thesis.

1.3.4.3 Computational Models

Computational models are useful in comparing the results obtained from the test specimens to the longer, larger cables on the Fred Hartman Bridge. Dowd (2001) developed a finite element model (FEM) of the laboratory test specimens. However, comparison of the FEM and test results show that the model created by Dowd overestimates the stiffness of the cable by a factor of 2. Current research at UT is underway to create accurate computational models.

1.3.4.4 Characterization of Vibration Data

Eggers (2003) used data collected by Johns Hopkins University to characterize the cable vibration. In his work, the displacement of the cables at the location of the accelerometer is determined. In addition, the number of cycles seen by the cables is estimated and the primary modes in which the cables vibrate are presented. This information is important in estimating the extent of fatigue damage already accumulated on the bridge.

1.4 TOPICS PRESENTED IN THIS THESIS

1.4.1 Full Scale Bending Fatigue Tests

This thesis describes the full-scale bending fatigue testing of Specimens 5 through 10. Details of the fatigue test setup and testing parameters are presented in Chapter 2, including the testing variables and parameters for Specimens 1 through 4 which were constructed and tested by Poser. The results of the fatigue tests, including the number of wire breaks and the number of loading cycles sustained by each cable, are presented in Chapter 4. A comparison of the fatigue results is presented in Chapter 5. The results of the bending fatigue tests will be used to establish the fatigue characteristics of the cable stay specimens in concurrence with computational models currently in development.

1.4.2 Single-Strand Tension Fatigue Tests

In-air tensile fatigue tests were performed to establish the fatigue characteristics of the strand used to construct Specimens 7 through 10. The results from these axial fatigue tests are compared with similar tests performed on the strand used to construct Specimens 1 through 6 by Eggers (2003). The results are also compared to established fatigue standards in Chapter 3.

CHAPTER 2

Overview of Cable Fatigue Tests

This chapter discusses the full-scale, cable-stay bending fatigue tests. Setup, details, and testing parameters for each specimen are included.

2.1 TEST SETUP

In general, the specimen assembly and test setup used for the full-scale fatigue tests followed those described by Poser (2001). To counteract the prestress and testing forces, the test specimens were constructed within a reaction frame consisting of two longitudinal wide flange columns with built-up crossbeams at each end. This reaction frame can be inclined for the grouting of the cable specimen, and the reaction frame is bolted to the floor during fatigue testing. A portal frame supported the hydraulic ram used to load the cable (Figure 2-1). This ram was then bolted to a steel clamp used to attach the cable to the loading apparatus (Figure 2-2). A photograph of the loading clamp is shown in Figure 2-3. To minimize stress concentrations along the loading region of the cable, a piece of polyethylene pipe acted as a cushion between the steel clamp and the test specimen over a length of 26 in. (660 mm). This PE cushioning pipe was tapered over a length of 6 in. (150 mm) at each end to provide a smooth stiffness transition from the stay cable to the clamp. The PE cushioning pipe is shown in Figure 2-2 and Figure 2-3.



Figure 2-1: Test setup

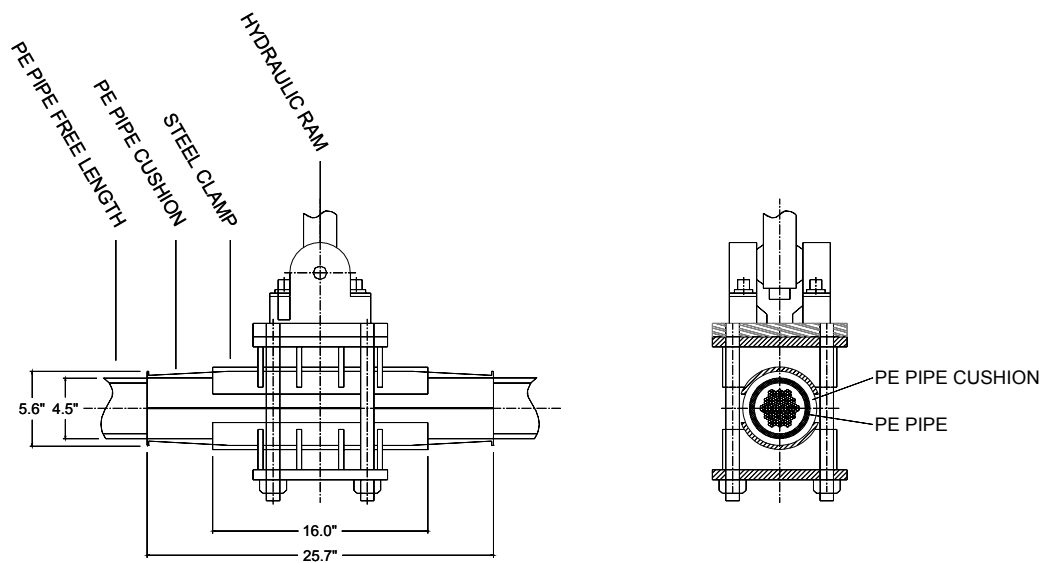


Figure 2-2: Geometry of loading clamp

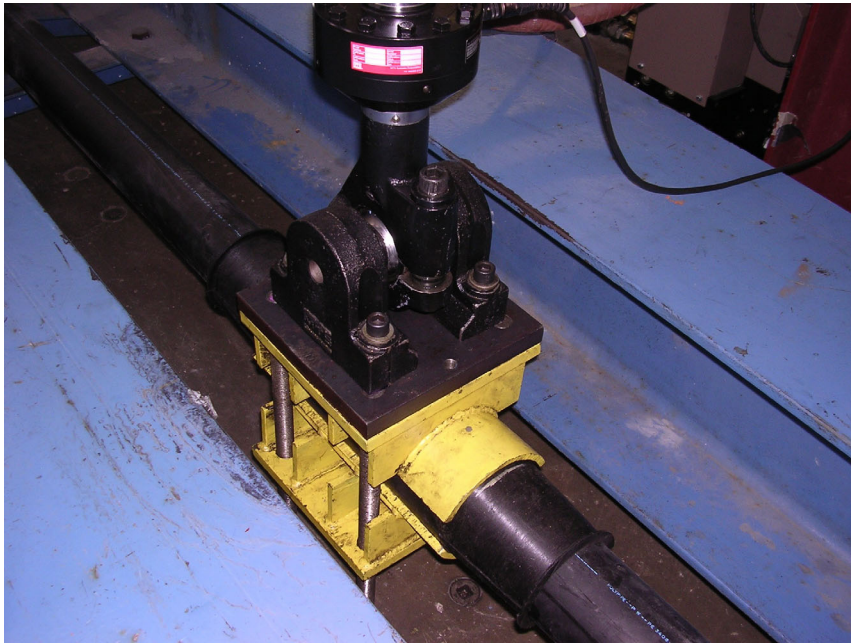


Figure 2-3: Loading clamp

2.2 CABLE STAY TEST SPECIMENS

Ten full-scale cable stay test specimens have been built and tested to date. Specimens 1 and 2 were tested and discussed by Poser (2001). Poser also oversaw construction and testing of Specimens 3 and 4, but those results were not included in the thesis by Poser (2001). Specimens 5 through 10 are reported in this thesis. A tabular summary of all tests is presented in Table 2-1. Details of Specimens 5 through 10 are presented in Section 2.2.4.

Table 2-1: Test parameters of all cable-stay test specimens

Stay	Number of Strands	Strand Type	Grout	Stressing End	Displacement (± in.)	Test Frequency (Hz)	Test Start Date	Test End Date
1	19	A	Grouted	Tower	1.6	0.9	3/8/2001	4/15/2001
2	19	A	Grouted	Tower	1.6	0.7	6/22/2001	8/9/2001
3	19	A	Grouted	Deck	1.6	2.2	11/31/01	12/27/2001
4	19	A	Grouted	Deck	1.1	3.0	2/1/2002	3/26/2002
5	19	A	Ungouted	Tower	1.6	2.1	3/11/2003	4/28/2003
6	13	A	Grouted	Tower	1.6	2.0	5/19/2003	7/2/2003
7	19	B	Grouted	Tower	1.6	2.0	7/15/2003	7/29/2003
8	19	B	Ungouted	Tower	1.6	1.8	12/17/2003	2/17/2004
9	19	B	Grouted	Tower	1.6	2.0	3/26/2004	4/11/2004
10	19	B	Grouted	Tower	1.1	3.1	5/7/2004	6/9/2004

Each specimen was either grouted or ungrouted. Grouted specimens were entirely filled with grout from anchor head to anchor head. Ungouted specimens were not grouted along the length; however, a 3-ft. section at the center was grouted for the purposes of clamping the cable to the loading apparatus. Other parameters were varied as well, such as the number of strands in the cross-section and the end from which the specimen was stressed. The parameters which apply to each specimen are presented in Table 2-1.

Each cable stay test specimen was composed of an arrangement of seven-wire, 0.6-in. prestressing strands and had a length of 33'-2³/₄". The longitudinal geometry is shown in Figure 2-4 and Figure 2-5. The anchorage components are shown in Figure 2-6 and were based on the most recent drawings for the Fred Hartman Bridge as produced by VSL International, the cable supplier for the bridge.

The geometry and anchorage components were slightly different from those used by Poser (2001). The shim plates were omitted from the tower anchorage region, thus making the cable symmetric about the loading point. Also, in the interest of economy and simplicity of construction, smooth end sleeves were substituted for the threaded nuts and flange plates used previously. The details of these can be seen in the exploded view of the anchorage elements (Figure 2-7).

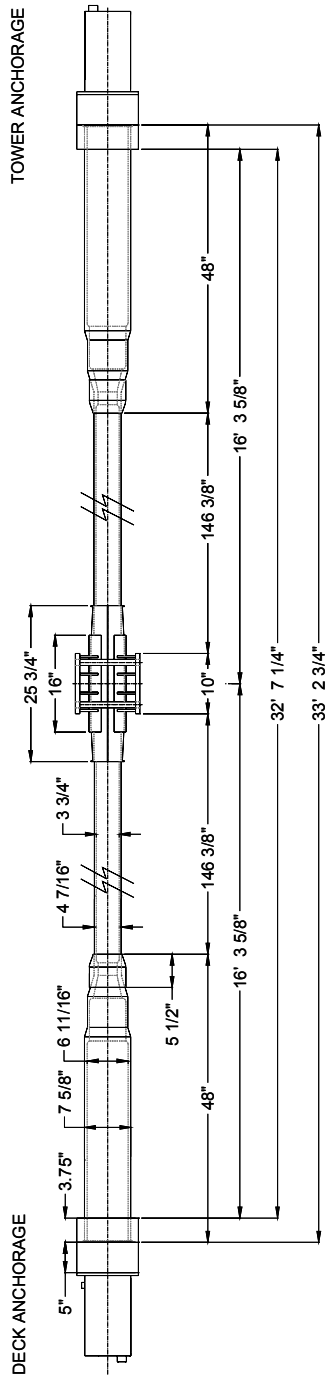


Figure 2-4: Longitudinal geometry of grouted test specimen

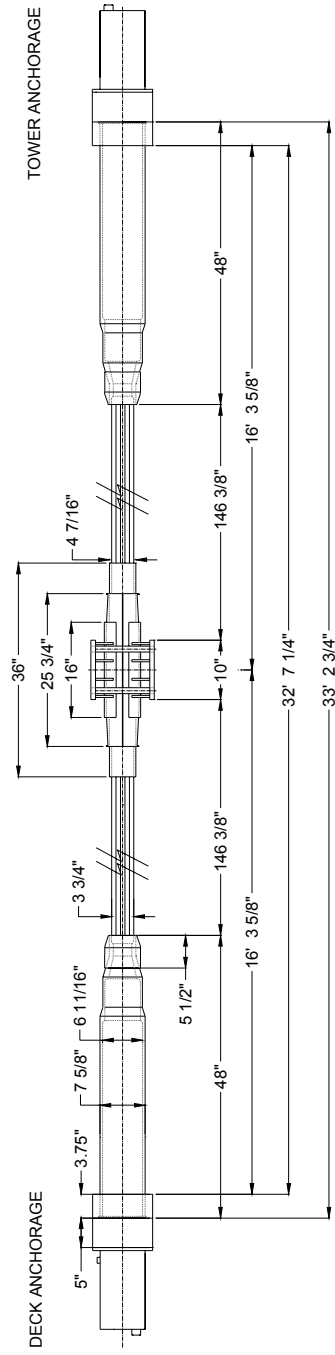


Figure 2-5: Longitudinal geometry of ungrouted test specimen

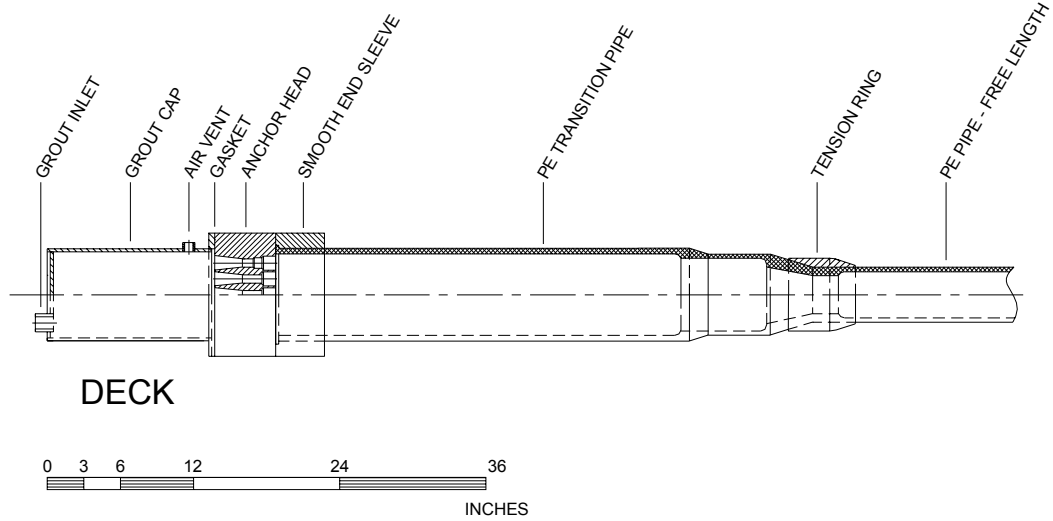
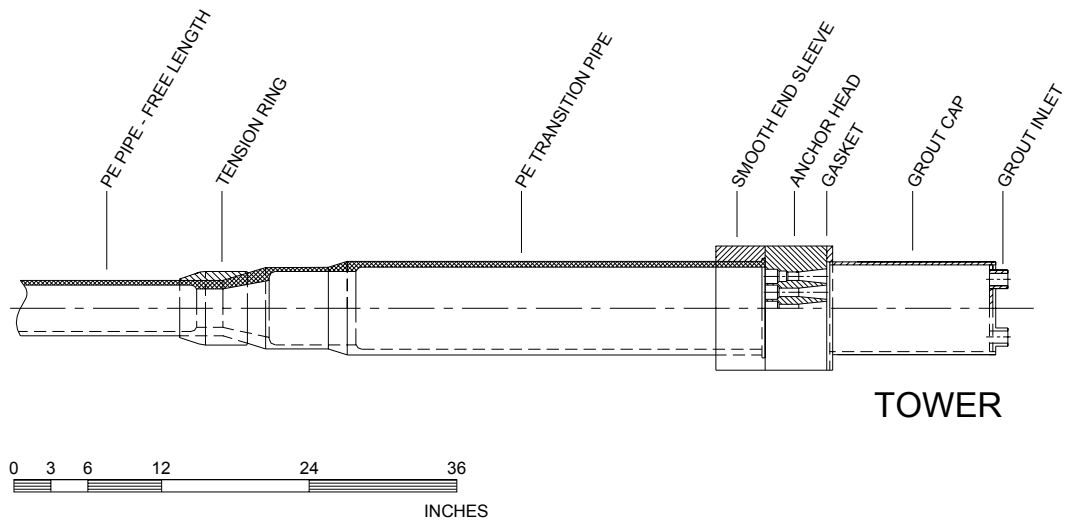


Figure 2-6: Geometry of anchorage regions

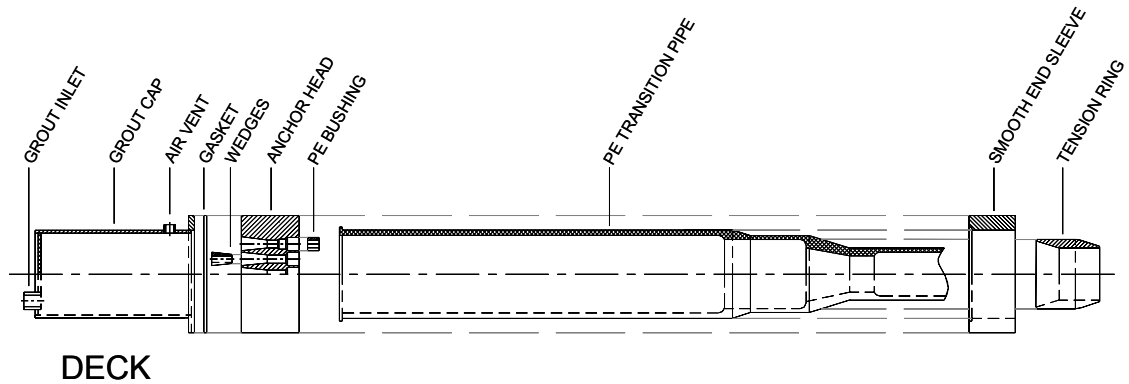


Figure 2-7: Exploded view of anchorage elements

2.2.1 Material Properties of Prestressing Strand

The prestressing strand used in all test specimens was seven-wire, 0.6-in. strand. However, strand from two different suppliers was tested. Strand B, which was manufactured with a larger center wire, is specifically for use in cable-stay applications. Table 2-2 shows the ASTM A416 specifications for this strand and the mill certificate values for each type. The area of each strand type was verified by the research team; the measured values, which varied from the mill certificate values by approximately 1%, are also presented. Both strand types satisfied the ASTM A416 minimum requirements.

In addition, the modulus of elasticity and breaking strength were verified for both types of strand. The measured values are presented in Table 2-3. Details of these tests are presented in Appendix A. It was observed that considering the measured breaking strength and the measured area, the ultimate stress for Strand A is only 269.9 ksi, which is less than the specified 270 ksi.

Table 2-2: Mechanical properties of prestressing strand

Grade 270 Strand	ASTM Standard	Strand A	Strand B
Modulus of Elasticity	27500 ksi	28000 ksi	28300 ksi
Breaking Strength	58.6 kip	58.992 kip	60.266 kip
Yield Point (1% Extension)	52.74 kip	54.363 kip	53.973 kip
Nominal Area	0.217 in ²	0.2185 in ²	0.2204 in ²

Table 2-3: Measured material properties for prestressing strand

Grade 270	Strand A	Strand B
Measured Area	0.220 in ²	0.223 in ²
Measured Area – Outer Wire	0.031 in ²	0.031 in ²
Measured Area – Center Wire	0.033 in ²	0.035 in ²
Modulus of Elasticity	28,900 ksi	28,600 ksi
Breaking Strength	59.4 kip	60.4 kip

2.2.2 General Assembly of Cable Stay Test Specimens

Cable stay test specimens were constructed as described in detail by Poser (2001). The process is divided into ten steps, which are described below.

1. First, 19 pieces of strand were cut from the spool. For Specimen 6, the geometry of the cross section was changed and only 13 pieces of strand were cut. The length of each piece was 48 ft. While only 36 ft was needed for the cable, the extra length was needed for the stressing operation.

2. The smooth end sleeve and tension ring were attached to the PE transition pipes (Figure 2-8). This apparatus was inserted into the frame at the deck end and the anchor head was placed behind it.

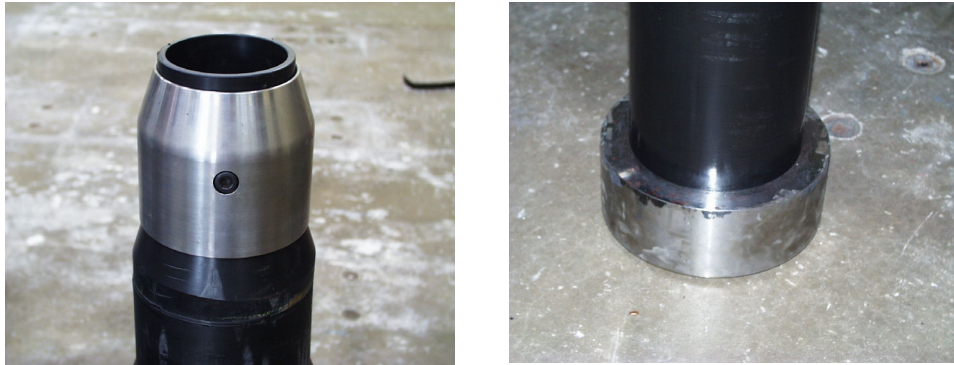


Figure 2-8: Tension ring (left) and smooth end sleeve (right) attached to transition pipe

3. Each strand was placed through the anchor head and transition pipe and pulled individually to the far end of the frame. Wooden shelves were built at two places along the length of the frame to ensure no strands crossed at any point. (Figure 2-9)



Figure 2-9: Wood shelf used to separate strands during construction

4. For the grouted specimens, the polyethylene pipe which acts as protection for the cable (including the helical spacer wire) was inserted

in the tower end of the reaction frame and pulled over the bundle of 19 strands. The helical spacer wire was 0.25-in. diameter steel wire which was wound into a coil and pulled through the pipe between the tension rings. This coil expanded to the interior diameter of the pipe and acted as a spacer such that the prestressing strand was not in contact with the pipe between the tension rings (Figure 2-10). For the ungrouted specimens, two PVC end caps which acted to seal the grouted section of the cable and 3-ft piece of polyethylene pipe (without a spacer wire) were pulled over the strands (Figure 2-11).

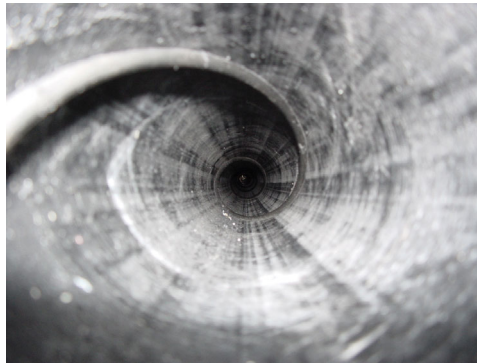


Figure 2-10: Helical spacer wire inside PE pipe (Poser, 2001)



Figure 2-11: PE pipe and white PVC end caps used on ungrouted specimens

5. The transition pipe, smooth end sleeve, and tension ring were placed outside the reaction frame on the tower end and each strand was pulled

through individually to ensure straightness. The transition pipe was then pushed into place within the frame.

6. Each strand was installed in the tower anchor head in the same position as the deck anchor head.
7. Wedges were installed around each strand at the anchor heads to fix the strands in the assembly. The wedges consisted of two halves that fit into the tapered opening in the anchor head and were supplied by VSL (Figure 2-12).

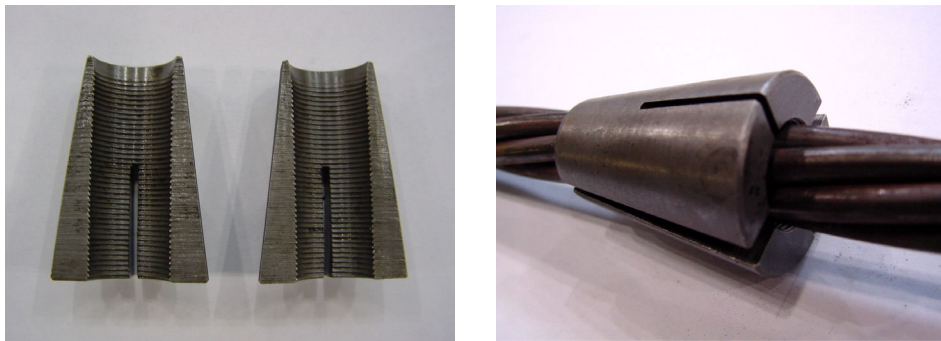


Figure 2-12: Wedges supplied by VSL (Poser, 2001)

8. After being anchored with the wedges, a prestress of approximately 2 kip was applied to each strand individually, starting with the center strand and working toward the outer strands. This step was done to allow for straightening of the assembly and seating of the wedges. The stress was applied using a mono-strand ram powered by a hand pump. Due to the congested nature of the anchor head area, a tapered adapter was needed to react against the anchor head. This adapter included a hole for a spring used to ensure wedge seating during the stressing operation. The setup for mono-strand stressing is shown in Figure 2-13. A close-up of the tapered adapter is shown in Figure 2-14.

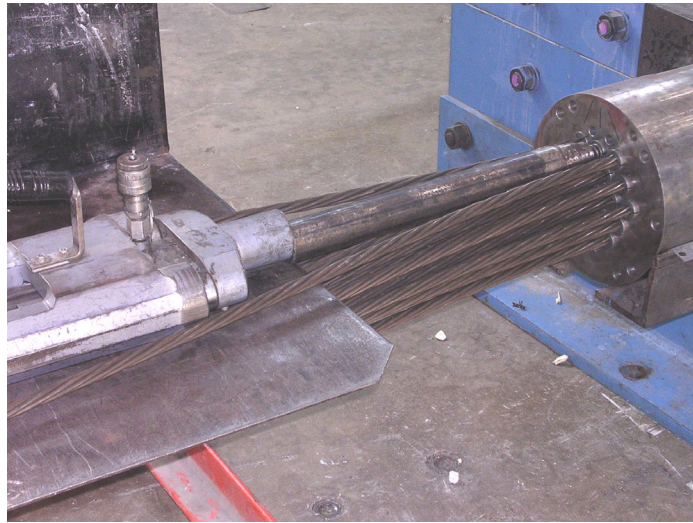


Figure 2-13: Setup for mono-strand stressing



Figure 2-14: Tapered adapter used for mono-strand stressing

9. After the assembly was straightened, all of the strands in the specimen were pulled together to prestress the cable. The prestressing ram was inserted over the extra length of cable at the tower end and an extra anchor head was installed behind the ram. This anchor head was used to react against during the stressing operation and was cut from the

cable before testing. The ram was powered by an electric pump, and a pressure gauge was attached to monitor the applied tension. A spring plate placed between the ram and the anchor head ensured that equal pressure was applied to all strands. Figure 2-15 shows the stressing assembly, and the spring plate is shown in Figure 2-16.

The stress was applied to the cable in increments to ensure equal stress on all the strands and to allow the wedges to seat equally. The cable was stressed in seven steps. Each step involved stressing the cable to a maximum value and then releasing the pressure on the ram to a minimum value as shown in Table 2-4, with both the maximum and minimum values increasing at each step. The values in Table 2-4 are given as a percentage of the pressure corresponding to the maximum tension.

Table 2-4: Stressing increments

Step	Maximum Stress (% Total)	Minimum Stress (% Total)
1	27	16
2	43	27
3	65	49
4	81	65
5	92	81
6	100	92
7	100	0

The nominal value of the full tension applied to the cable was 40.4% of the guaranteed ultimate tensile strength (GUTS) of the strand. This nominal value was 450 kip for the 19-strand specimens and 308 kip for the 13-strand specimen. Force during stressing was monitored using a gage which measured the pressure in the hydraulic system. The pressure at the maximum force of 450 kip was calculated

to correspond to a hydraulic pressure of 1850 psi. For Specimens 5 through 8, a gage with a maximum capacity of 5,000 psi was used. A more precise 2,000 psi gage was used during stressing of Specimen 9 and Specimen 10 to improve the accuracy of the stressing operation.



Figure 2-15: Setup for stressing



Figure 2-16: Spring plate used during stressing

10. After stressing was completed, the polyethylene pipe was welded to the transition pipe at both ends to seal the cable. This was done using a commercially available polyethylene welder. This step was only necessary for the grouted specimens.

2.2.3 Grouting of Cable Stay Specimens

2.2.3.1 Grouted Specimens

The reaction frame was inclined at approximately 30 degrees as shown in Figure 2-17 for the fully-grouted specimens. The end of the stay at the top of the grouting tower was designated the tower end and the end of the stay nearest the floor was designated the deck end. A combined grout mixer and pump was used to fill the tensioned cable with grout, which consisted of Type I portland cement and tap water with a water-to-cement ratio of 0.42. An anti-bleed admixture (Sikament 300 SC) was also added in the recommended proportion of 2.2% by weight of cement. The mixture proportions remained constant for all portland cement grout used for Specimen 5 through 10, except for a small amount of repair grout used to fill an intentional void left in Specimen 9.

To begin the grouting process, the cement, water, and admixture were added to the mixer. After the grout was thoroughly mixed, it was released into the trough from which it was pumped into the deck end grout cap. This continued until the grout flowing out of a transparent hose connected to the grout cap was an acceptable consistency, at which point the grout was pumped through the stay. Pumping of the grout continued until it flowed out of the tower grout cap. The pressure of the grouting operation was carefully monitored to stay between 40 psi and 70 psi to prevent the hoses and polyethylene pipe from rupturing.



Figure 2-17: Inclination of stay for grouting

2.2.3.2 UngROUTed Specimens

The grouting process for ungrouted specimens (5 and 8) was modified for the small volume of grout needed in the 3-ft section at the center of the cable. The reaction frame was propped on concrete blocks as shown in Figure 2-18, resulting in an inclination of approximately 10 degrees. Specimen 5 was grouted at the same time as a fully grouted specimen, thus the same large electric pump/mixer was used to fill the grouted cable and the small grouted section of Specimen 5. Because a small volume of grout was required for Specimen 8, it was mixed using a hand-held electric drill and paddle mixer (Figure 2-19) before being pumped into the cable stay using a small hand pump.



Figure 2-18: Grouting setup for Specimen 8



Figure 2-19: Grout mixing using electric drill and paddle mixer

2.2.4 Details of Cable Stay Test Specimens

A tabular summary of all specimen and testing parameters can be found in Table 2-1. Specimens 1 and 2 were tested and discussed by Poser (2001). Poser also oversaw construction and testing of Specimens 3 and 4, but those results

were not previously reported. Specimens 5 through 10 are discussed in this thesis.

2.2.4.1 Details of Specimen 5

Specimen 5 was composed of 19 strands and was oriented as shown in Figure 2-20 with the grout inlet holes at the top and bottom of the anchor head. Strand A was used for construction.

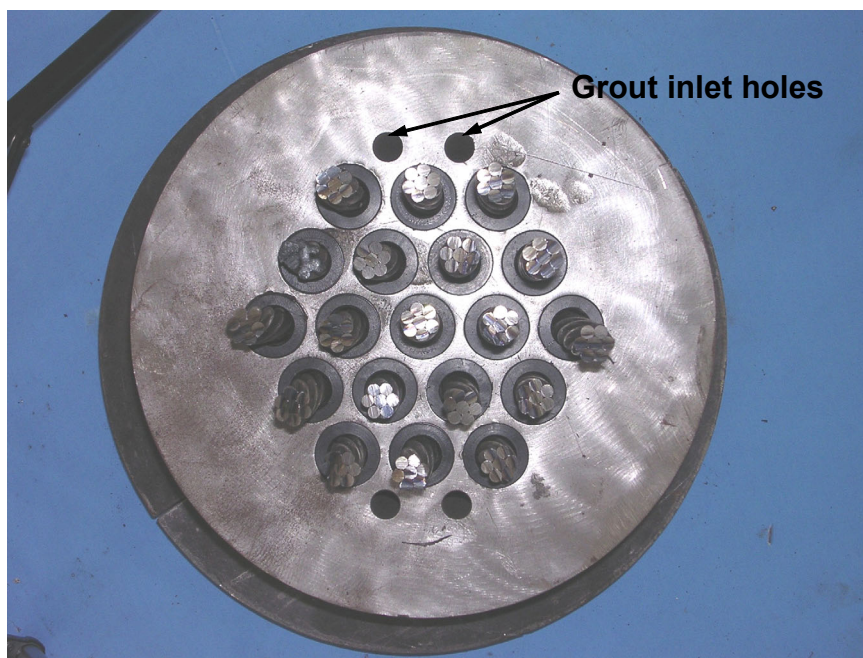
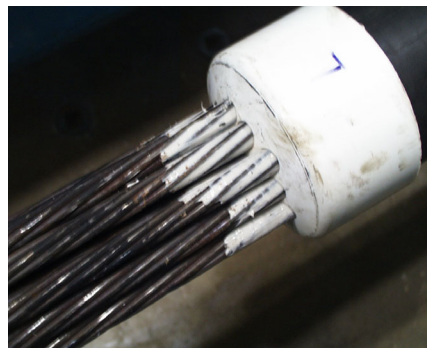


Figure 2-20: Orientation of Specimen 5

The cable was ungrouted along its length, with the exception of a 3-ft section located at the center of the cable. This grouted section allowed for the clamping and loading of the specimen as described previously and consisted of 4.5-in. diameter polyethylene pipe sealed at each end with a PVC pipe cap as shown in Figure 2-21 (a). To limit the leaking of grout from the ends of the grouted section, holes were drilled in the pipe caps to match the strand pattern of

the cable and caulk was applied both inside the pipe cap and around the exterior of the polyethylene pipe as shown in Figure 2-21 (b).



(a) Grouted section in clamp region (b) PVC end cap sealed with caulk

Figure 2-21: Center section of Specimen 5

The absence of grout in the stay allowed for the use of strain gages to monitor strand stresses near the anchor head. Eight strain gages were applied at the deck end of the stay, two each on strands 1, 3, 17, and 19 as shown in Figure 2-22. The distance of each gage from the face of the anchor head, measured before stressing the cable, is shown in Table 2-5. Gages were placed on the extreme exterior wire of the strand at the point of application, thus the gages on each strand were not attached to the same wire.

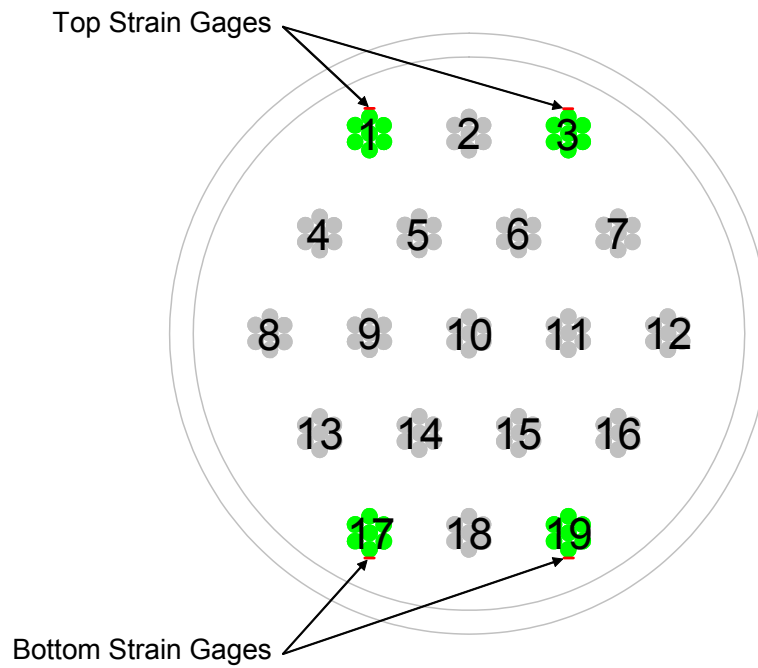


Figure 2-22: Placement of strain gages – Specimen 5

Table 2-5: Distance of strain gages from deck anchor head – Specimen 5

Gage	Strand	Location* (in.)
1	1	2.82
2	1	4.32
3	3	2.74
4	3	4.3
5	17	1.99
6	17	3.73
7	19	2.29
8	19	3.76

* Distance from face of anchor head to strain gage was measured before the specimen was stressed.

2.2.4.2 Details of Specimen 6

Specimen 6 was built using only 13 strands of type A to test the effect of a reduced moment of inertia on the bending fatigue properties of the specimen. Six strands were removed from the standard strand pattern as shown in Figure 2-23. The anchorage system and loading apparatus were identical to that used for the standard 19-strand specimens, and the anchor heads were oriented with the grout inlet holes at the top and bottom of the stay (Figure 2-24).

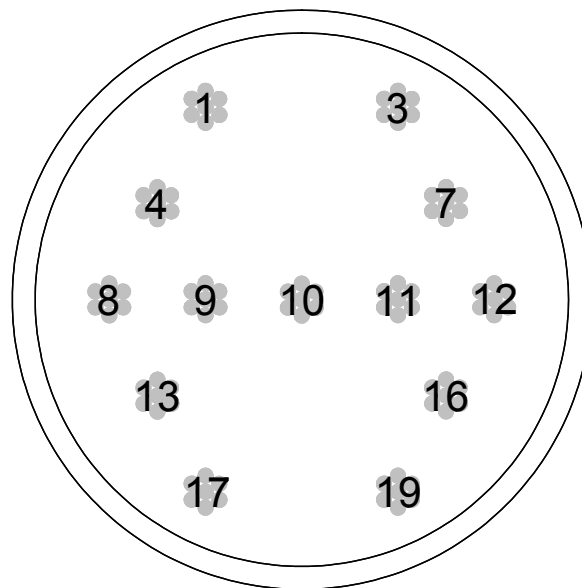


Figure 2-23: Strand layout - Specimen 6

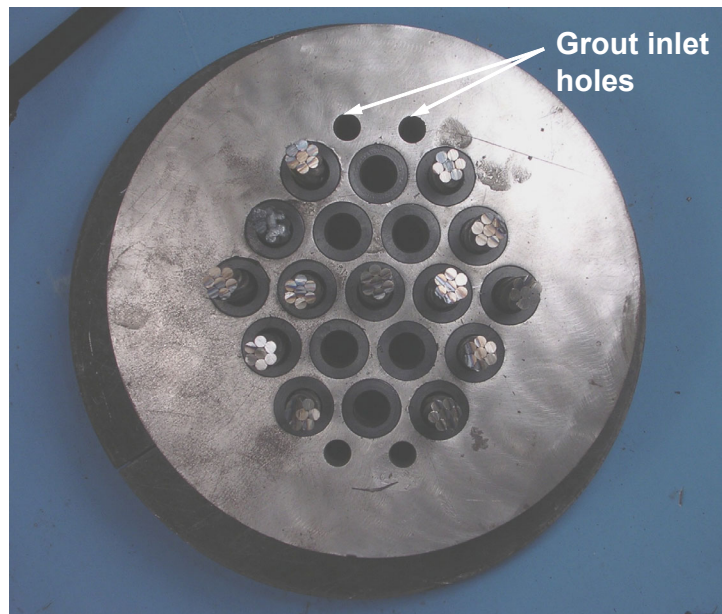


Figure 2-24: Orientation of Specimen 6

2.2.4.3 Details of Specimen 7

Specimen 7 was composed of 19 strands of type B and was a duplicate of Specimen 2 (Poser, 2001). The anchor heads were oriented with the grout inlet holes at the top and bottom of the stay.

2.2.4.4 Details of Specimen 8

Specimen 8 was similar to Specimen 5, composed of 19 strands and ungrouted along the length. The anchor heads were oriented with the grout inlets at the top and bottom of the specimen. Like Specimen 5, a 3-foot section at the center of the cable was grouted for clamping and loading purposes and sealed as described previously. However, Specimen 8 was built with strand of type B.

2.2.4.5 Details of Specimen 9

Specimen 9 consisted of 19 strands and was built with strand type B. The anchor heads were oriented such that the grout inlet holes were at the top and bottom of the stay.

The specimen was grouted along the entire length; however, a grout outlet was deliberately placed approximately 2 ft from the tower anchor head. This was done to generate a grout void in the specimen. A void had been identified near the tower anchor head of one stay on the Fred Hartman Bridge. TxDOT personnel were interested in testing the efficacy of a proposed method to fill the void and determining if the added grout influenced the fatigue life of the stay.

Ten days after the main grouting of the stay, this void was filled with SikaGrout 300 PT, a non-bleed, high-flow, sand-free grout mixture. The grout in this region was a mixture of SikaGrout and tap water. The ratio of water to grout mix, by weight, was 0.27, which corresponds to the highest amount of water recommended by the manufacturers. A funnel and tube system was attached to a grout inlet hole in the tower anchor head and gravity was used to fill the void as shown in Figure 2-25.



Figure 2-25: Filling of grout void near tower anchor head

2.2.4.6 Details of Specimen 10

Specimen 10 was composed of 19 strands of type B and was a duplicate of Specimen 4. The anchor heads were oriented with the grout inlet holes at the top and bottom of the stay.

2.3 TESTING OF SPECIMENS

2.3.1 Free-Vibration Testing

Before clamping the cable stay specimen to the hydraulic ram used for fatigue testing, a free-vibration test was performed to determine the natural frequency of each test specimen. A free-vibration test was also performed after fatigue testing was completed and the stay had been disconnected from the ram.

The free-vibration test was performed by connecting a weak link, a steel wire, to both the stay and the ram as shown in Figure 2-26. The ram was then raised until the steel wire broke, letting the cable vibrate freely. Displacement data were taken using a linear potentiometer and the CR 9000 data acquisition system. The natural frequency of the specimen was extracted from the data using a fast Fourier transform. The initial and final natural frequency of each specimen is presented in Chapter 4.

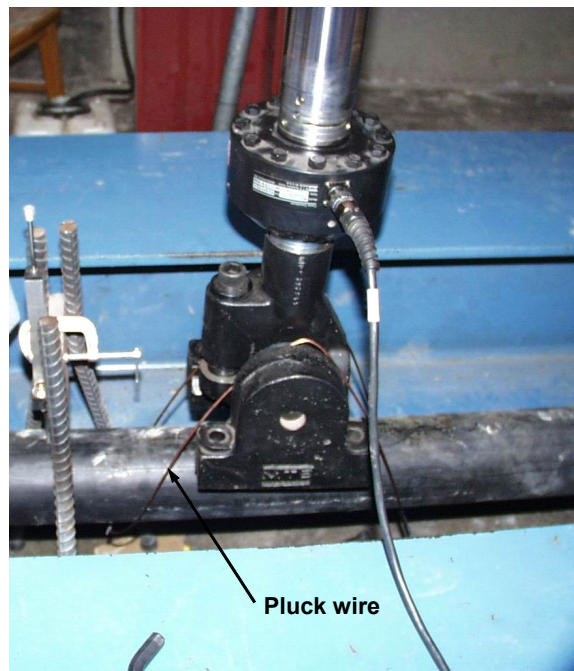


Figure 2-26: Setup for free-vibration test

2.3.2 Static Testing

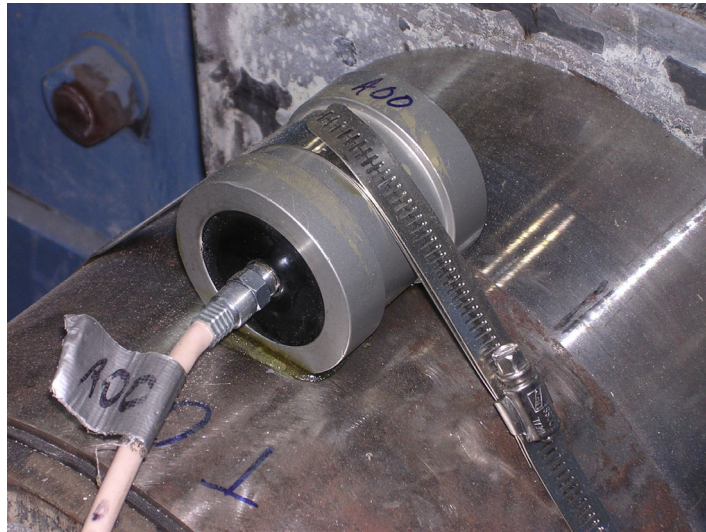
Before testing each specimen in fatigue, a static load test was also performed. The neutral level of the specimen was determined by finding the ram displacement that corresponded to zero load. Using displacement control, the midspan deflection was increased from the neutral level to its maximum positive value of 1.6 in. for Specimens 5 through 9 and 1.1 in. for Specimen 10 and then back to the neutral level. Load and displacement values were taken from the controller unit of the ram at approximately $\frac{1}{4}$ -in. intervals. The test process was then repeated from the neutral level to the maximum negative value of -1.6 in. for Specimens 5 through 9 and -1.1 in. for Specimen 10. The data from these tests were used to determine the stiffness of each specimen as presented in Chapter 4. Static tests were performed throughout fatigue testing of the specimen and after testing was completed.

2.3.3 Fatigue Testing

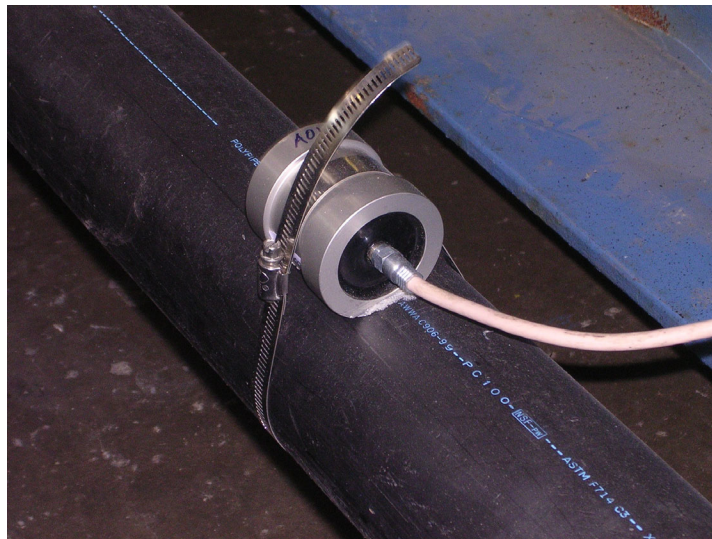
To test each cable stay specimen in fatigue, the controller unit of the ram was programmed to impose the desired displacement to the cable as a sine wave with a defined frequency. The testing frequency was slowly increased from 0.2 Hz to the desired testing frequency, which was controlled by the pumping capacity of the hydraulic system. The desired displacement values were determined such that the specimen was cycling about the zero load point. The specific testing parameters of each specimen are shown in Table 2-1. During the fatigue testing, strict error limits were imposed on the system, ensuring that the test stayed within closely-defined parameters. If the load, deflection, or error between the controller input and the ram output became too high, the system shut off automatically.

2.4 FATIGUE TEST MONITORING

The fatigue tests were monitored using a system provided by Soundprint, a division of Pure Technologies, Ltd. Acoustic sensors were placed on each anchor head as shown in Figure 2-27, and at two points along the free length within 2 ft of the tension ring (on the fully grouted specimens only). **Error! Reference source not found.** and **Error! Reference source not found.** show the placement of the sensors on the grouted and ungrouted stays. The sensors were connected with a computer that was monitored remotely by Soundprint. Sensors were set up in an automatic trigger mode that was calibrated to detect wire breaks. Wire break events were recorded and time stamped by the system, located and classified by Soundprint, and made available to the research team on the company's website.



(a) Sensor attached to anchor head



(b) Sensor attached to PE pipe near tension ring

Figure 2-27: Soundprint acoustic sensors

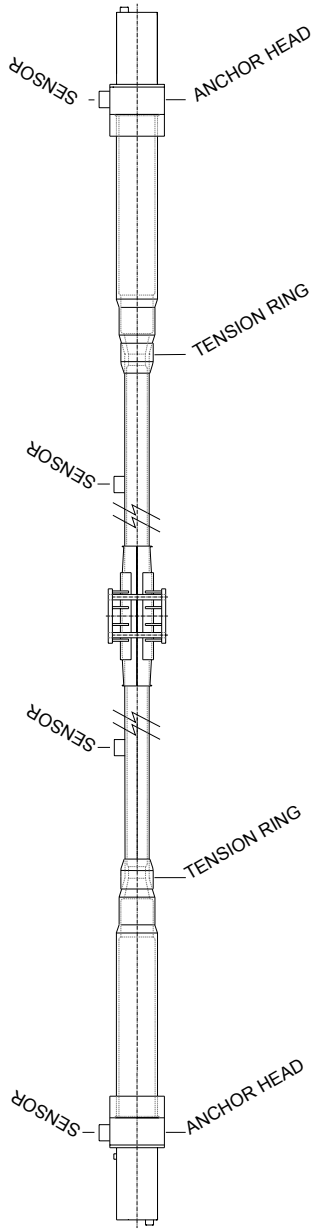


Figure 2-28: Placement of Soundprint sensors on a gouted specimen

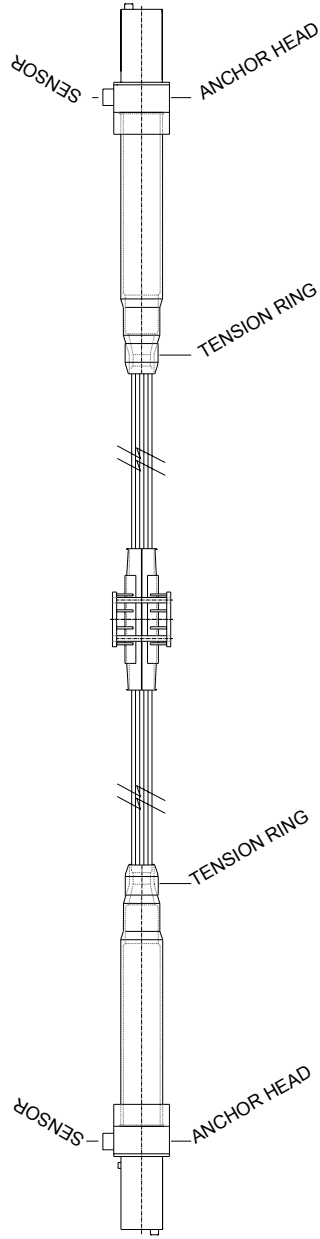


Figure 2-29: Placement of Soundprint sensors on an ungrouted specimen

CHAPTER 3

Single-Strand Tension Fatigue Tests

This chapter discusses in-air axial fatigue tests performed on the prestressing strand used to construct the full-scale test specimens. A detailed description of the test program is presented and the results are compared with established fatigue specifications.

3.1 INTRODUCTION

In order to determine whether bending accelerates the fatigue damage of cable stays, it is necessary to understand the fatigue performance of the individual components of the cables. Tensile fatigue tests were performed in air to determine the fatigue properties of the 0.6-in. diameter prestressing strand used in the cable stay specimens 7 through 10 (Strand B). Eggers (2003) provided similar data for Strand A, which was used to construct cable-stay specimens 1 through 6. The results are compared with the PTI specifications for axial fatigue of prestressing strand.

3.2 TEST PROGRAM

Axial fatigue tests were performed on a total of sixteen specimens. Nine of the specimens were considered in evaluating the fatigue performance of the strand; the other seven specimens exhibited premature failures at the grip. Data from these specimens are presented for the sake of completeness only.

Each fatigue specimen was subjected to a stress range of either 20, 30, or 40 ksi. The number of tests was not determined before testing began. Rather, testing was continued within each stress range until three specimens sustained wire fractures away from the grips or resisted 4,000,000 loading cycles without a

wire fracture, which was considered to be a run out. The only exception to this was Test 16, which was stopped after 2,758,249 loading cycles with a stress range of 20 ksi. The test was stopped with no wire failures because it had already surpassed the fatigue requirements of PTI (2001), which states that a test with a stress range of 20 ksi should sustain over 2,000,000 loading cycles.

The average stress applied to each specimen was 108 ksi. This value corresponds to 40% of the guaranteed ultimate tensile strength (GUTS) of the strand and is the prestress applied to the bending fatigue test specimens.

3.2.1 Test Set-up

The axial tensile tests were performed in a 220-kip MTS load frame shown in Figure 3-1. This load system consists of two heads with hydraulically-controlled clamps which may be used to fix a specimen in the load frame. Once a specimen is clamped in place, the bottom head may be moved to apply static or dynamic loads to the specimen.



Figure 3-1: 220-kip MTS load frame

The loading was controlled by PC-based software (MTS TestStar II) which was connected to the MTS system. Each test was run under load control with the necessary loads being calculated based on the area of the strand as measured by the research team. This value was within 1.2% of the value reported on the mill certificate for the strand. The input for the cyclic loading was a sine wave with feedback compensation, which automatically compensates for the error between the input load and the load actually measured by the test specimen. Test frequency was the highest frequency that did not cause excessive errors due to the degradation of the loading history or dynamic movements of the load frame. The testing frequency for each stress range is presented in Table 3-1.

Table 3-1: Test frequency for axial fatigue testing

Stress Range (ksi)	Test Frequency (Hz)
20	9.0
30	7.5
40	5.0

Each test specimen was approximately 48” long measured between the grips and was carefully aligned in the load frame to minimize eccentricity in loading. The grips used at either end were specially designed to minimize added stress to the strand and are described in Section 3.2.2. Approximately $\frac{3}{4}$ ” of the grip was left outside the clamp on each end of the MTS load frame. (Figure 3-2) This was done to provide a stiffness transition between the grip and the strand in an attempt to eliminate wire fractures at the face of the grip.

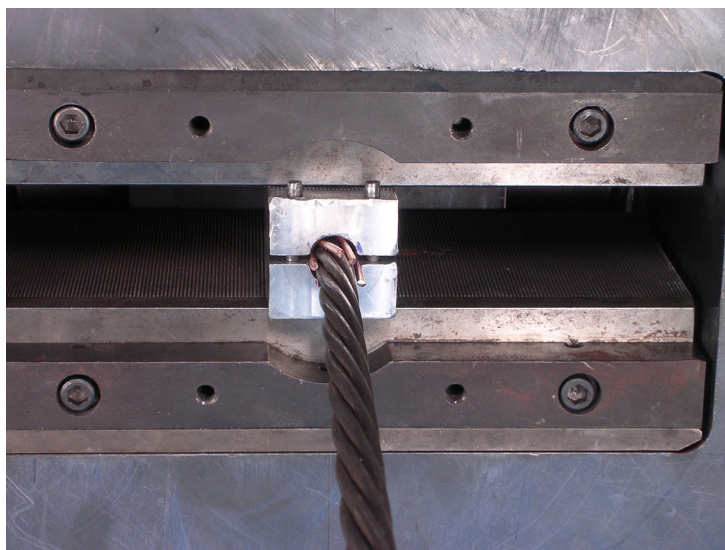


Figure 3-2: Grips in position during testing

3.2.2 Aluminum Grips

The aluminum grips used to clamp the specimen into position during fatigue loading were designed to keep the specimen from slipping during testing without crushing the specimen or the aluminum grips. The grip design was similar to that developed by Heller (2003). A schematic of this design is shown in Figure 3-3 and a photograph of the finished grips is shown in Figure 3-4.

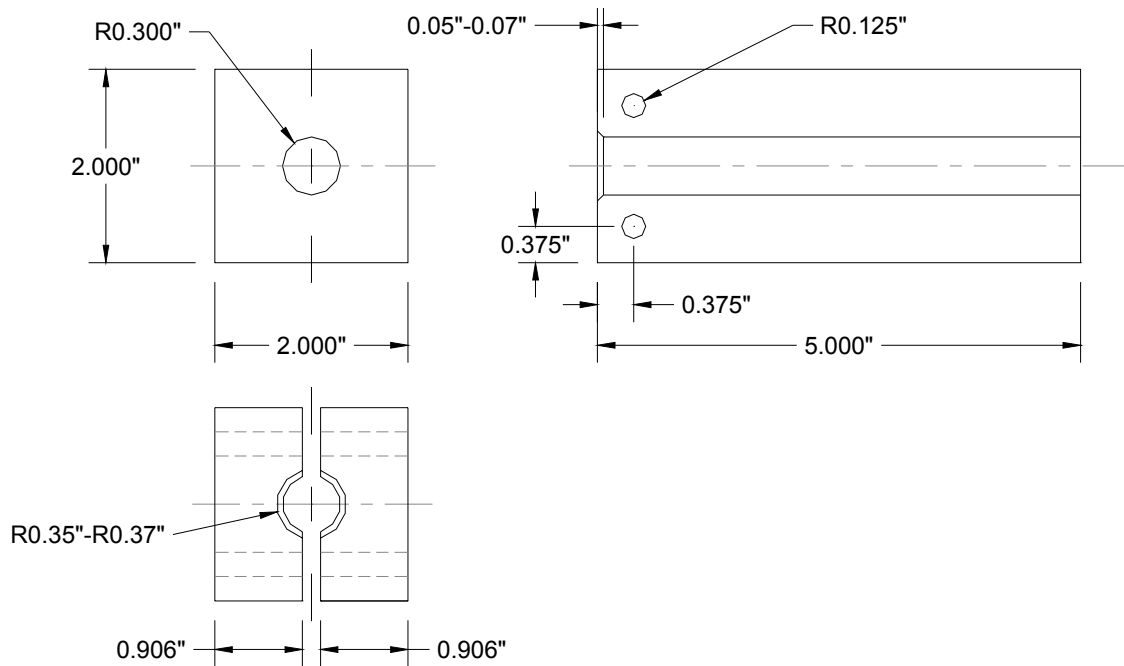


Figure 3-3: Aluminum grip design



Figure 3-4: New aluminum grips used for axial fatigue testing

The grips used were modifications of those fabricated for Eggers (2003). Originally, a 2-in. aluminum block with a 5/8-in. diameter threaded hole was cut in half longitudinally. The clamps were modified by taking 0.015" off the face of each clamp and re-drilling a 0.6-in. diameter smooth hole. The end of each grip was then filed down approximately 0.05" to eliminate a sharp transition between the grip and the strand. The two halves of the grip are aligned on either side of the strand using steel pegs that fit through the small holes shown in Figure 3-4.

Before placing the grips on the test specimen, the specimen was wrapped in the grip region with 8-gauge solid copper wire following the helix of the strand (Figure 3-5). The copper wire was crushed during clamping of the specimen and acted as a cushion between the strand and the aluminum grip, preventing crushing of the strand. The clamp pressure was carefully controlled to avoid crushing the aluminum clamps during testing, although the aluminum did deform due to the copper wire (Figure 3-6). Because the pressure was carefully controlled and due to the cushioning effect of the copper wire, the aluminum grips were used for multiple tests.

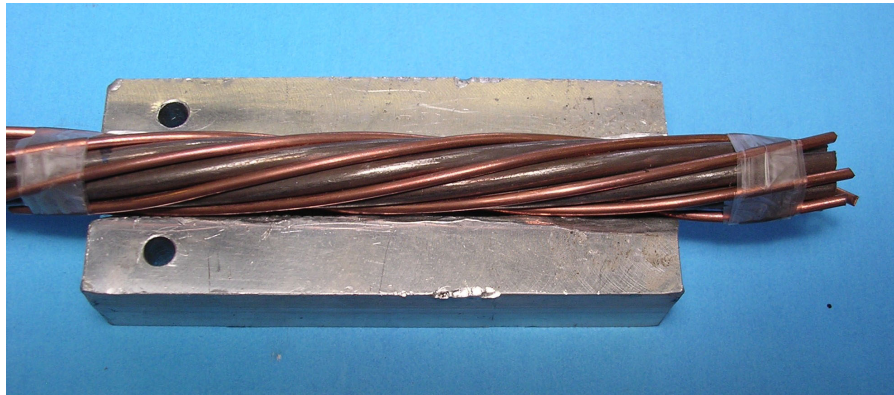


Figure 3-5: Strand wrapped with copper wire before fatigue testing



Figure 3-6: Grips after use in multiple axial fatigue tests

3.3 RESULTS

Fatigue tests were performed at stress ranges of 20, 30, and 40 ksi. The stress range and cycle at breaking of each test is presented in Table 3-2. The results from the seven strands that failed prematurely at the grips were not included in the evaluation of the data and are identified in Table 3-2.

Table 3-2: Axial fatigue test results

Test	S_r (ksi)	N (cycles)	Notes
1	40	918,237	
2*	40	319,823	Grip failure
3*	40	154,303	Grip failure
4	40	2,743,778	
5*	40	480,528	Grip failure
6	40	218,335	
7*	30	647,023	Grip failure
8	30	430,914	
9*	30	1,366,485	Grip failure
10*	30	513,931	Grip failure
11	30	4,494,437	Run-out: stopped without failure
12*	30	2,400,387	Grip failure
13	30	4,077,677	Run-out: stopped without failure
14	20	4,630,117	Run-out: stopped without failure
15	20	4,013,272	Run-out: stopped without failure
16	20	2,758,249	Run-out: stopped without failure

* Specimens were not used to evaluate strand and are presented for completeness only.

3.3.1 Comparison with Published Fatigue Standards

The results of the axial fatigue tests on Strand B are compared with the fatigue standards published by the Post-Tensioning Institute (2001). These standards specify a lower limit to the fatigue life of ASTM A416 uncoated, seven-wire, low-relaxation strand for use in stay cables. Both the 2001 and 1986 specifications are presented, as there was a significant increase in the required fatigue life between these two editions. The 1986 requirements are understood to be based on tests by Paulson et. al (1983) which were similar to those described in

this thesis. The basis for the 2001 requirements is not documented. Table 3-3 summarizes the fatigue requirements for the strand as set forth by PTI.

Table 3-3: PTI Specifications for Strand Fatigue Life

Number of Cycles	2001 PTI Required Stress Range (ksi)	1986 PTI Required Stress Range (ksi)
100,000	64.3	55.0
500,000	43.8	37.5
2,000,000	33.1	28.0
> 2,000,000	30.9	26.0

The testing parameters presented in this thesis closely match the testing requirements of both editions of the PTI specification. PTI specifies that the maximum stress during cycling be $0.45 f'_s$, where f'_s represents the tensile strength of the strand. The maximum stresses for the axial fatigue tests are shown in Table 3-4. The maximum stress during cycling was $0.47 f'_s$, less than 5% higher than the prescribed value.

Table 3-4: Maximum Stress During Axial Fatigue Testing

Test Stress Range (ksi)	Maximum Stress
20	$0.44 f'_s$
30	$0.46 f'_s$
40	$0.47 f'_s$

The test data are plotted with both the 2001 and 1986 PTI minimum values in Figure 3-7. Seven of the nine tests satisfied the 2001 PTI minimum requirements. Tests that were stopped without failures (run-outs) satisfied the PTI minimum. The two tests that did not satisfy the 2001 PTI requirements also did not satisfy the lower 1986 PTI requirements. These results indicate that Strand B, used to construct full-size Specimens 7 through 10, has a satisfactory fatigue life.

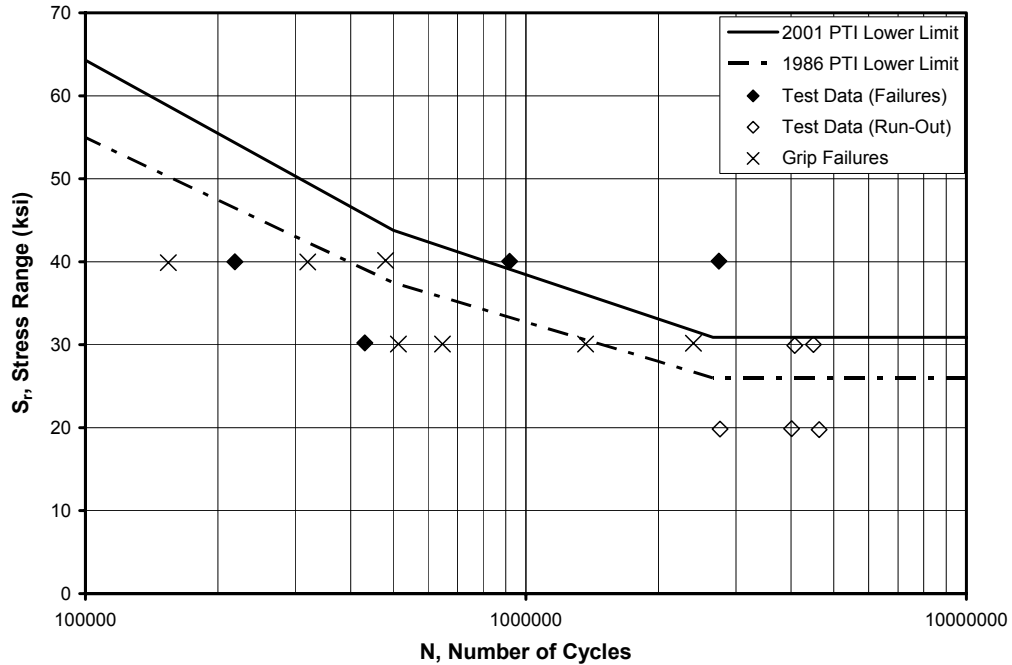


Figure 3-7: Results of Tensile Fatigue Tests

3.3.2 Comparison with Previous Fatigue Testing

Similar fatigue tests were performed by Eggers (2003) on Strand A, which was used to construct Specimens 1 through 6. Figure 3-8 compares the data from the fatigue tests of Strand B with the data for Strand A as presented by Eggers. Seven out of eight of the axial fatigue tests performed on Strand A did not pass the 2001 PTI specifications, compared with only two out of nine of the Strand B specimens which did not pass. However, the scatter in the data for Strand B is greater than that for Strand A. Overall Strand B, which is specifically fabricated for cable stay applications, exhibits better fatigue performance in-air than Strand A.

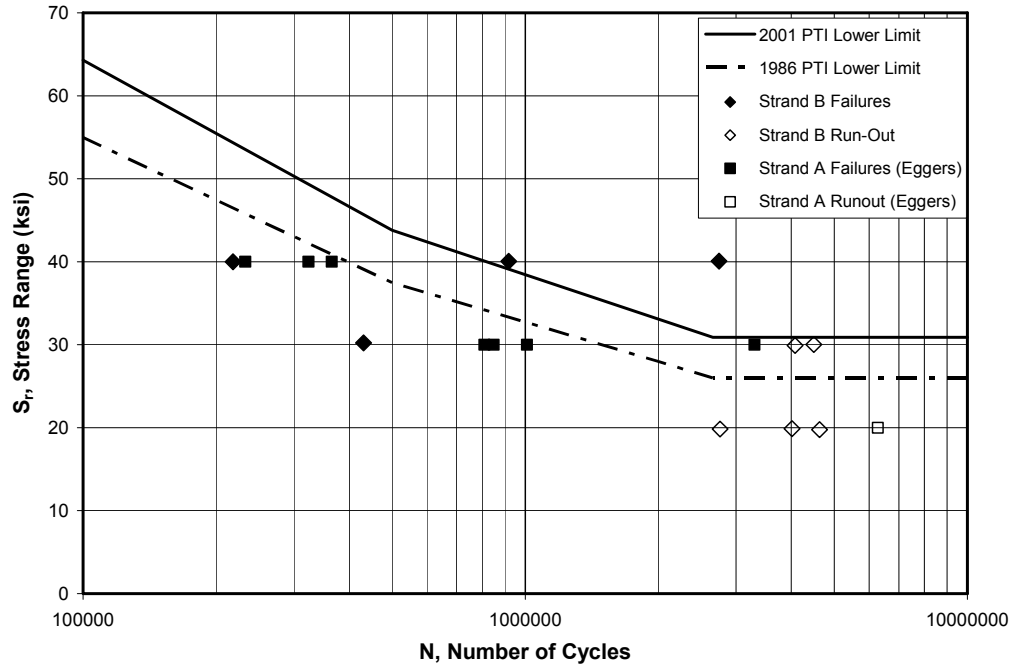


Figure 3-8: Fatigue Test Results of Strand B vs. Strand A

CHAPTER 4

Bending Fatigue Test Results

This chapter presents the results of the full-scale bending fatigue tests on Specimens 5 through 10. Observations made during the post-mortem (autopsy) investigation of each cable stay specimen are also reported. The testing parameters for each specimen are listed in Table 2-1.

4.1 METHODS OF ANALYSIS

After fatigue testing was completed and the specimen had been disconnected from the ram, a final free-vibration test was performed to determine the final natural frequency of the stay. The reaction frame was then moved out from under the ram and an autopsy investigation was performed.

4.1.1 Method of Autopsy Investigation

To begin the autopsy of each stay, it was cut into three portions, the tower end, the deck end, and the center portion. For the ungrouted specimens (5 and 8), the stay was first torch-cut just outside the grouted region near the center of the cable. The stay was then cut again on the other side of the grouted portion using a disc grinder. For the grouted specimens (6, 7, 9, and 10), a 4-in. section of the polyethylene pipe was removed and the grout was removed before torch-cutting the strand. Further cross-sectional cuts were made using a disc grinder.

4.1.2 Types of Fatigue Fractures

The fracture surface of each wire break was examined using a microscope. The wire breaks were caused primarily by fretting fatigue, which occurs when two adjacent wires rub against each other during cyclic testing. The initiation of a

fatigue crack occurs at the contact point between the two wires; the fatigue crack continues to grow outward in a semi-circular manner until the loss in gross wire area due to the crack causes a tension failure.

Two types of fretting fatigue failures were dominant. The first type occurred due to fretting between the center wire and an outer wire, as shown in Figure 4-1. This type of fretting can lead to fracture of the center wire, the outer wire, or both wires at the contact point (Figure 4-2).

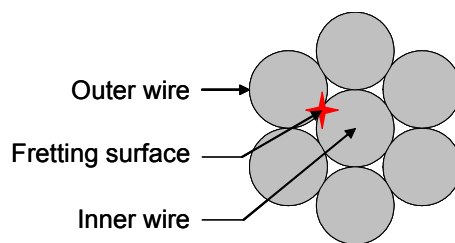


Figure 4-1: Fretting between the center wire and an outer wire

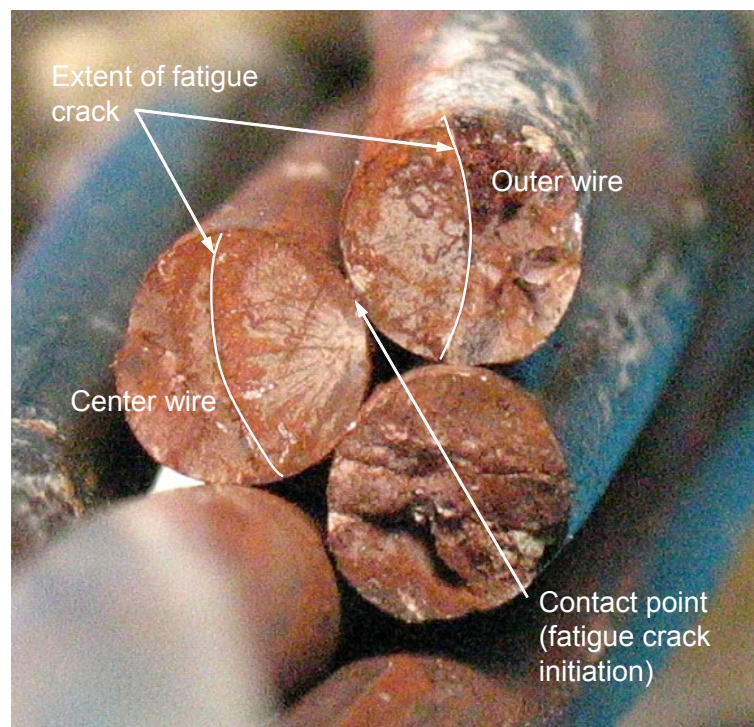


Figure 4-2: Fretting fatigue of center and outer wires

The second type of fatigue failure was due to fretting between two adjacent outer wires as shown in Figure 4-3. An example of this type of failure is shown in Figure 4-4.

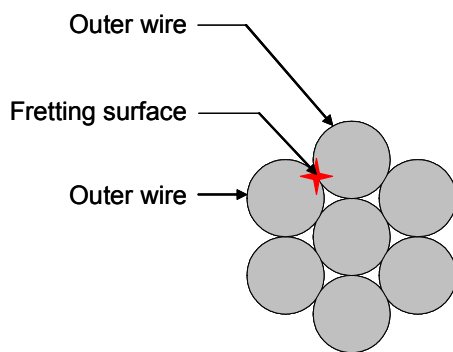


Figure 4-3: Fretting between adjacent outer wires

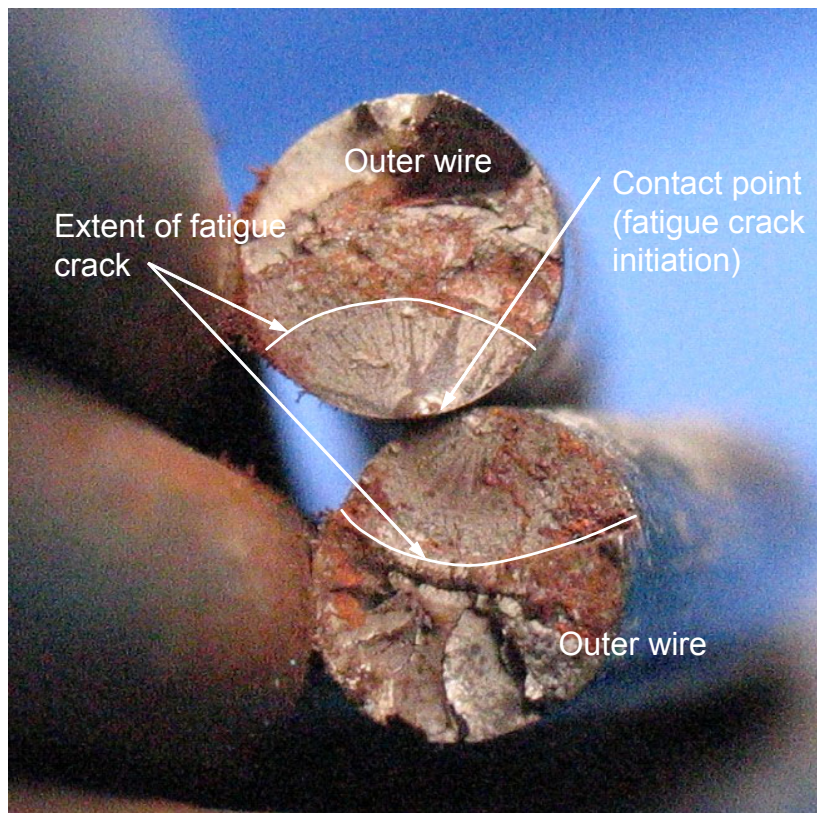


Figure 4-4: Fretting fatigue between outer wires

A third, less common type of fatigue failure was also observed where the fatigue crack was initiated at a point that was not in contact with other wires in the strand. This type of failure tended to occur near the wedges at the stressing end of the cable where fatigue cracks were initiated by a wedge. Figure 4-5 shows an external wire that failed near the wedge.

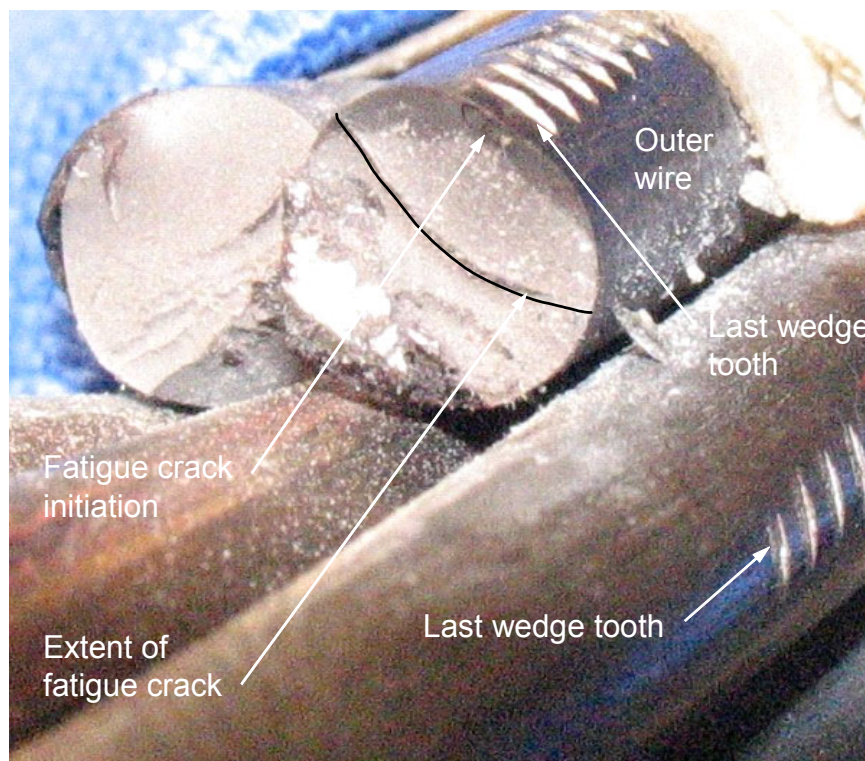


Figure 4-5: Isolated fatigue failure at wedge

Occasionally fatigue failures were also observed to initiate at a point where an exterior wire was not in contact with the other wires in the strand. It is unknown what caused this type of failure, although possible sources are corrosion, defects on the wire, or fretting with the helical spacer wire (Figure 4-6).

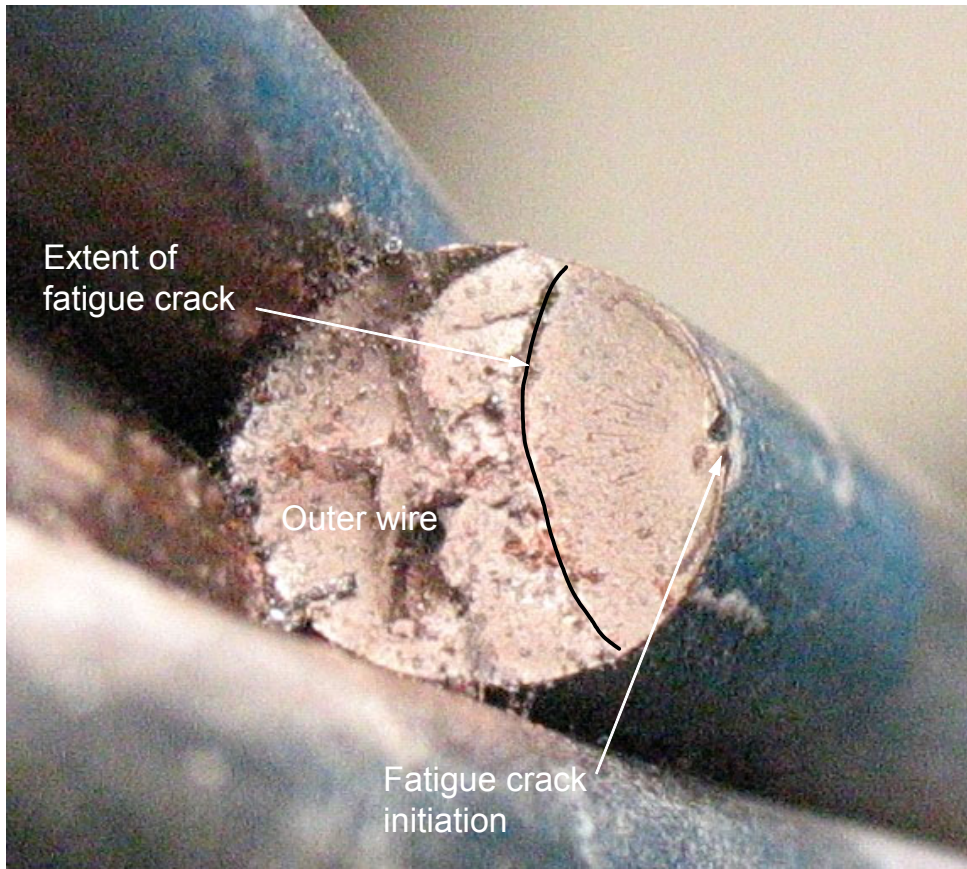


Figure 4-6: Fatigue caused by external source

4.1.3 Nomenclature

To maintain consistency among specimens, the nomenclature established by Poser (2001) to identify strands and wires was adopted in this thesis as well (Figure 4-7 and Figure 4-8). The strands were numbered 1 through 19 from right to left as looking from the tower end to the deck end. This numbering of the strands was maintained for all specimens, even those that were fabricated with fewer than 19 strands. The individual wires in a strand were numbered clockwise from 1 to 7, with 1 being the top wire and 7 being the center wire.

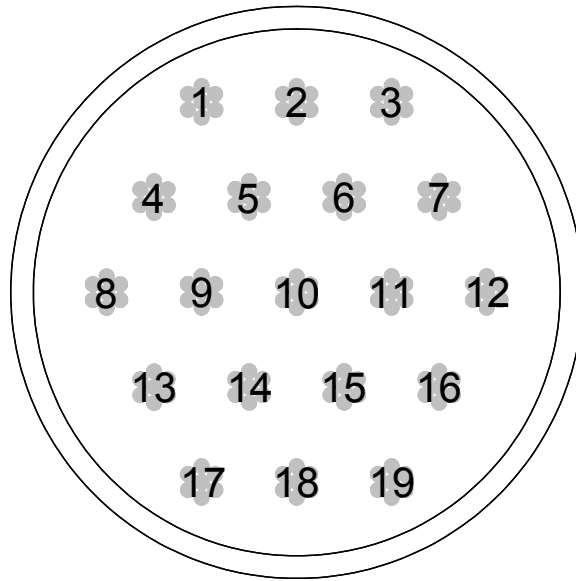


Figure 4-7: Nomenclature of strands looking from tower end to deck end

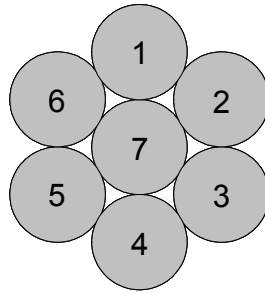


Figure 4-8: Nomenclature for wires in a strand

4.2 FATIGUE TEST RESULTS

A summary of the fatigue results of all specimens is presented in Table 4-1. Specimens 1 and 2 were discussed by Poser (2001). Specimens 3 and 4 were constructed and tested by Poser but have not been previously reported. Specimens 5 through 10 are documented in this thesis.

Table 4-1 presents the number of cycles, static stiffness, natural frequency, and number of wire breaks of each cable. The stiffness of each cable before and after the fatigue tests was determined by a static test as described in Chapter 2.

The final static stiffness of Specimens 1 through 4 is not known. The natural frequency of each specimen before and after the fatigue test was determined by a free-vibration test. An initial free-vibration test was not performed for Specimen 1. No data are available for the initial or final natural frequency of Specimen 3 and the initial natural frequency of Specimen 4.

Table 4-1 also presents the number and location of wire fractures found in each specimen after the fatigue test. The tower end was the end of the stay elevated during grouting. The deck end was the lower anchorage during grouting. The center of the cable was the portion under the load point.

Table 4-1: Summary of Fatigue Test Results

Stay	Number of Cycles	Initial Static Stiffness	Final Static Stiffness	Initial Natural Frequency	Final Natural Frequency	Number of Wire Fractures		
		(kip/in)	(kip/in)	(Hz)	(Hz)	Tower	Center	Deck
1	2,808,398	4.8	No data	No data	12.0	14	11	0
2	2,865,103	4.8	No data	12.5	11.5	51	16	1
3	4,961,560	4.7	No data	No data	No data	9	62	14
4	8,775,245	4.5	No data	12.9	No data	28	0	3
5	5,211,106	4.1	3.9	13.8	13.5	0	0	0
6	6,483,024	3.3	3.0	11.5	11.0	17	11	0
7	2,246,869	5.0	3.4	13.3	11.1	37	65	17
8	6,200,593	4.1	3.9	13.9	13.4	2	0	2
9	2,566,126	4.5	4.2*	12.5	10.5	12	61	3
10	5,614,211	4.8	4.0	13.0	11.8	23	21	8

*Note: Final static test was performed at 1,748,800 cycles.

4.2.1 Specimen 5

Specimen 5 sustained 5,211,106 loading cycles without a wire fracture. The specimen was ungrouted and the cross-section consisted of 19 strands.

Specimen 5 was stressed from the tower end and grouted from the deck end. The cable displacement was ± 1.6 in. at midspan.

4.2.1.1 Grout Condition

The only portion of Specimen 5 that was grouted was a 3-ft section at the center. Following completion of the fatigue test, the polyethylene pipe was opened using a router. The grout had no appreciable voids apart from a small defect at the location of the vent hole used for grouting and appeared to be homogeneous. The grout appeared to be essentially uncracked immediately upon opening the PE pipe, as shown in Figure 4-9. The only large crack was directly under the line cut by the router; no longitudinal cracks characteristic of regions where wire breaks are present were found. However, within minutes of opening the polyethylene pipe, circumferential shrinkage cracks began to appear and the grout began to fall away in pieces.



Figure 4-9: Grout condition - Specimen 5

4.2.1.2 Corrosion

Specimen 5 was cured for 46 days after grouting the center portion and then tested for 48 days. Corrosion was evident at the interface between the grout and caulk in the grouted portion of the specimen, as shown in Figure 4-10. The color indicates the presence of corroded fretting product but the source of this

fretting is unclear. Very little corrosion or corroded fretting product was observed along the ungrouted portion of the specimen.



Figure 4-10: Interface between caulk and grout – Specimen 5

4.2.1.3 Wire Breaks

Specimen 5 did not experience any wire breaks during the fatigue tests. To ensure accurate calibration of the Soundprint monitoring system, the research team intentionally generated two wire breaks (Figure 4-11). A Dremel tool was used to cut the wires, and then the cable was displaced until the damaged wire broke. The acoustic monitoring system accurately captured the simulated wire breaks.

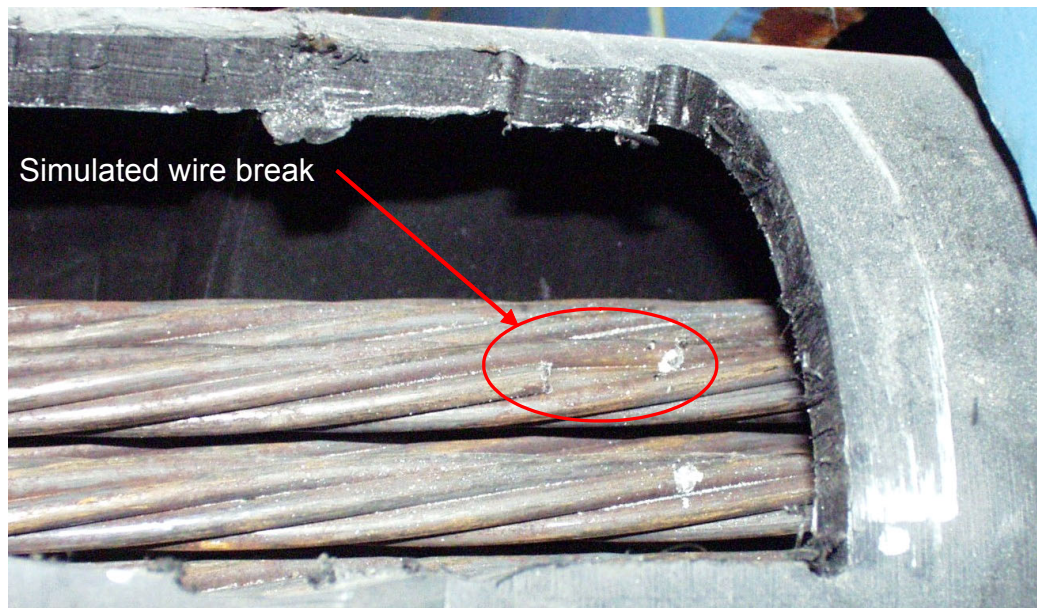


Figure 4-11: Simulated wire break – Specimen 5

4.2.1.4 Lateral Stiffness

The lateral stiffness of the test specimen was monitored throughout the fatigue test, both by daily monitoring of the load required to reach the desired displacement and also by stopping the programmed fatigue test periodically to perform static displacement tests as described in Chapter 2.

Figure 4-12 shows the variation of the peak loads required to reach the desired displacement during fatigue tests. The maximum applied load did not vary appreciably during the fatigue tests. This observation is consistent with the fact that the specimen did not experience any wire breaks. Wire breaks decrease the stiffness of the specimen because as wires break, both the tension and the moment of inertia decrease, requiring less load to reach the required displacement.

Figure 4-13 compares the initial and final static tests. The stiffness, determined by fitting a linear trendline through the data, changed by less than 5%,

from 4.1 k/in. initially to 3.9 k/in. after the completion of tests (Table 4-1). This small decrease in stiffness is most likely due to strand relaxation and further wedge seating during testing.

Another measure of the change in stiffness may be obtained from the free-vibration tests, which were performed before and after the fatigue tests. As wires break, the tension in the cable is reduced, thus reducing the natural frequency of the specimen. For Specimen 5, the initial natural frequency was 13.8 Hz and the final natural frequency was 13.5 Hz (Table 4-1), resulting in a difference of 2.2%. This decrease is most likely due to strand relaxation.

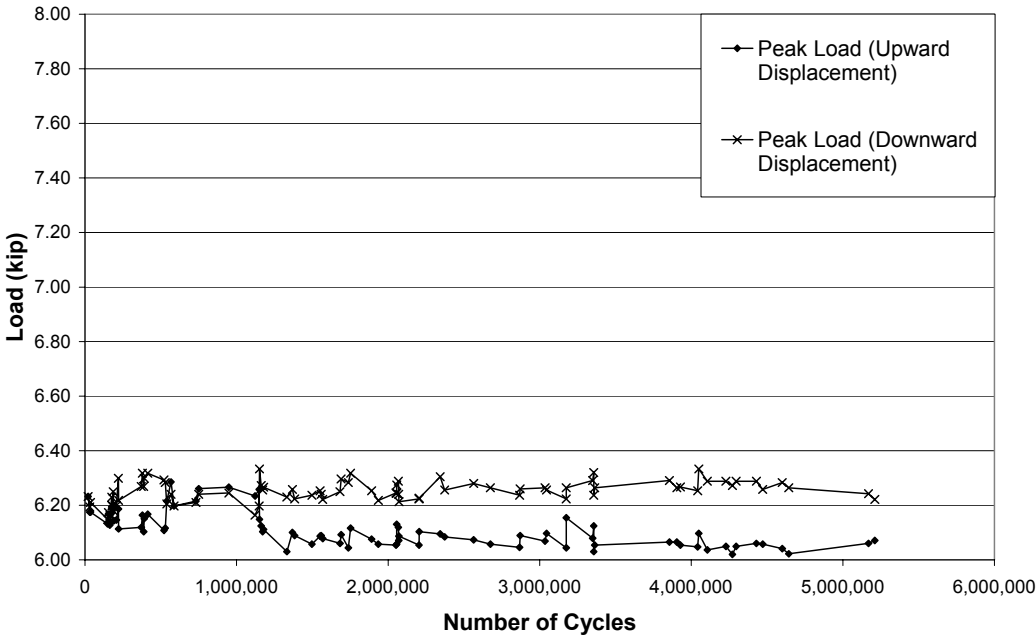


Figure 4-12: Peak loads during fatigue test - Specimen 5

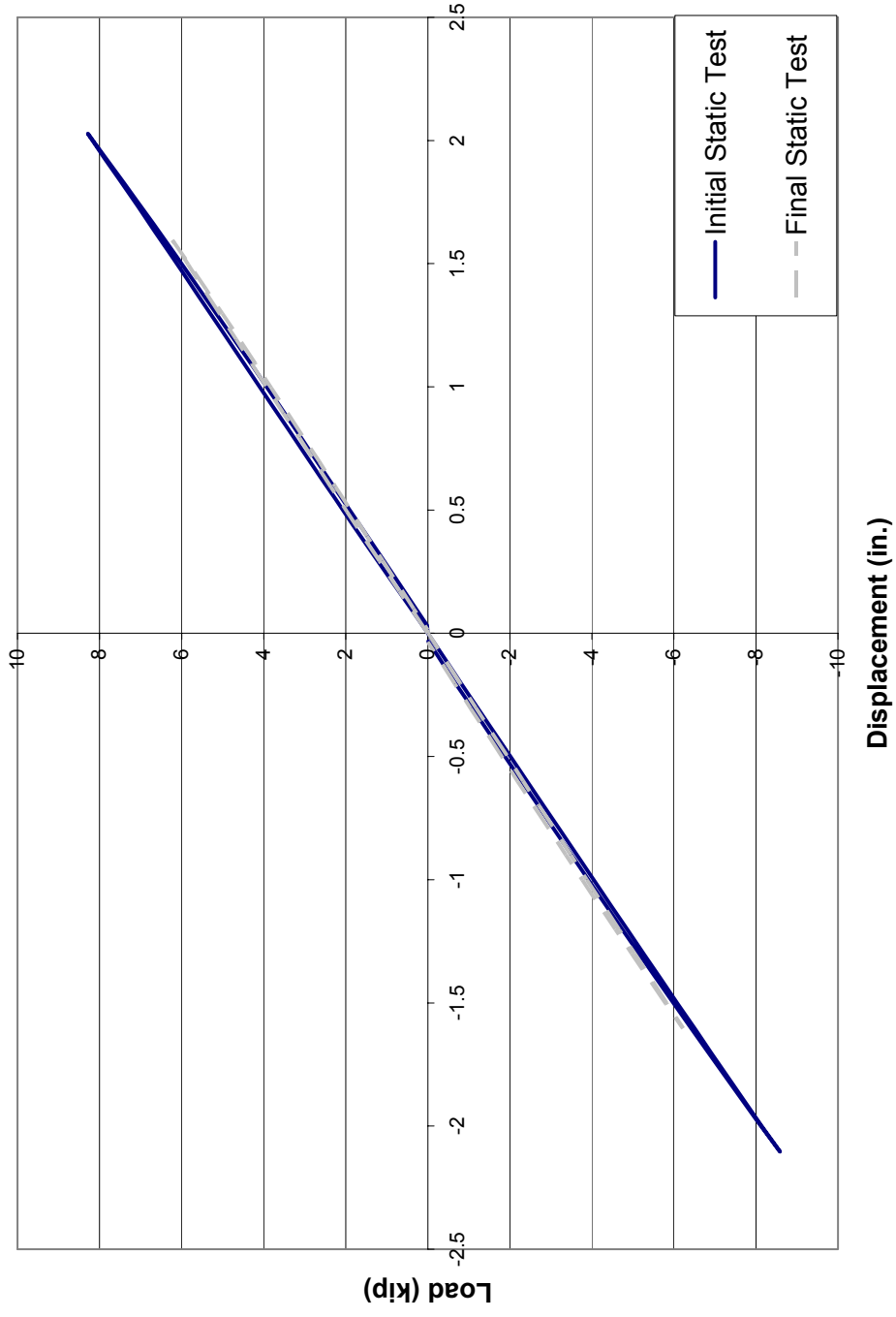


Figure 4-13: Load - displacement response from static tests - Specimen 5

4.2.1.5 Stress Range Near End of Stay

Because Specimen 5 was instrumented with eight strain gages, it was possible to calculate the stress range in the strand in the region near the anchor head. The strain gages were located near the anchor head on the deck end as described in Chapter 2. The gage length was 3 mm. The surface of the strand was prepared before applying the gages to ensure bond between the gage and the strand by removing the millscale from the surface of the steel and carefully cleaning the area with acetone.

Strain data were taken during each static test as well as periodically during the fatigue tests. Figure 4-14 presents the strain data from two gages taken during a static test. Gage 2 was on the top of Strand 1, 4.3 in. from the anchor head. Gage 8 was on the bottom of Strand 19, 3.8 in. from the anchor head. The strain was considered to be zero when the midspan displacement of the cable was zero. Positive strain values in Figure 4-14 represent an increase in tension and negative strain values represent a decrease in tension which occurs as the cable experiences bending stress near the anchor head. Due to the prestress, no strand in the specimen actually experiences compressive strain. Based on the maximum strain reported by any gage during the test, the section remains elastic throughout the test.

The measured strains did not vary linearly with the applied load. While the maximum positive and negative displacements at the midspan of the cable were the same, the amplitude of the maximum strain is greater than the amplitude of the minimum strain for both the top and bottom gages. This occurs because as the cable is displaced in either direction, the net tension on the cable increases. A change in cable tension is also caused by the bending effects due to the displacement. The interaction between these two phenomena is shown in

Equation 1.1. ΔT represents the change in tension due to elongation of the cable during loading, A is the cross-sectional area of the cable, M is the bending moment applied to the section, c is the distance from the neutral axis of the cross-section to the strain gage, and I is the moment of inertia of the section.

$$\sigma = \frac{\Delta T}{A} \pm \frac{Mc}{I} \quad (1.1)$$

There is also a discrepancy in the amplitude of the gages relative to each other. Because Gage 8 is farther from the anchor head than Gage 2, Gage 2 should experience higher strains. While this behavior is seen on the side of decreasing tension (negative strain), the strain values on the positive side (increasing tension) are nearly equal for the two gages. In addition to this, while the response of both gages appears to be linear as the strand tension increases (strain becomes more positive), the response becomes nonlinear as the strand tension decreases (strain becomes more negative). These trends were representative of all data taken.

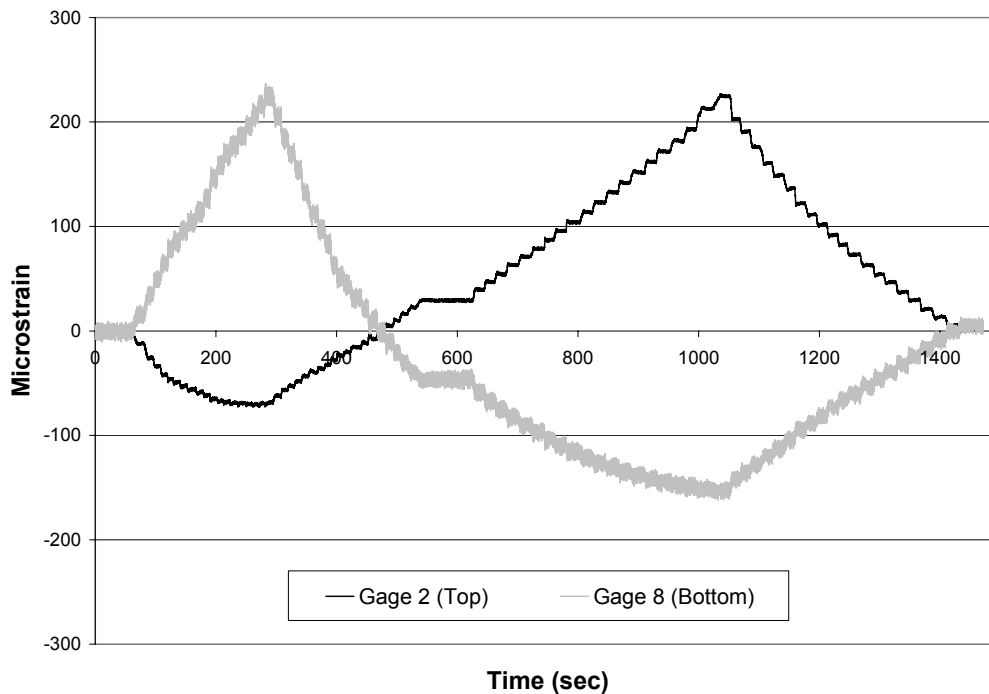
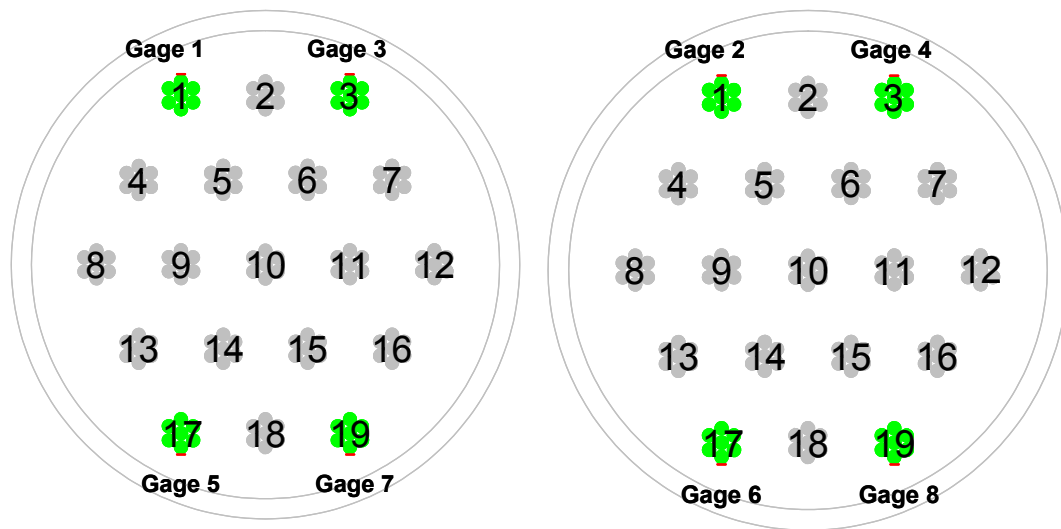


Figure 4-14: Strain data from static test - Specimen 5

Figure 4-16 shows the stress range calculated for each gage during the fatigue tests. The stress was calculated assuming linear-elastic behavior of the strand, with the stress directly proportional to the strain and an elastic modulus of $E = 28,900$ ksi. After an initial drop, the stress range recorded by each gage remains relatively constant. The gage nearest the anchor head on Strand 17 (Gage 5) stopped functioning early in the test, and the gage farthest from the anchor head on Strand 19 (Gage 8) provided intermittent data throughout the test.

After examining Figure 4-16, it appears that the stress range at the bottom of the cable (Gages 5-8) tends to be higher than that at the top (Gages 1-4). On any given strand, the gages farther away from the anchor head experience a lower stress range than those nearer the anchor head. The values presented are calculated based on the placement of the strain gages before stressing the cable

(Figure 4-15). Because the gages were applied to the surface of the strand before stressing the cable, the actual location of the gages was not known. Access to the anchor head region was blocked by the reaction frame. The cable was stressed from the tower end and the gages were placed at the deck end, thus they were farther from the anchor head during the fatigue tests than indicated by the initial measurements due to the elongation of the strands during stressing (although the difference in distance is estimated to be less than 0.05 in). In addition, the moment gradient in the region near the anchor head is very high (Eggers, 2003), thus the stresses near the actual face of the anchor head may be much higher than those estimated by strain gages over 2 in. away.



a) Gages nearest to the anchor head b) Gages farther from the anchor head

Figure 4-15: Location of strain gages

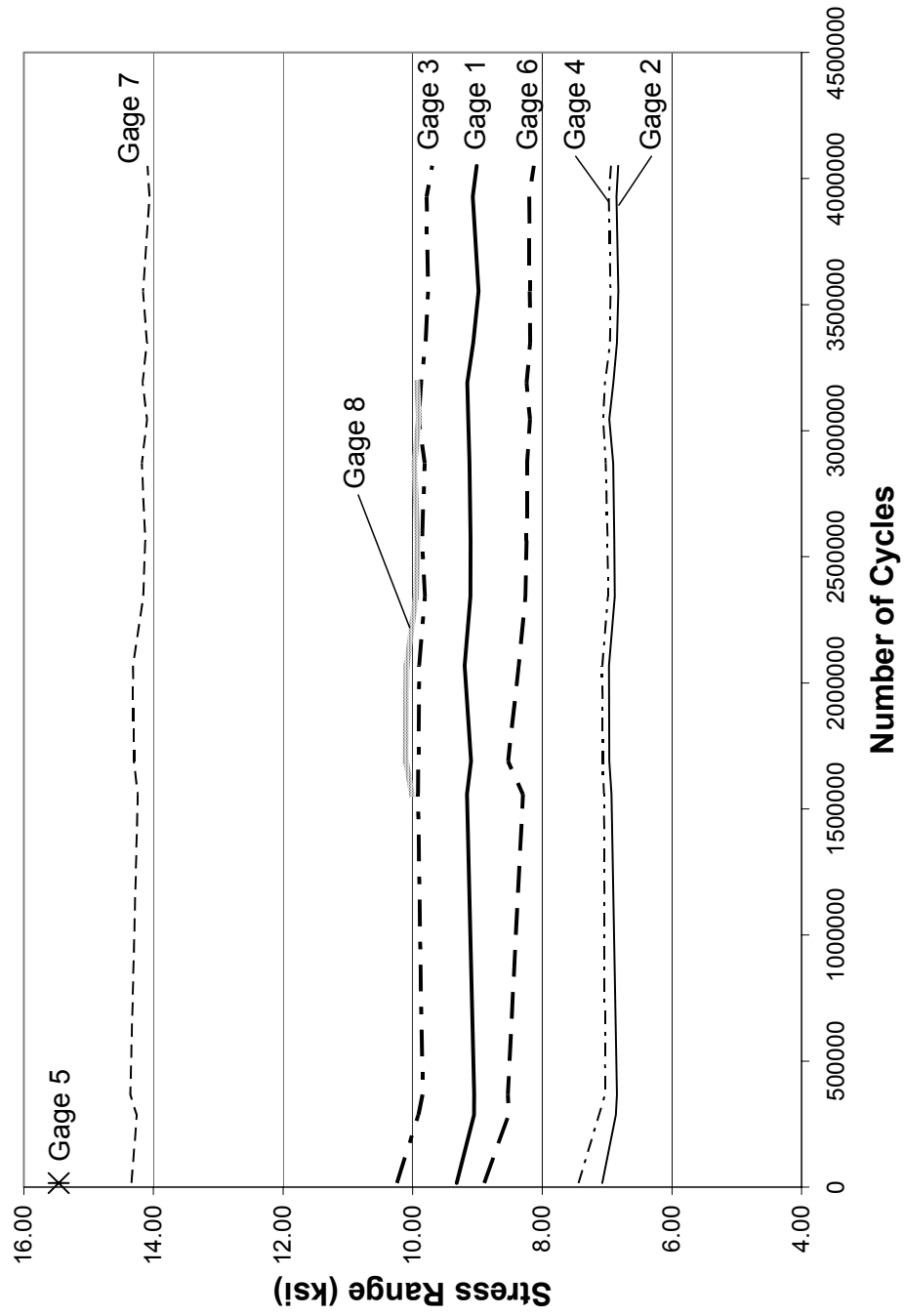


Figure 4-16: Estimated stress range during fatigue test near deck anchorage - Specimen 5

4.2.2 Specimen 6

Specimen 6 sustained 6,483,024 loading cycles. A total of 28 wire fractures were found in the stay; seventeen breaks occurred at the tower end and 11 breaks occurred at the center of the specimen under the load point. No breaks were found at the deck end. The specimen was grouted and the cross-section consisted of 13 strands. Specimen 6 was grouted from the deck end and stressed from the tower end. The cable displacement was ± 1.6 in. at midspan during the fatigue test.

4.2.2.1 Grout Condition

Figure 4-17 shows the grout condition upon opening the polyethylene pipe. At the deck anchorage, a large grout crack was observed on the bottom of the specimen near the ring formed in the grout due to the weld in the polyethylene transition pipe. Other than this large crack and several small (less than 0.25-in. diameter) air voids, no other visible grout damage was seen at the deck end.

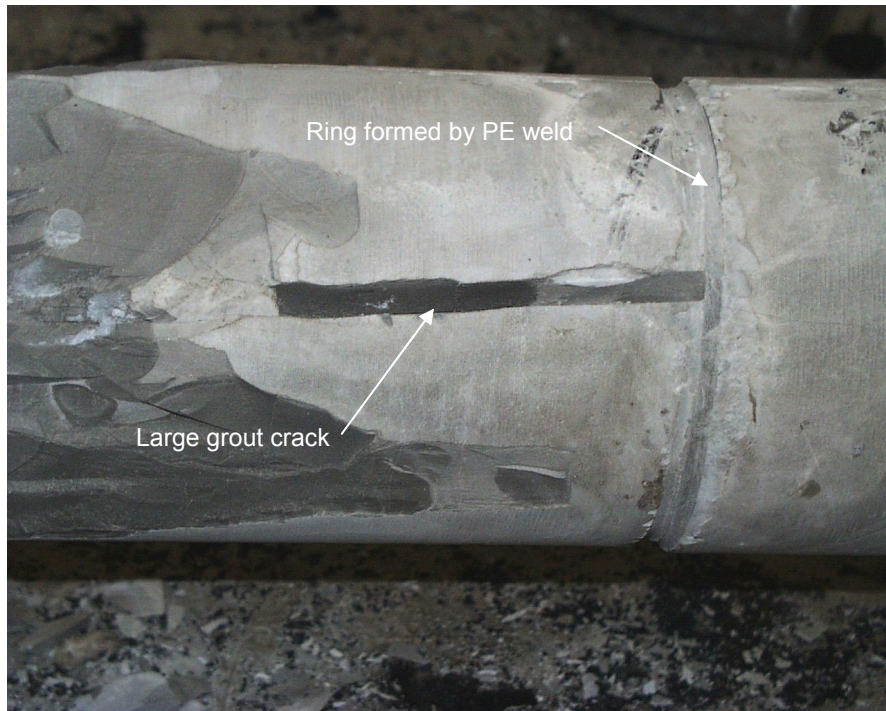


Figure 4-17: Large grout crack at deck anchorage - Specimen 6

At the tower end, large longitudinal cracks characteristic of areas where wire breaks were present immediately upon opening the stay. As the grout was exposed to the open air, parallel circumferential cracks began to form and pieces of grout began to fall away, exposing two strands as seen in Figure 4-18. Apart from the cracking, the grout had no visible imperfections and appeared to be homogenous.

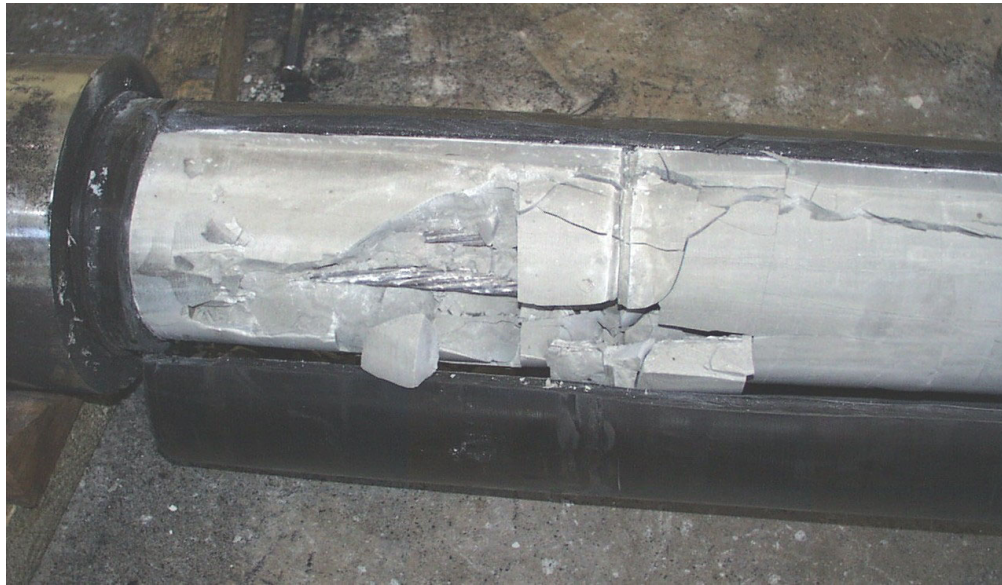


Figure 4-18: Grout cracking at tower end - Specimen 6

The grout in the portion of the cable under the ram during fatigue testing showed severe longitudinal cracks characteristic of regions near wire breaks as shown in Figure 4-19. Thin, parallel circumferential cracks can also be seen. As with the other portions of the stay, the cracking in the center portion of the specimen became more severe upon exposure to the air.

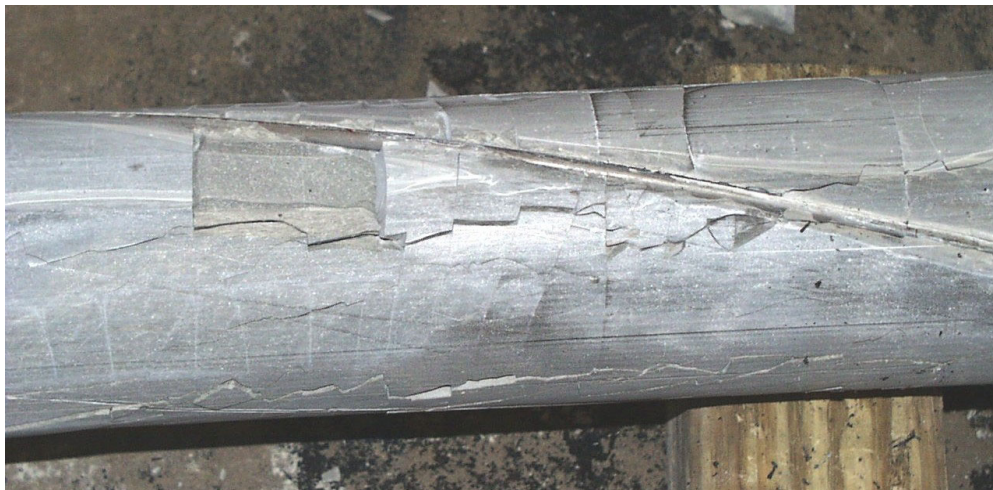


Figure 4-19: Grout cracking under the ram - Specimen 6

4.2.2.2 Corrosion

Specimen 6 was cured for 115 days after grouting and was then tested for 44 days.

Upon opening the specimen, corroded fretting product was observed near wire breaks. As wires fret against each other, microscopic particles of steel begin to rub off the wire surfaces. These particles have a very high surface area to volume ratio, thus corrode very easily to form an abrasive product that aggravates fretting (Frank, 2004). In most cases, this corroded fretting product was not evident on the exterior of the strand and could only be seen by taking apart the strand and inspecting the contact surfaces between wires. An example of corroded fretting product can be seen in Figure 4-20.

The abrasive nature of the corrosion product formed by fretting may initiate fatigue cracking or may be a product formed after a wire breaks. After one wire of a strand is fractured, the increased relative movement between the adjacent intact wires and the sharp fracture surface may increase the production of fretting product and surface abrasion, thus instigating further fatigue cracking.

In the case of Specimen 6, the evidence of fretting near the wire breaks at the tower anchor head was more severe than the evidence of fretting found elsewhere. In some places, corrosion was evident on the exterior of the strand and was accompanied by a white substance that coated the strand, shown in Figure 4-21. In this region, corrosion was also seen on the grout surface at the interface between the grout and the strand (Figure 4-22).



Figure 4-20: Corroded fretting product on Strand 19 – Specimen 6



Figure 4-21: Corrosion on Strand 19 near tower anchor head - Specimen 6



Figure 4-22: Corrosion product on grout from tower end - Specimen 6

4.2.2.3 Location of Wire Breaks

A total of 28 wire breaks occurred during the fatigue test; all 28 were reported by Soundprint. Table 4-2 shows the distribution of wire breaks along the cable. Both the actual autopsy data and the Soundprint data are reported.

Table 4-2: Wire break distribution on Specimen 6

	Tower	Center	Deck	Total
Autopsy	17	11	0	28
Soundprint	17	11	0	28

Figure 4-23 shows the cycle at which each wire broke based on the Soundprint data. The first break at the tower end occurred at 612,000 cycles and the first break under the loading point occurred at 3,835,000 cycles. The breaks occurred with as few as 6,200 cycles between consecutive breaks. The small number of cycles between some breaks may indicate the last few wires on a strand breaking due to the increased relative movement between broken and unbroken wires, which increases the fretting effects.

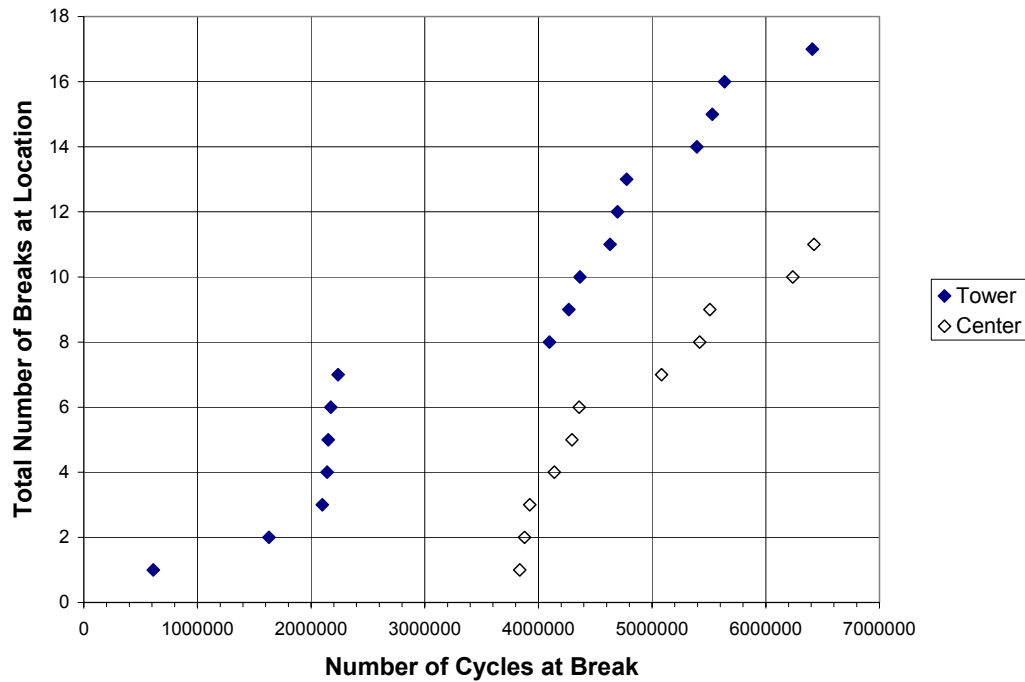


Figure 4-23: Wire breaks based on Soundprint data - Specimen 6

Figure 4-24 shows the location in the cross-section of each wire break near the tower anchorage. The 17 wire breaks occurred on four strands (1, 4, 17, and 19), most of which are located on the top and bottom of the specimen cross-section. Assuming a composite section and a linear variation of strain, the strands at the top and bottom of the cross section would experience the highest stress range during the bending fatigue test.

Figure 4-25 also shows the longitudinal location of wire breaks near the tower anchorage. Nearly all breaks at the tower end of the specimen occurred within 2 in. of the front face of the anchor head in the region of the smooth end sleeve. Examples of breaks occurring in this region are shown in Figure 4-26 and Figure 4-27. The only breaks which did not occur in this region were found inside the anchor head.

Two wires broke inside the anchor head at the contact point between the strand and the wedge. At the wedge, the fatigue of the strand due to bending stress is accelerated by the first tooth of the wedge which creates a localized stress concentration.

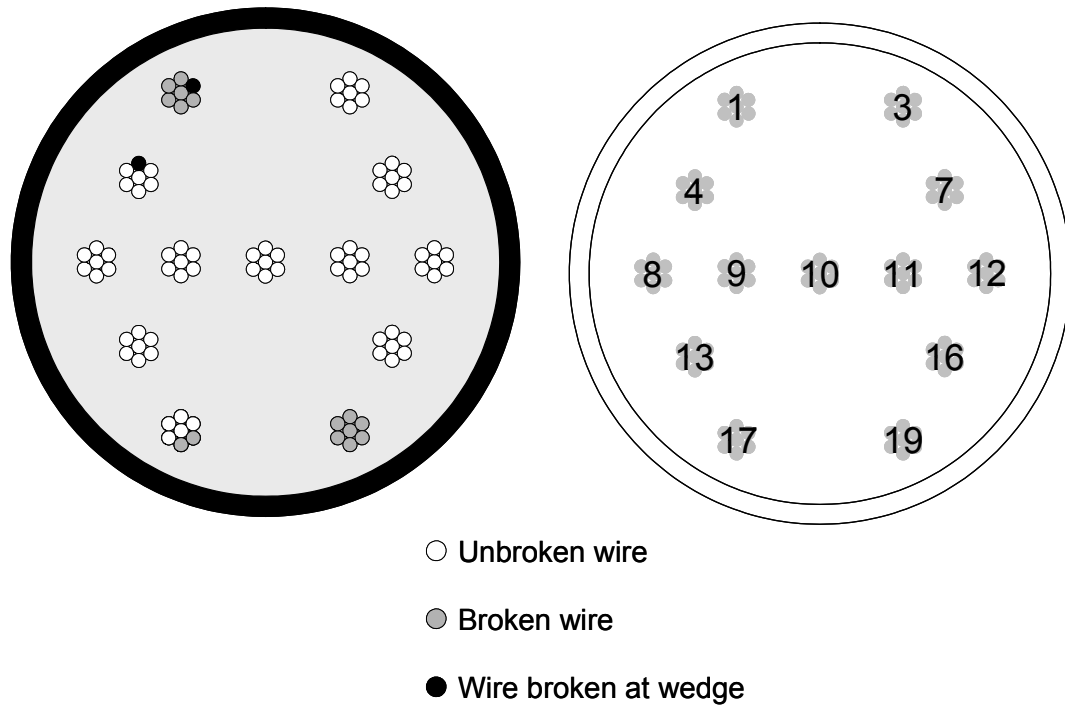


Figure 4-24: Wire breaks at the tower end - Specimen 6

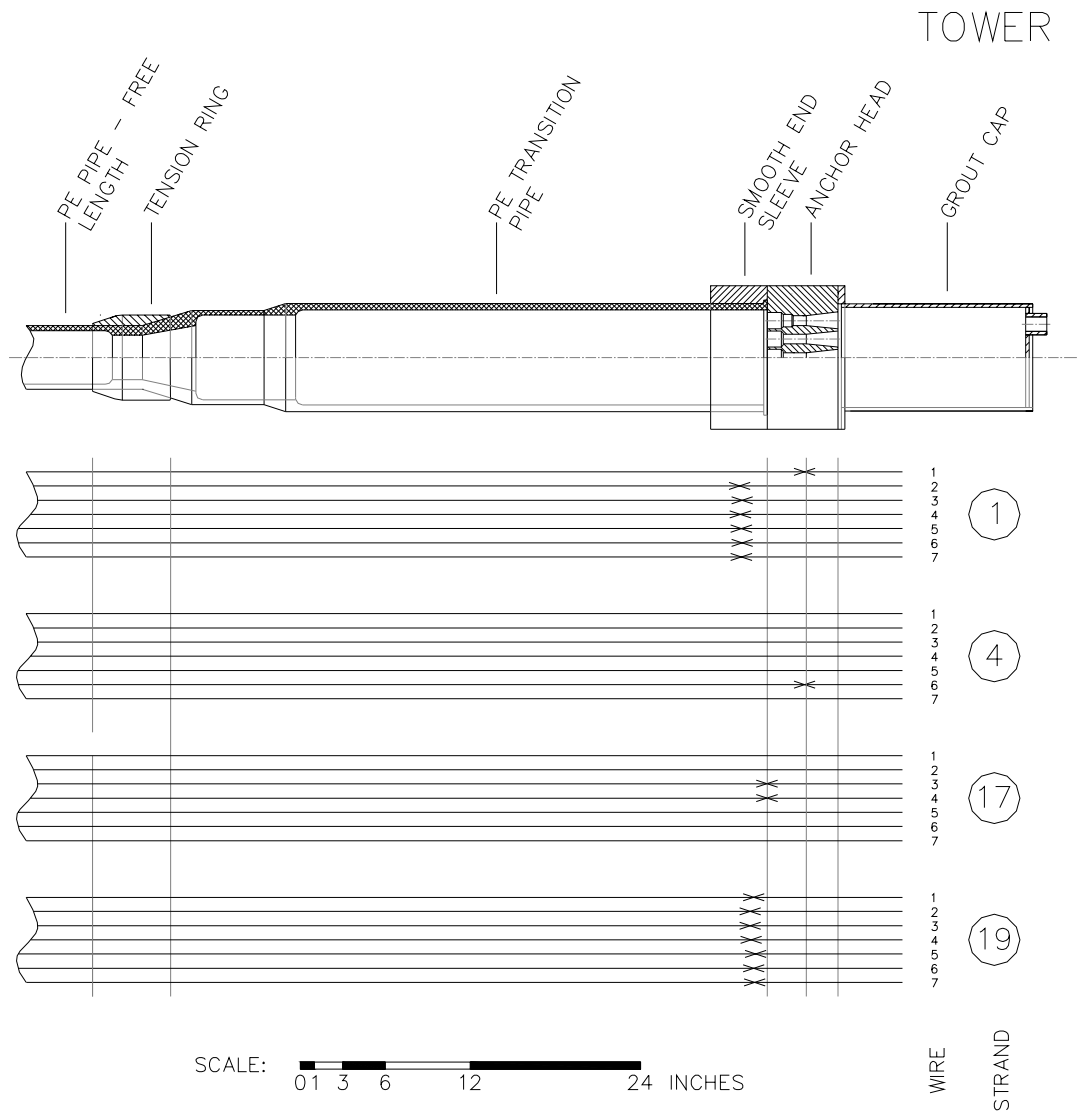


Figure 4-25: Location of wire breaks near tower anchorage of Specimen 6



Figure 4-26: Wire breaks on strand 1 near the tower anchor head - Specimen 6



Figure 4-27: Wire breaks on strand 17 at the face of the tower anchor head - Specimen 6

Figure 4-28 shows the location in the cross-section of each break that occurred under the load point. These wire breaks occurred on strands 16, 17, and 19 which are all on the bottom of the section at or near the extreme fiber of the cross section.

Figure 4-29 shows the location of wire breaks near the load point relative to the loading apparatus. All breaks occurred just outside the tapered polyethylene cushioning pipe.

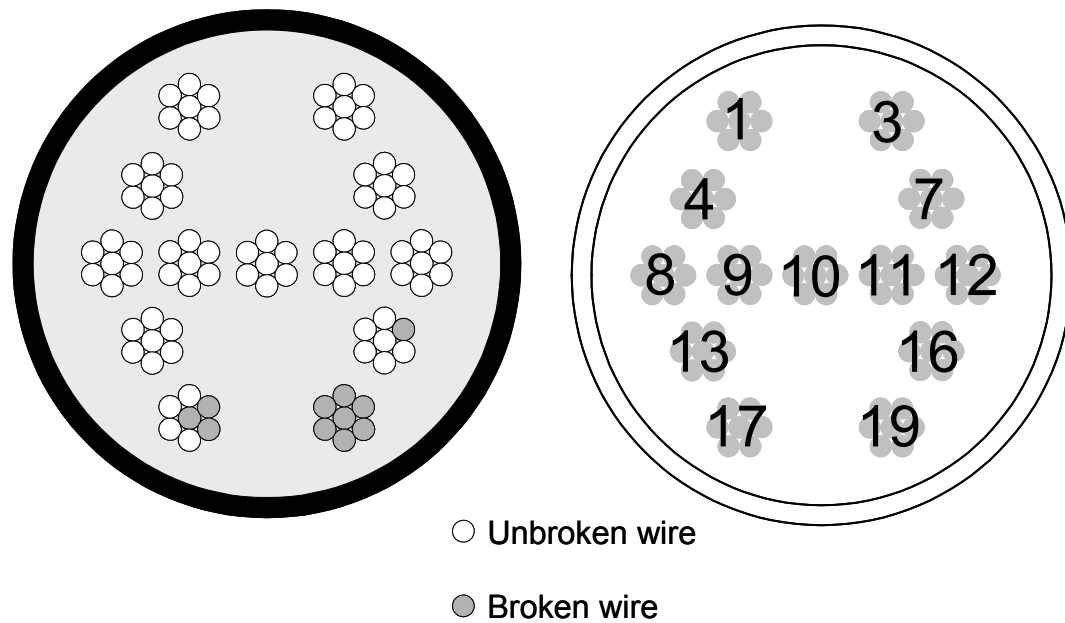


Figure 4-28: Wire breaks under the load point - Specimen 6

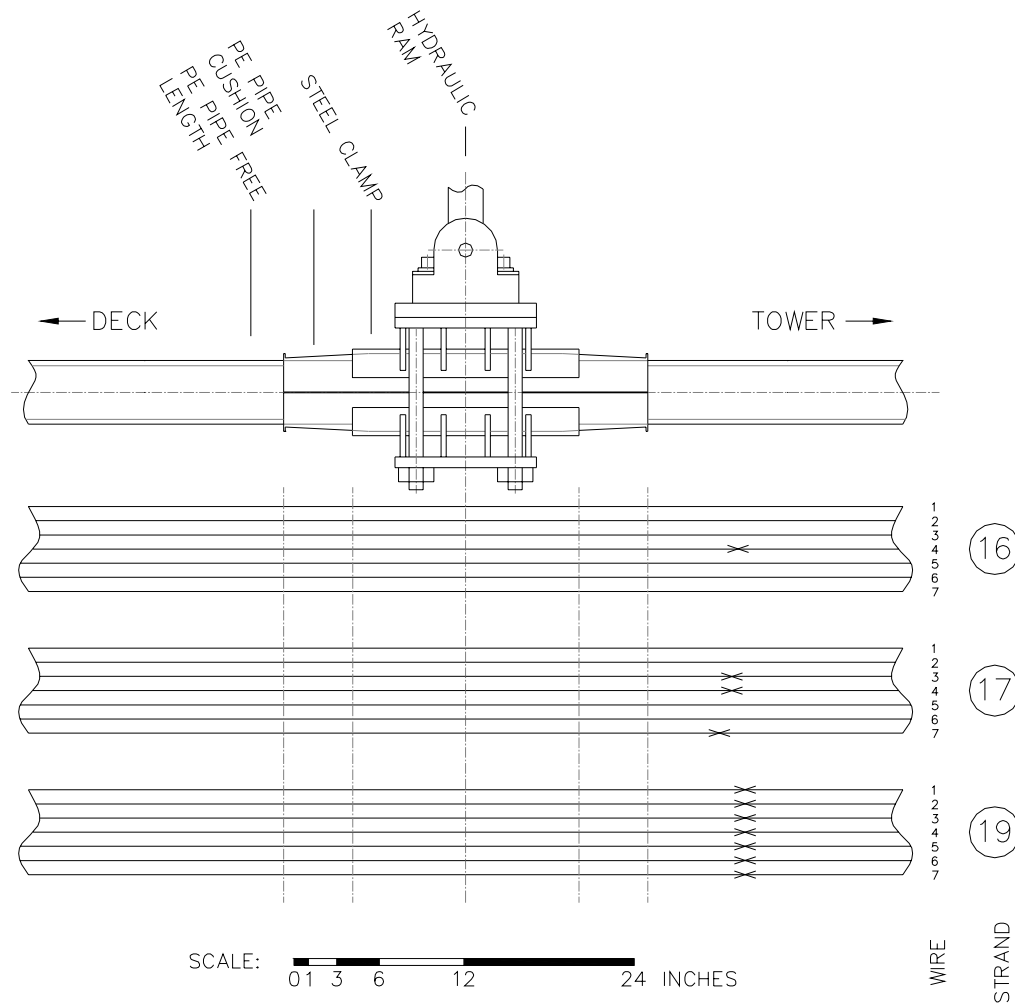


Figure 4-29: Location of wire breaks under load point - Specimen 6

4.2.2.4 Characteristics of Wire Breaks

The relative occurrences of the four fretting fatigue mechanisms discussed in Section 4.1.2 are shown in Figure 4-30 and Figure 4-31. For Specimen 6, fretting between wires of the same strand led to 89% of the wire breaks in the

specimen. Figure 4-30 shows that the dominant mode of failure at the tower end was due to fretting between the center wire and outer wires. At the center of the specimen, equal numbers of breaks were attributed to fretting between adjacent outer and fretting between an outer wire and the inner wire. Considering all wire breaks, fretting between the center and outer wires was the dominant failure mode as shown in Figure 4-31.

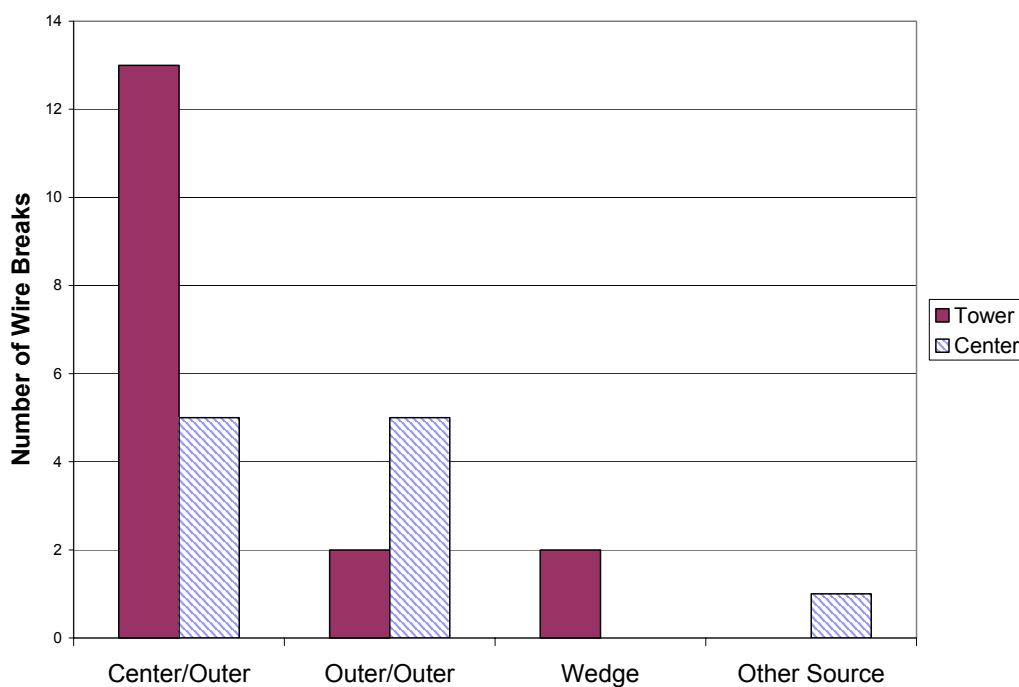


Figure 4-30: Observed fretting fatigue mechanisms – Specimen 6

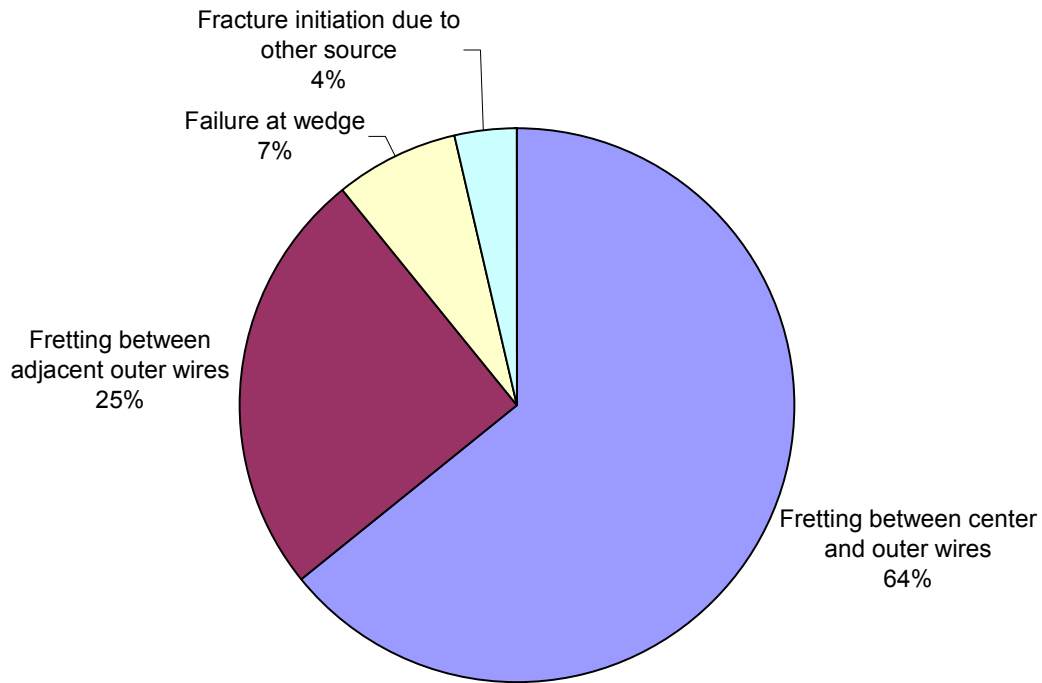


Figure 4-31: Distribution of fretting fatigue mechanisms - Specimen 6

4.2.2.5 Lateral Stiffness

The lateral stiffness of the test specimen was monitored throughout the test by recording the load required to reach the desired displacement on a daily basis. Figure 4-32 shows the peak loads required to reach the desired displacement of ± 1.6 in. during the fatigue tests. The vertical lines on this plot represent each wire break as reported by Soundprint. The plot shows that between wire breaks, the stiffness stays fairly constant. As wire breaks occur, the stiffness is reduced because the tension and the moment of inertia of the specimen decrease. While a single wire break does not cause a large decrease in stiffness, the stiffness drops more dramatically as multiple wire breaks occur on the

specimen. The overall decrease in load was 8%, from approximately 5.0 kip initially to approximately 4.6 kip at the end of the test.

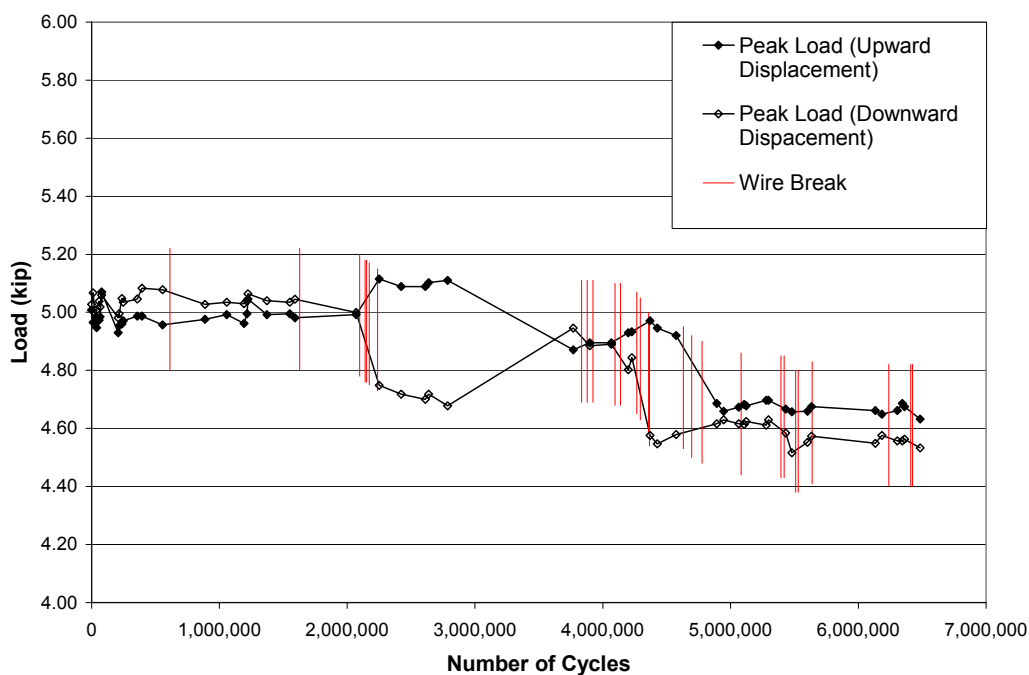


Figure 4-32: Peak loads during fatigue tests - Specimen 6

Figure 4-33 shows the measured load-displacement response from the initial and final static tests. The stiffness, determined by fitting a linear trendline through the data, decreased by 9% from 3.3 k/in. initially to 3.0 k/in. at the end of the test. These data are consistent with the stiffness decrease observed from the load data taken during fatigue testing.

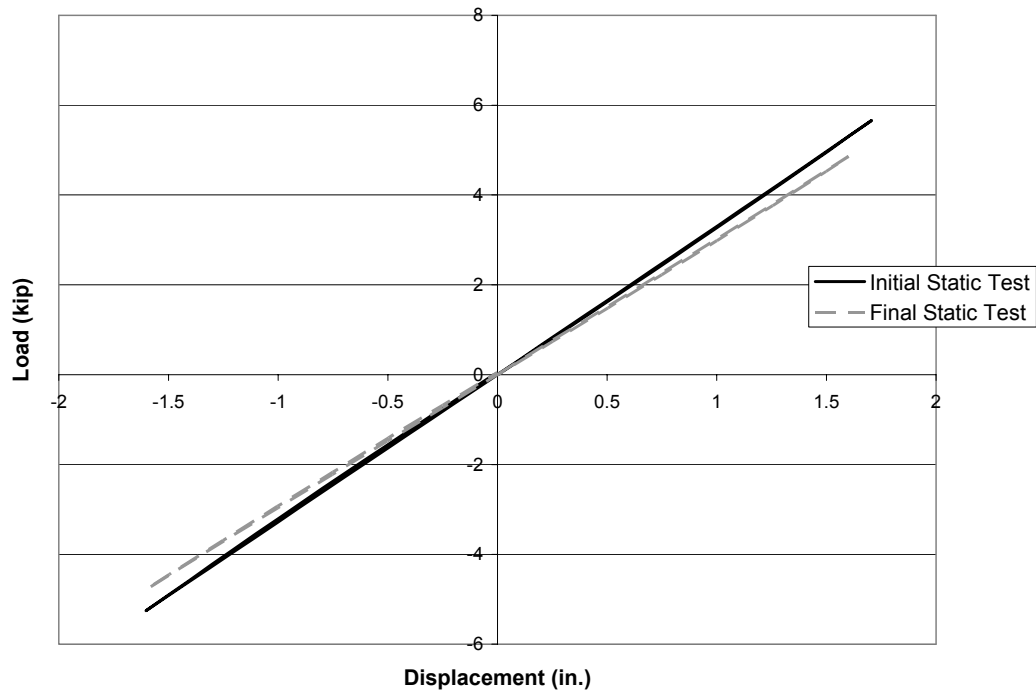


Figure 4-33: Load – displacement response from static tests - Specimen 6

Another measure of the change in stiffness is the natural frequency, which is determined from free-vibration tests performed before and after the fatigue tests. The natural frequency of the specimen decreased 4.3% due to wire breaks, which reduce the tension in the stay. The initial frequency was 11.5 Hz and the final natural frequency was 11.0 Hz (Table 4-1).

4.2.3 Specimen 7

Specimen 7 sustained 2,246,869 loading cycles and 117 wire breaks were found. Thirty-seven breaks were found at the tower end, 65 were found in the center under the load point, and 17 were found at the deck end. The specimen was nominally identical to Specimen 2, but was constructed with Strand B; it was grouted and the cross-section consisted of 19 strands. It was grouted from the

deck end and stressed from the tower end. The cable displacement was ± 1.6 in. at midspan during the fatigue test.

4.2.3.1 Grout Condition

Several air voids, approximately $\frac{1}{2}$ in. in diameter, were found after exposing the grout at the tower end of the stay, as shown in Figure 4-34. Longitudinal cracks indicative of wire breaks were also observed. Figure 4-34 also shows the ring-shaped deformity in the grout caused by the weld in the polyethylene transition pipe.



Figure 4-34: Grout condition at tower end - Specimen 7

The grout at the deck end appeared homogeneous with no significant air voids. Some circumferential cracks, most likely due to bending stress, were observed (Figure 4-35). Despite the presence of wire breaks in the region, the grout appeared to be in good condition immediately upon opening the specimen

(Figure 4-35). However, after being exposed to the open air, the grout cracked violently as observed when opening Specimen 6. This cracking is due to a loss of confinement which occurs when the PE pipe is removed. The condition of the stay after this cracking is shown in Figure 4-36.

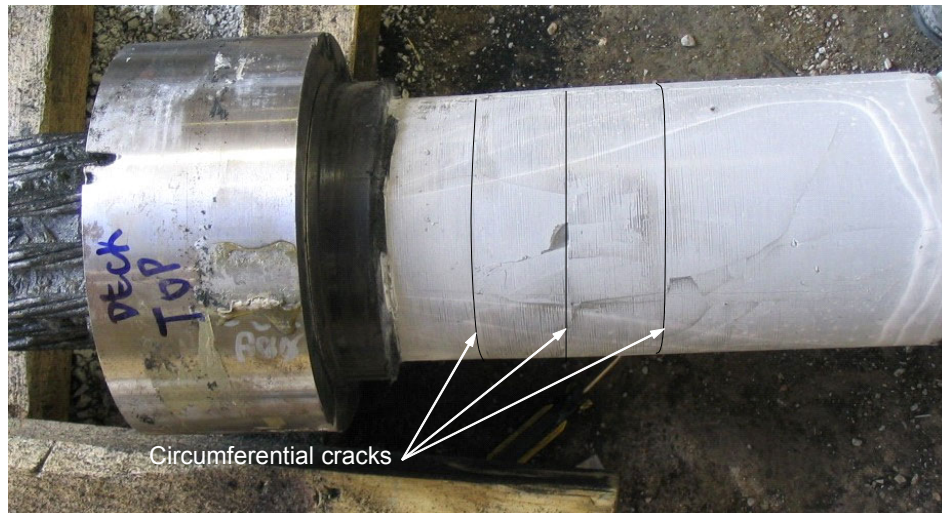


Figure 4-35: Grout condition at deck anchor head immediately after removing polyethylene pipe - Specimen 7



Figure 4-36: Condition of grout at deck anchor head several minutes after removing polyethylene pipe - Specimen 7

Grout in the section of the cable under the ram during the fatigue tests was severely damaged immediately upon opening the specimen, as shown in Figure 4-37. No further cracking was observed after removing the PE pipe, most likely due to the high level of damage already sustained by the grout. Some evidence could be seen of circumferential cracks.



Figure 4-37: Grout condition under load point - Specimen 7

4.2.3.2 Corrosion

Specimen 7 was cured for 21 days after grouting and was then tested for 14 days.

Most of the corrosion and corroded fretting product found upon opening the specimen was near wire breaks. Figure 4-38 shows a typical example of the corroded fretting product found in these areas.



Figure 4-38: Corrosion found near anchorage on strand 18 - Specimen 7

In the region at the center of the stay, a thick white substance was found near most wire breaks as well as at several isolated points away from wire breaks in addition to some spots of corrosion which were not related to fretting product (Figure 4-40). In addition to the white substance found, red-orange corroded fretting product was typically found between the strands on which wire breaks occurred. The corroded fretting product was not visible on the exterior of the strand.



Figure 4-39: White substance on strand 17 at midspan - Specimen 7



Figure 4-40: Corrosion on strand 17 at midspan - Specimen 7

4.2.3.3 Location of Wire Breaks

A total of 119 wire breaks occurred during fatigue testing of Specimen 7. The distribution of wire breaks along the cable based on both the autopsy data and the Soundprint data is shown in Table 4-3.

Table 4-3: Wire break distribution on Specimen 7

	Tower	Center	Deck	Total
Autopsy	37	65	17	119
Soundprint	36	62	16	114

Figure 4-41 shows the cycle at which each wire break occurred based on the Soundprint data. The first wire break at the tower end occurred after 667,300 cycles, the first wire break at the deck end occurred after 1,122,300 cycles, and the first wire break at the center (under the load point) occurred after 894,200 cycles.

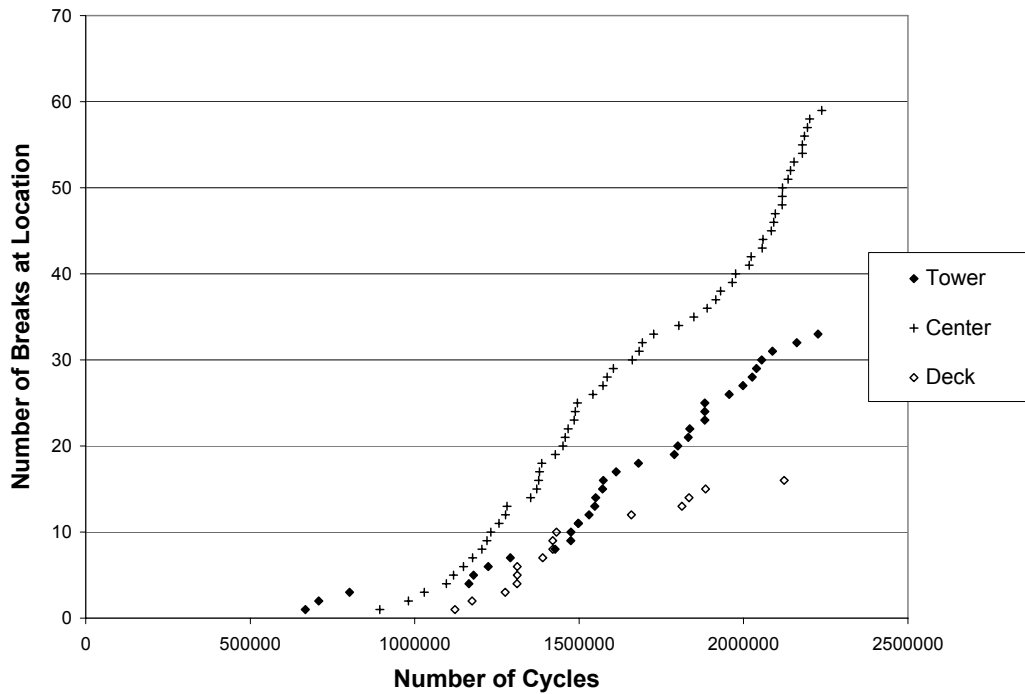


Figure 4-41: Wire breaks based on Soundprint data – Specimen 7

Figure 4-42 shows the location in the cross section of each wire break near the tower anchorage. The 37 breaks occurred on six strands (1, 2, 3, 17, 18, and 19), which are the strands farthest from the neutral axis of the composite cross section. One wire on strand 17 broke in two places approximately 2 in. apart. Four wire breaks occurred at the wedges.

Figure 4-43 shows the longitudinal location of each wire break near the tower anchorage. A majority of the breaks occurred within 9 in. from the face of the anchor head. Wire breaks on Specimen 7 occurred as far as 16 in. from the face of the anchor head, well outside the region of high moment calculated by Eggers (2003).

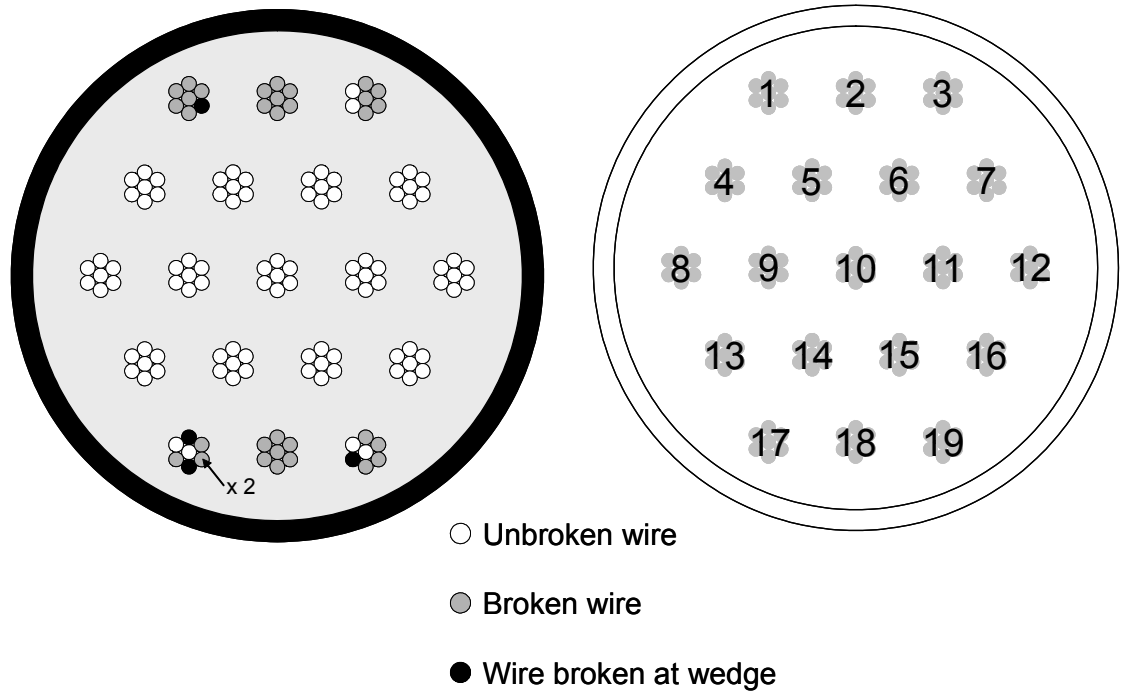


Figure 4-42: Wire breaks at tower anchorage - Specimen 7

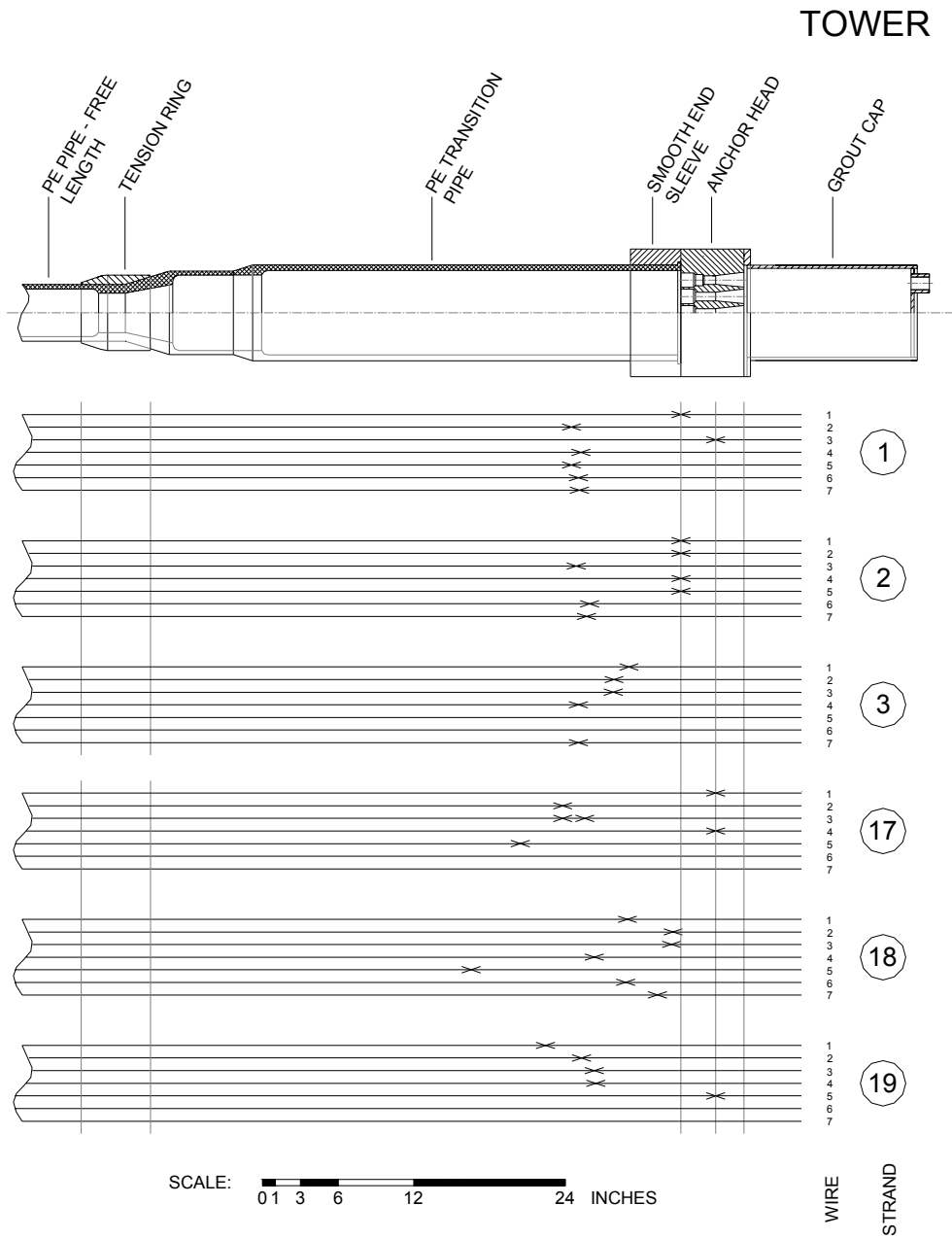


Figure 4-43: Location of wire breaks near the tower anchorage - Specimen 7

Figure 4-44 shows the location in the cross section of each wire break near the deck anchorage. The 17 breaks occurred on 5 strands (1, 3, 17, 18, and 19), which are the strands farthest from the neutral axis of the composite cross section. One break occurred at the wedge.

Figure 4-45 shows the longitudinal location of each wire break near the deck anchorage. Most of the wire breaks occurred within 4 in. of the anchor head or inside the anchor head, either at the face of the polyethylene bushing used to cushion the strand or at the face of the wedge. One wire on strand 18 broke approximately 14 in. from the face of the anchor head, but no other wire breaks occurred in this area. The wire breaks on strand 1 all occurred within 5 in. of the stiffness transition at the face of the smooth end sleeve.

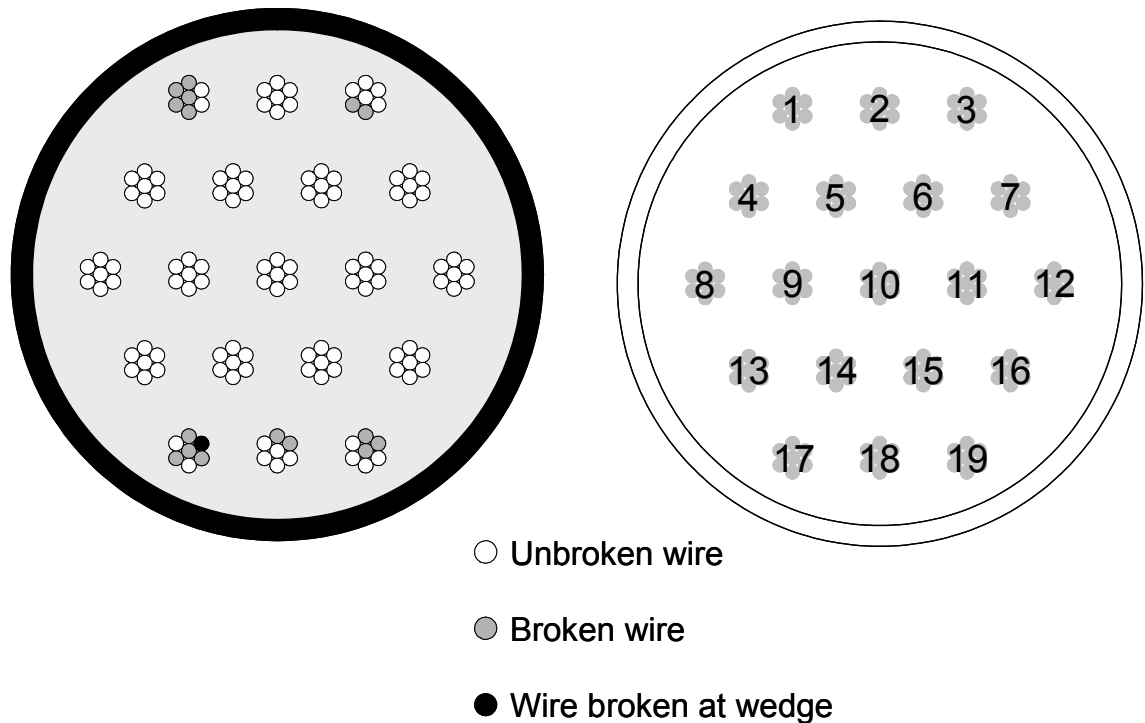


Figure 4-44: Wire breaks at the deck anchorage - Specimen 7

DECK

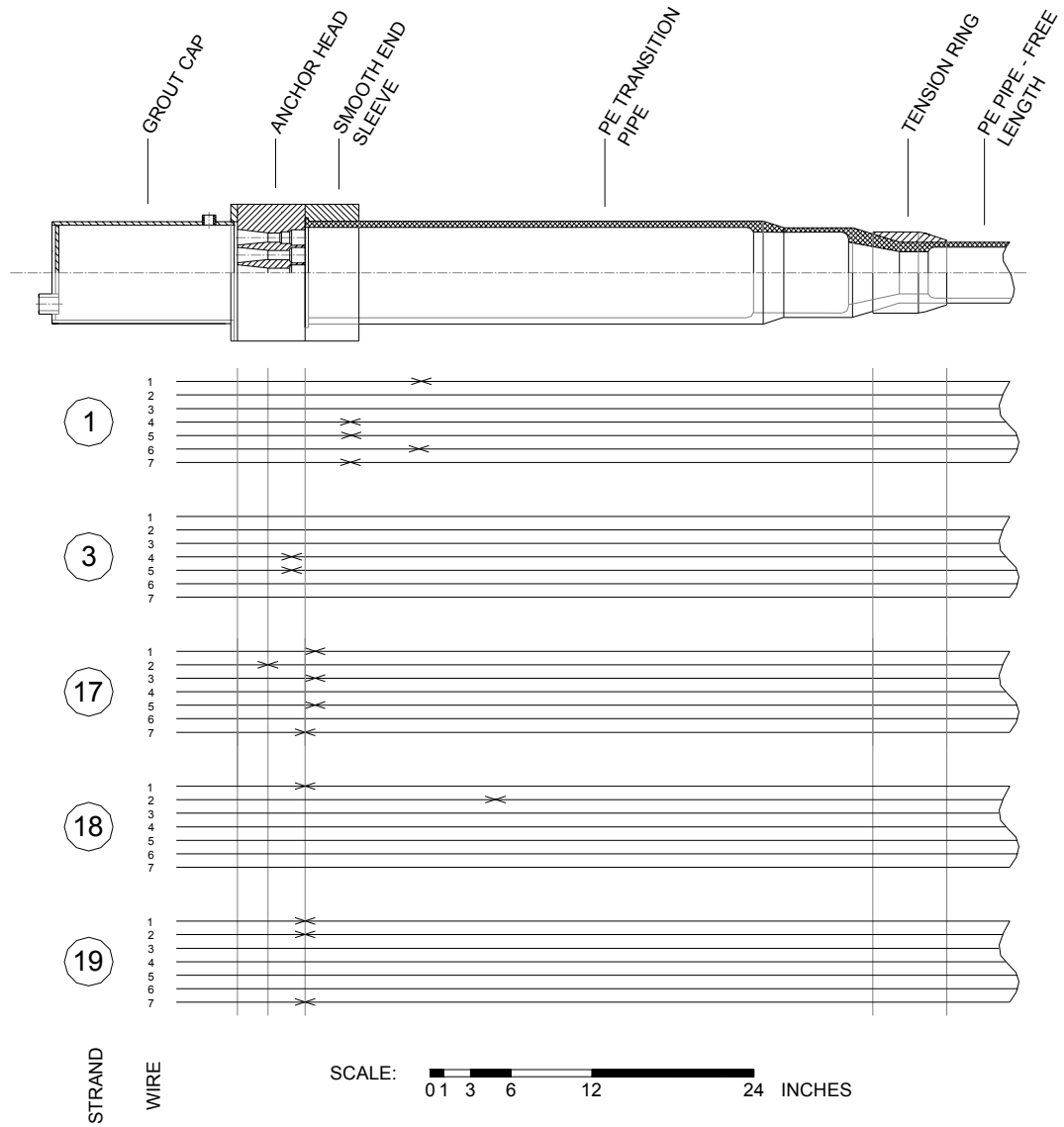


Figure 4-45: Location of breaks near the deck anchorage - Specimen 7

Figure 4-46 shows the location in the cross section of each wire break under the load point. Sixty-five percent of the wire breaks at midspan occurred

on the outer strands (1, 2, 3, 17, 18, and 19). The wires also exhibited a tendency to break near the bottom of the specimen, with 66% of the breaks occurring below the neutral axis of the cross section.

Figure 4-47 and Figure 4-48 show the longitudinal location of each wire break relative to the loading apparatus. The breaks tend to be centered around the edge of the load plate where the clamp is bolted to the cable and favored the tower side of the clamp. High stresses are found in this area due to the high localized curvature of the cable caused by the sudden change of stiffness of the loading apparatus.

The center wire on strand 2 fractured in three places; two breaks were found near the edge of the load plate on the tower side, and one break was located at the edge of the steel clamp on the deck side of the load point.

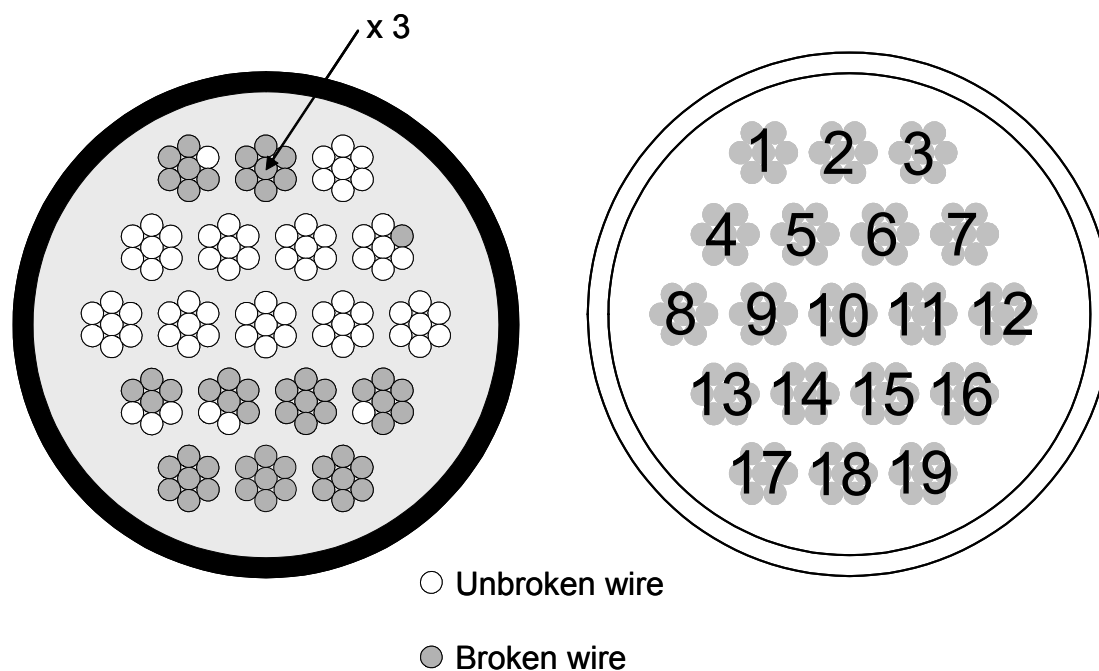


Figure 4-46: Wire breaks under the load point - Specimen 7

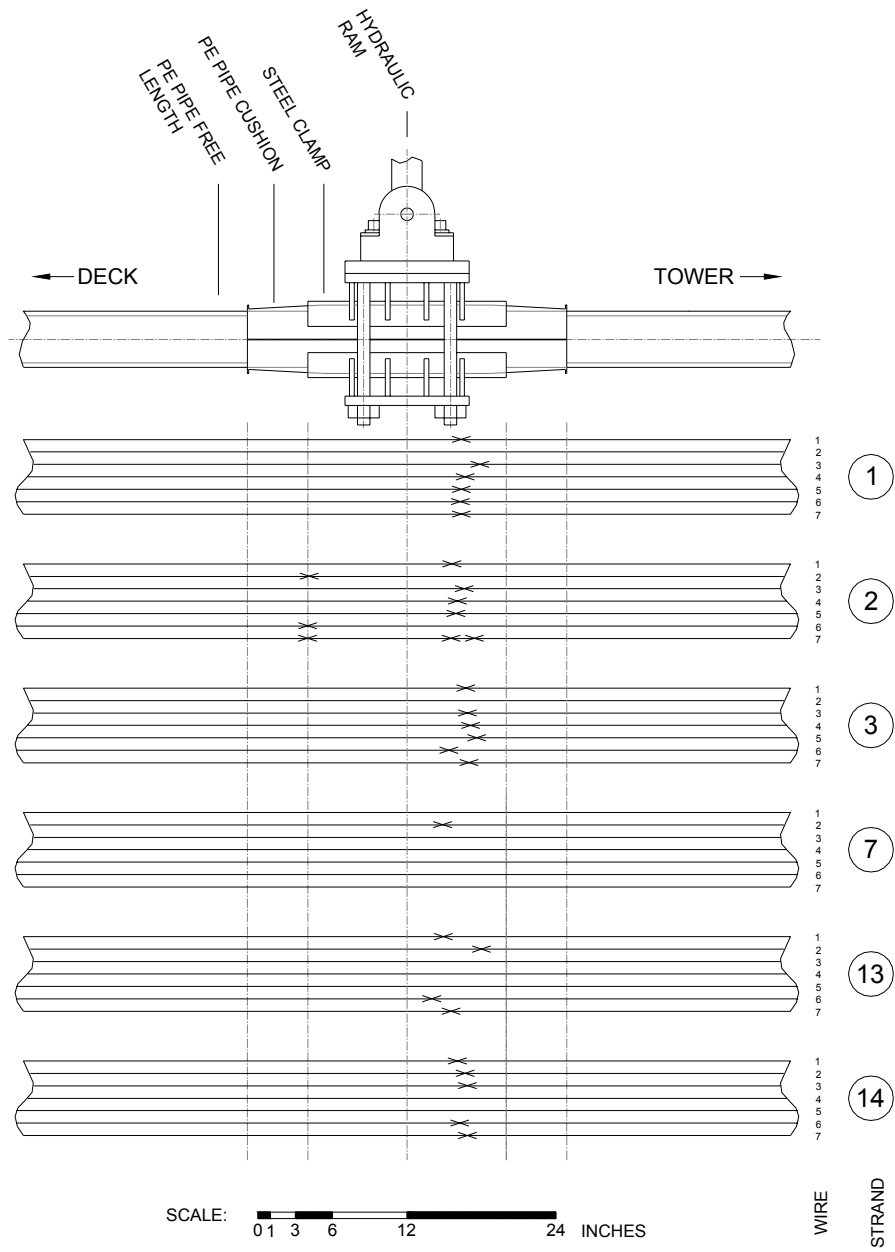


Figure 4-47: Location of wire breaks under the load point - Specimen 7

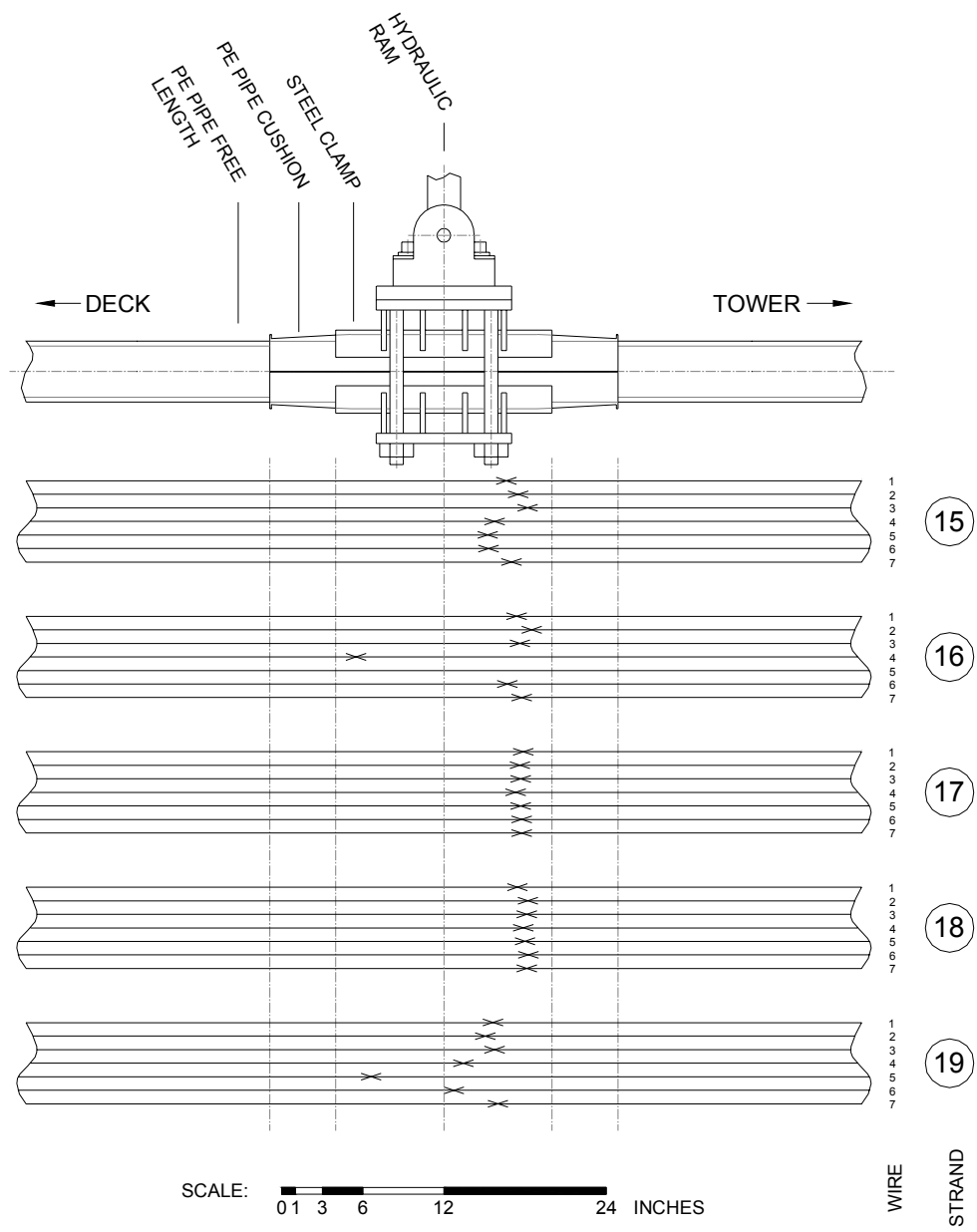


Figure 4-48: Location of wire breaks under the load point - Specimen 7

4.2.3.4 Wire Break Characteristics

Ninety-one percent of all wire breaks found in Specimen 7 were caused by fretting between the wires of a strand (Figure 4-49). No failures were found due to fretting along the free length. In addition to fretting fatigue failures, several wire breaks on Specimen 7 were not caused by fatigue. These non-fatigue failures are direct tension failures that most likely occurred because the wire was the last wire of the strand to break, leaving one wire to carry almost seven times the tension an intact strand would carry.

The relative occurrences of each failure type at different locations along the stay are represented in Figure 4-50. The distribution of failure mechanisms for the specimen as a whole is presented in Figure 4-49. Fretting between adjacent outer wires led to 49% of all wire breaks found in the stay. However, the dominant failure mechanism at midspan is not the same as the dominant failure mechanism near the anchorages. Near the anchorages, fatigue fractures due to fretting between adjacent outer wires were the most common failure mechanism, constituting 62% of the wire breaks at the tower end and 70% of the wire breaks at the deck end. Under the load point, the opposite is true; fretting between the center wire and an outer wire was the cause of over 56% of the wire breaks.

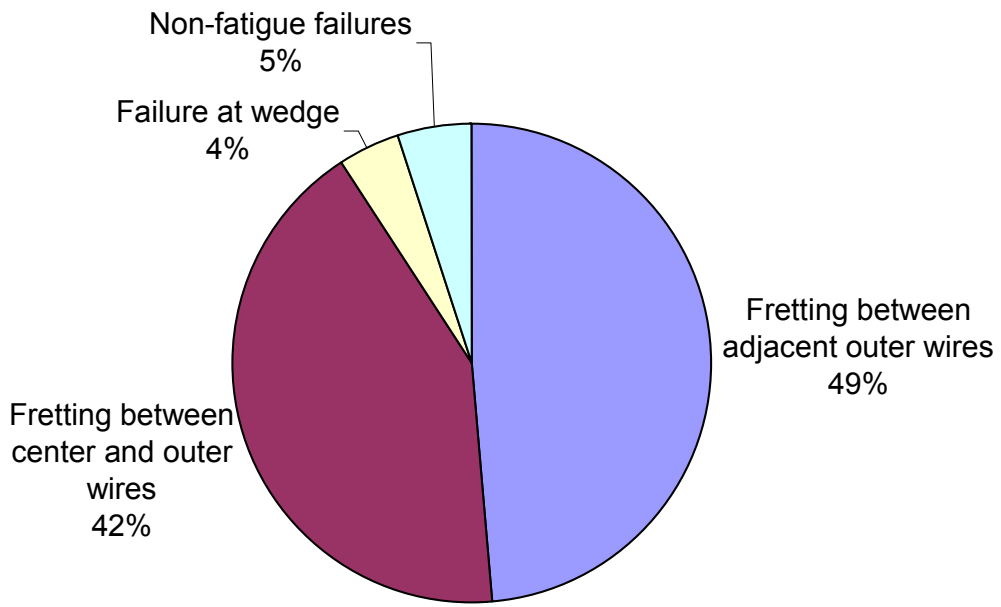


Figure 4-49: Distribution of failure mechanisms - Specimen 7

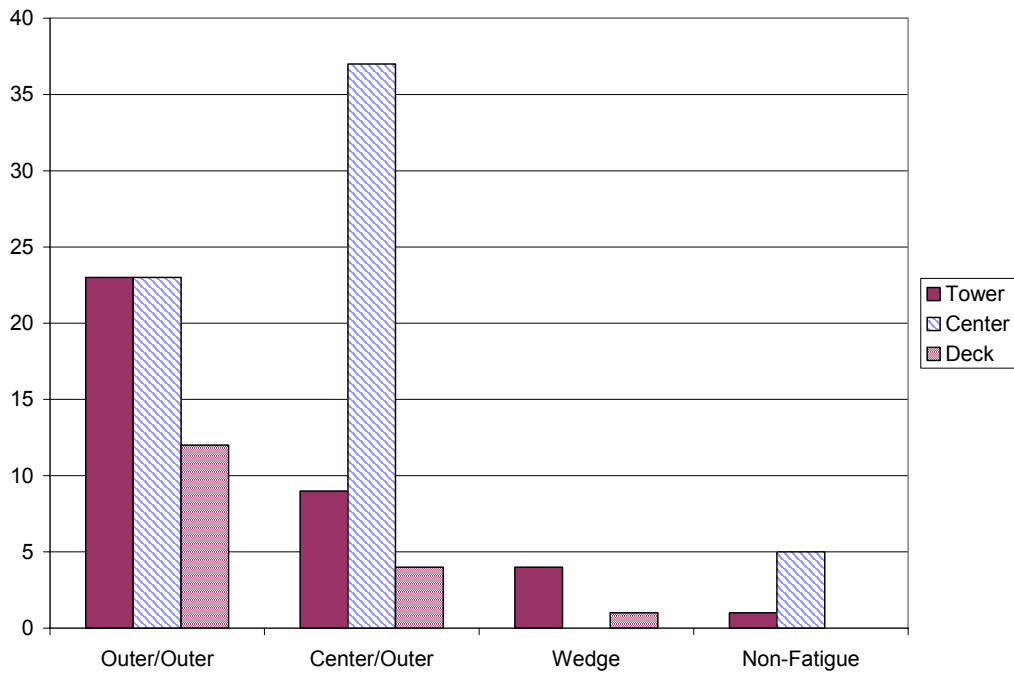
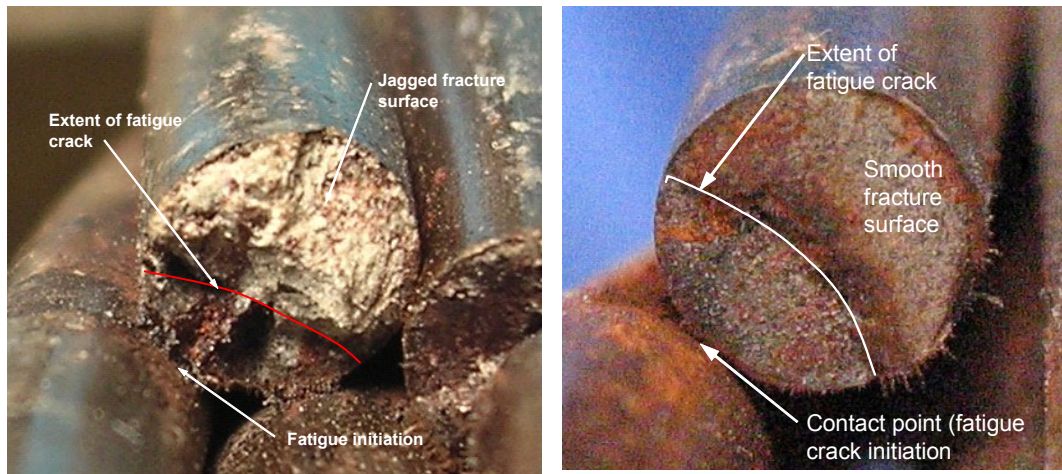


Figure 4-50: Observed fretting fatigue mechanisms - Specimen 7

In the case of multiple wire breaks on the same wire, inspection of the fracture surfaces of the wire breaks can be used to determine the order in which the breaks occurred. When a fatigue crack forms and grows, the gross area of the wire is reduced until the wire fails in tension. Such a tension failure is typically characterized by a rough, jagged fracture surface. After the release of tension in the wire, other fatigue cracks may continue to grow. However, when the wire fractures again at the site of another crack (possibly due to small tensile forces still being carried by the wire transmitted through the grout or other wires) the nominal tensile force on the wire allows a smooth fracture surface. This can be seen by observing the two fracture surfaces on strand 2 at the tower anchorage as seen in Figure 4-51 (the tension failure of Figure 4-51(a) is somewhat obscured by grout remaining on the fracture surface).



(a) First fracture to occur on the wire (b) Subsequent fracture on same wire

Figure 4-51: Multiple wire breaks on the same wire

4.2.3.5 Lateral Stiffness

The lateral stiffness of Specimen 7 was monitored throughout the fatigue test by daily recording the load required to reach the desired displacement of ± 1.6 in. Figure 4-52 shows the peak loads during the fatigue tests of the specimen. The vertical lines on this plot represent each wire break occurrence as reported by Soundprint. The stiffness remains relatively constant through the first several wire breaks. However, as wire breaks began to occur more frequently, the stiffness decreased dramatically. The average load decreased 12%, from approximately 7.6 kip to approximately 6.5 kip over the course of testing.

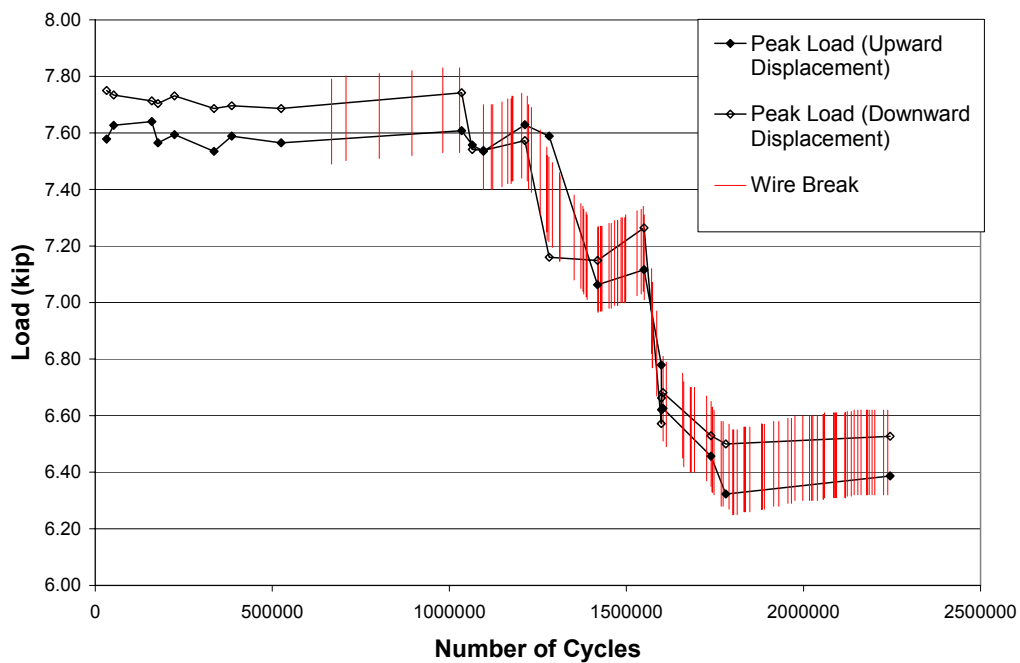


Figure 4-52: Peak loads during fatigue tests - Specimen 7

A comparison between the initial and final static tests is shown in Figure 4-53. The stiffness decreased by 32% (from 5.0 kip/in. to 3.4 kip/in.). This indicates an approximate static stiffness reduction of 0.3 k/in. per wire break.

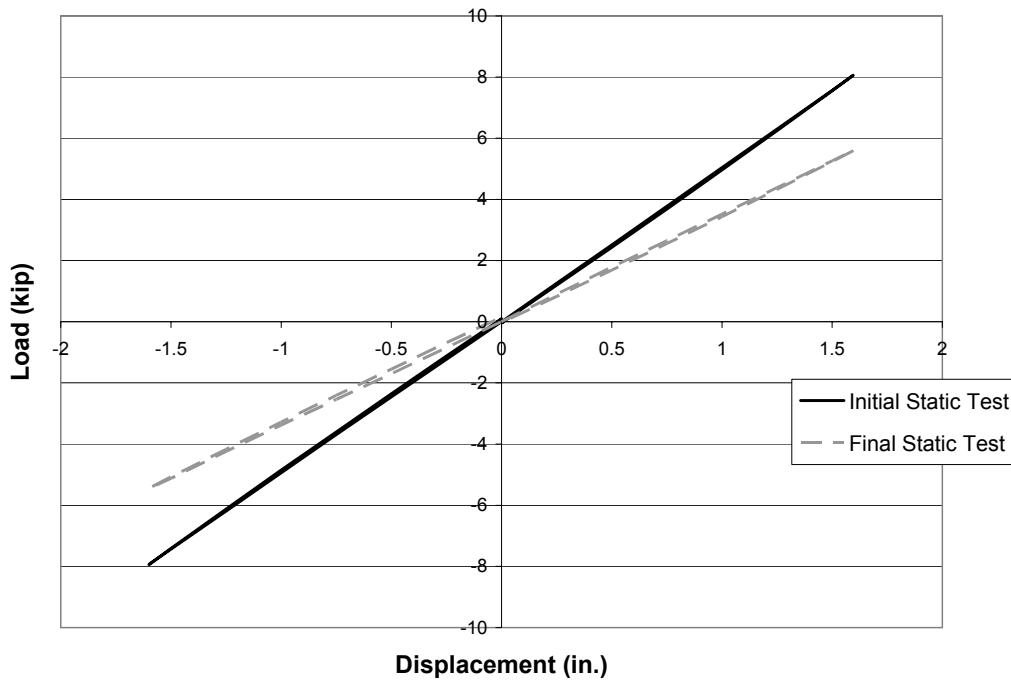


Figure 4-53: Load - displacement response from static tests - Specimen 7

Another measure of the lateral stiffness of the cable stay specimen is the natural frequency which is determined by a free-vibration test. The initial natural frequency of the specimen was 13.3 Hz and the final natural frequency was 11.1 Hz (Table 4-1), a 16% difference. This decrease in stiffness is due to the decrease in axial tension caused by the wire breaks as well as the decreased moment of inertia caused by both the wire breaks and the cracked grout.

4.2.4 Specimen 8

Specimen 8 sustained 6,200,593 loading cycles and four wire breaks. Two wire breaks were found at the tower end and two wire breaks were found at the deck end. The specimen was ungrouted, stressed from the tower end, and the cross-section consisted of 19 strands. The cable displacement was ± 1.6 in. at midspan during the fatigue test.

4.2.4.1 Grout Condition

The only portion of Specimen 8 that was grouted was a 3-ft section at the center. The grout had no appreciable voids apart from a small defect at the site of the grouting vent hole and appeared to be homogeneous. Longitudinal cracks were found along the entire length of the grouted section, as well as circumferential cracks which were found primarily near the PVC end caps as seen in Figure 4-54. The grout cracking was more severe near the ends of the section.

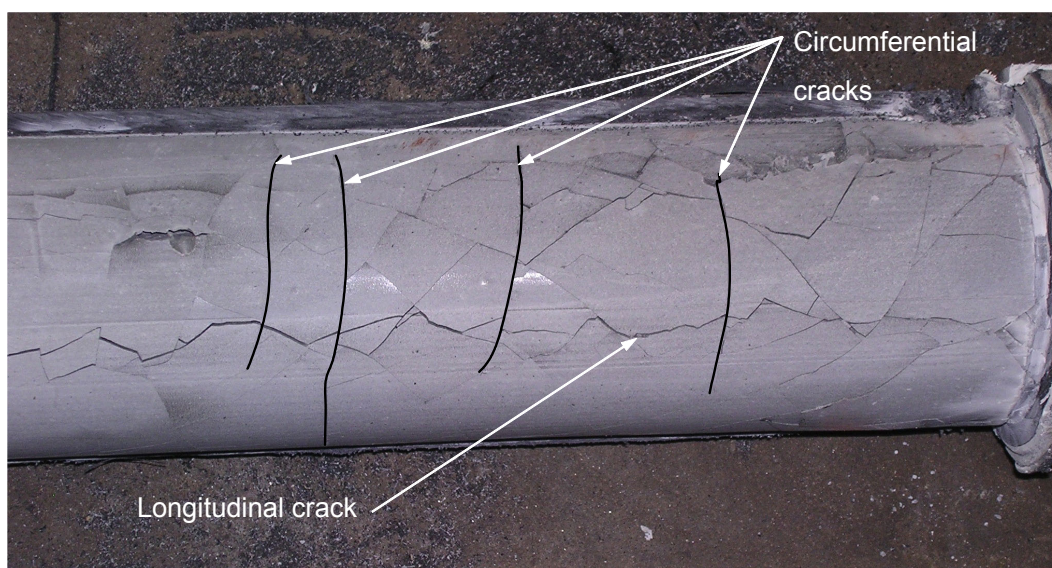


Figure 4-54: Grout condition at center of Specimen 8

4.2.4.2 Corrosion

Specimen 8 was cured for 12 days after grouting the center portion and was then tested for 62 days.

Corroded fretting product between the strands at the tension ring was observed on both the tower and the deck ends after less than 1,000,000 cycles. Fretting was more severe at the deck end due to a misalignment of the strands. Although the strands were not crossed, an interior strand (11) was caught between

strands 7 and 12, creating an extra strand on the exterior of the strand pattern at the tension ring (Figure 4-55). This misalignment was observed between the PVC end cap and the tension ring on the deck end of the cable; the strands on the tower end stayed in alignment. Wear of the wires at the contact point due to the fretting was observed upon opening the cable (Figure 4-56).

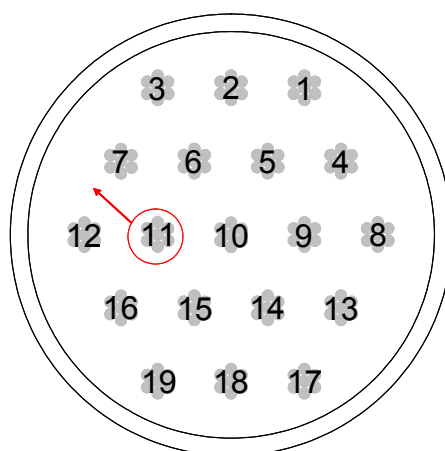
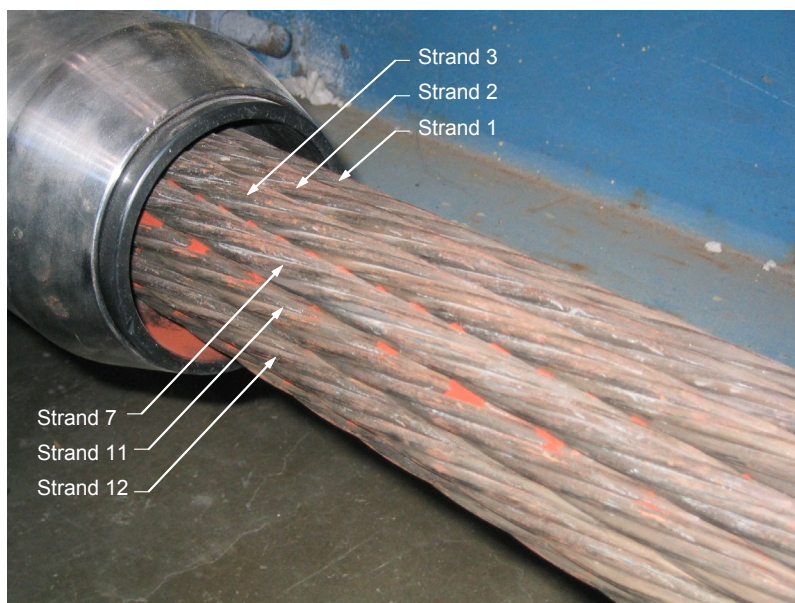


Figure 4-55: Evidence of fretting fatigue at deck tension ring – Specimen 8



Figure 4-56: Wearing of the strands due to fretting - Specimen 8

Near the tension ring, the friction due to the contact between the strands caused a noticeable temperature increase. The temperature difference between the tension ring and the free length of the cable, measured using a Type-K thermocouple, was 20°F at the deck end and 18°F at the tower end.

Severe corrosion was also found at the interface between the strand and the silicone caulk used in the PVC end caps of the grouted section as seen in Figure 4-57, although this corrosion did not appear to impair the performance of the stay.



Figure 4-57: Corrosion at interface between strand and caulk - Specimen 8

4.2.4.3 Location of Wire Breaks

Four wire breaks occurred on Specimen 8 during the fatigue tests. The distribution of wire breaks is presented in Table 4-4.

Table 4-4: Wire break distribution on Specimen 8

	Tower	Center	Deck	Total
Autopsy	2	0	2	4
Soundprint	2	0	2	4

Figure 4-58 shows the cycle at which each wire break occurred based on Soundprint data. The first wire break occurred after 300,000 cycles at the tower anchorage. The first wire break at the deck anchorage occurred after 1,308,000 cycles.

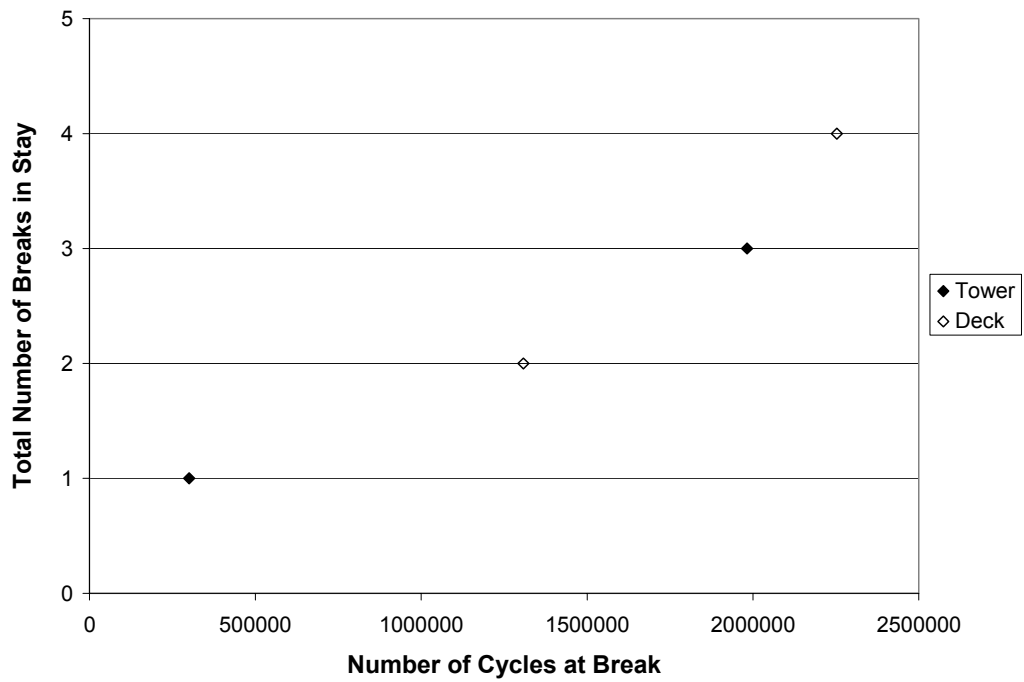


Figure 4-58: Wire breaks based on Soundprint data - Specimen 8

Figure 4-59 shows the location in the cross section of each wire break at the tower anchorage. The breaks occurred on strands 1 and 9.

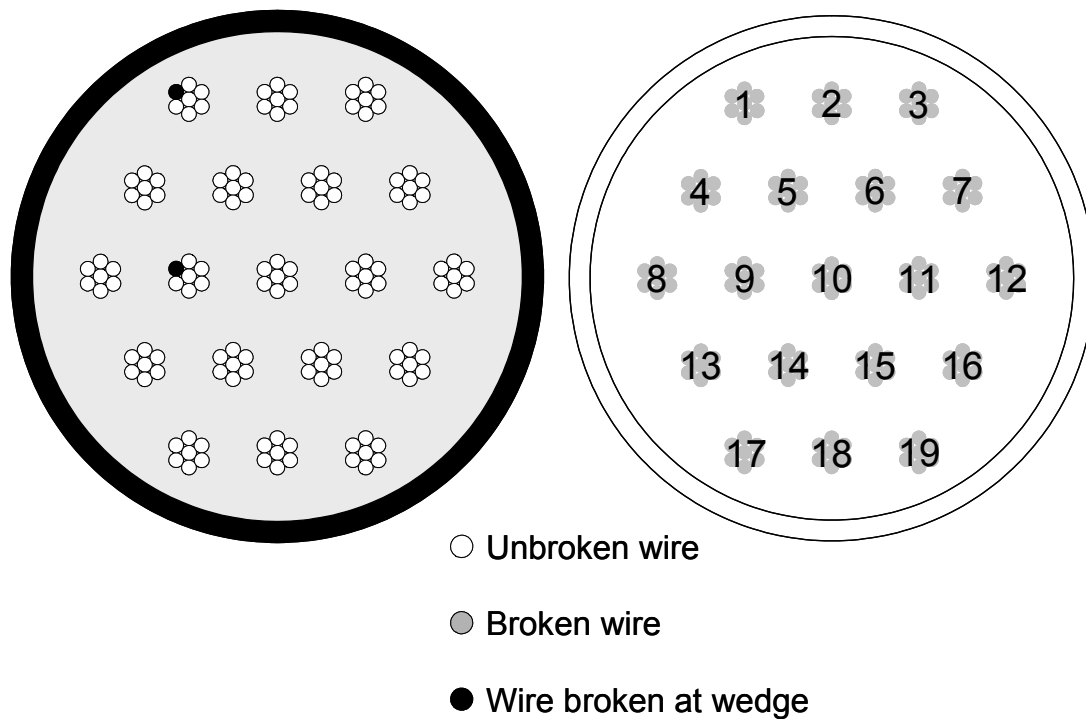


Figure 4-59: Wire breaks at the tower anchorage - Specimen 8

Figure 4-60 shows the location in the cross section of each wire break at the deck anchorage. The breaks occurred on strands 9 and 11. Specimen 8 was the only stay which experienced wire breaks within the center layer of strands at the anchorages.

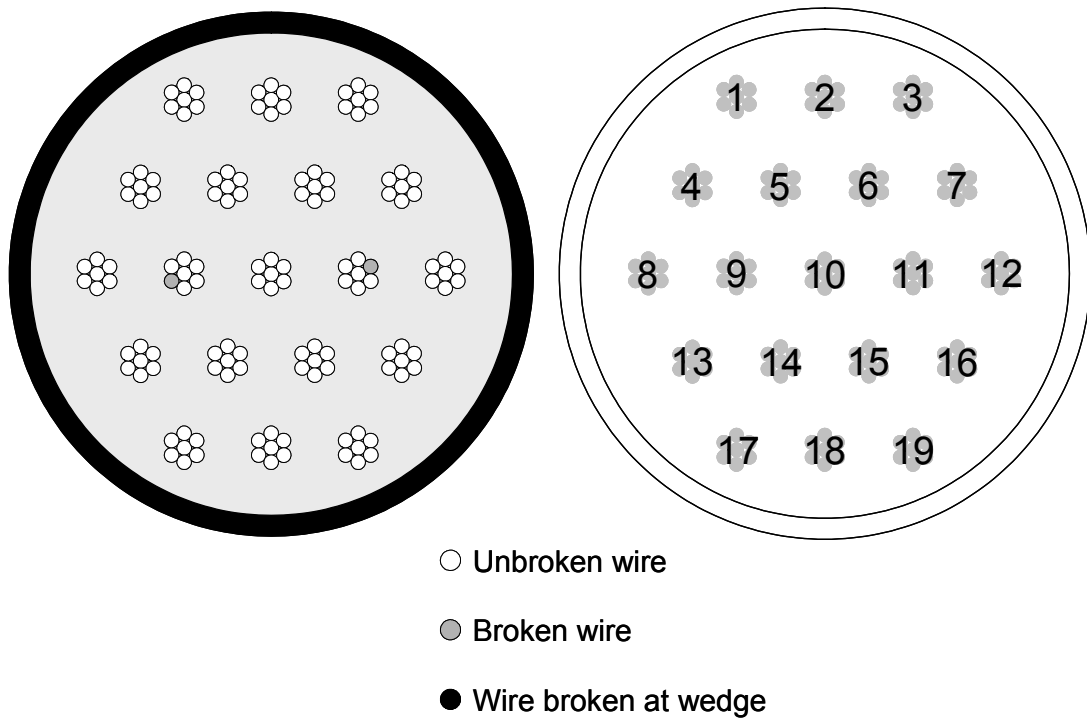


Figure 4-60: Wire breaks at deck anchorage - Specimen 8

Figure 4-61 shows the longitudinal location of each wire break near the tower anchorage. Both wire breaks occurred at the contact point between the strand and the wedge. The first tooth of the wedge causes a stress concentration that accelerates fatigue cracking.

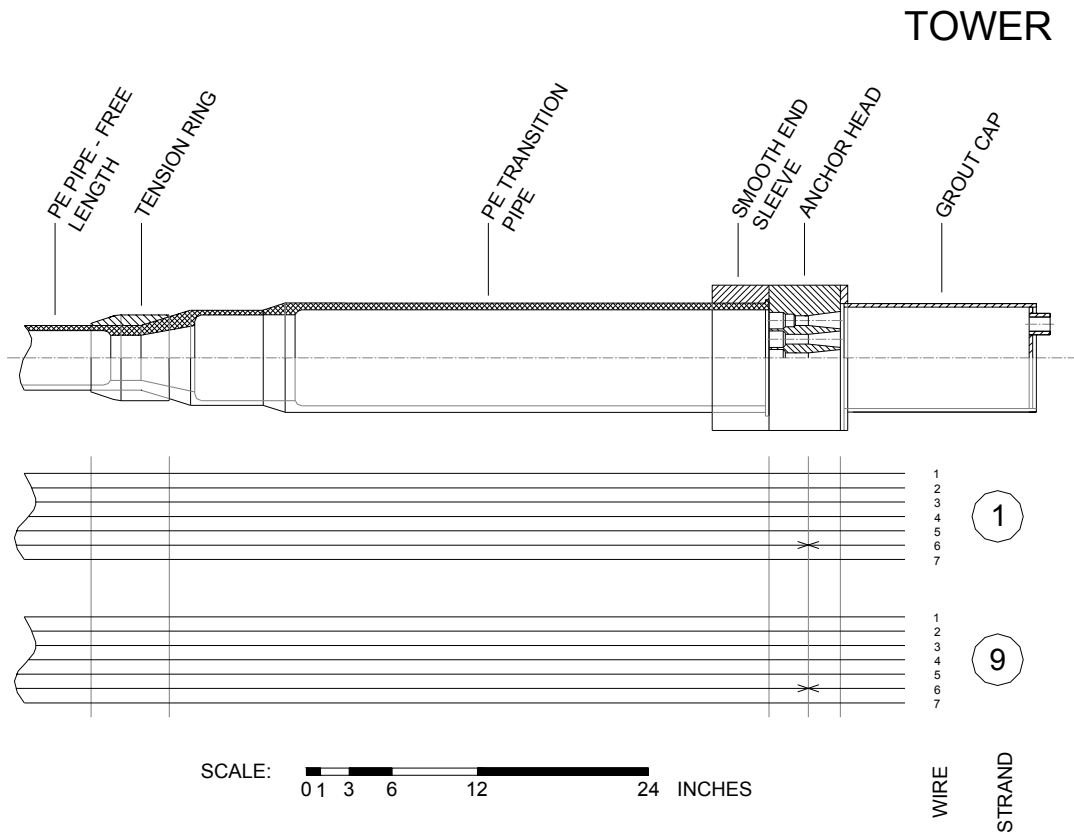


Figure 4-61: Location of wire breaks near the tower anchorage - Specimen 8

Figure 4-62 shows the longitudinal location of each wire break near the deck anchorage. The fracture on strand 9 was inside the wedge, $\frac{1}{4}$ in. behind the first wedge tooth (Figure 4-63). The fracture on strand 11 was $\frac{1}{2}$ in. outside the wedge (Figure 4-64).

DECK

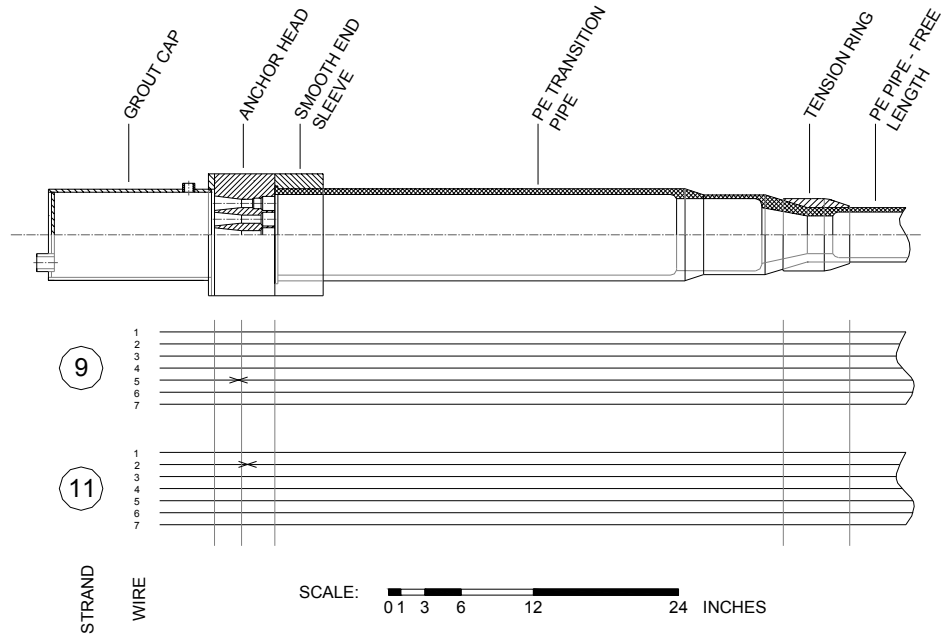


Figure 4-62: Location of wire breaks near the deck anchorage - Specimen 8



*Figure 4-63: Wire break on strand 9
at deck end*



*Figure 4-64: Wire break on strand 11
at deck end*

4.2.4.4 Wire Break Characteristics

All wire breaks occurred inside the anchor head at or near the contact between a strand and the wedge used to anchor it. However, the type of wire break found varied between the deck and tower ends.

At the deck end, which was the dead end during the stressing of the cable, the wire breaks were caused by fretting between the wires of the strand and occurred away from the first wedge tooth. The wire breaks were similar to those that typically occur away from the wedges. The wire break at the deck end on strand 11 was caused by fretting between the center wire and an outer wire (Figure 4-65) and the fracture at the deck end on strand 9 was caused by fretting between two adjacent outer wires (Figure 4-63).

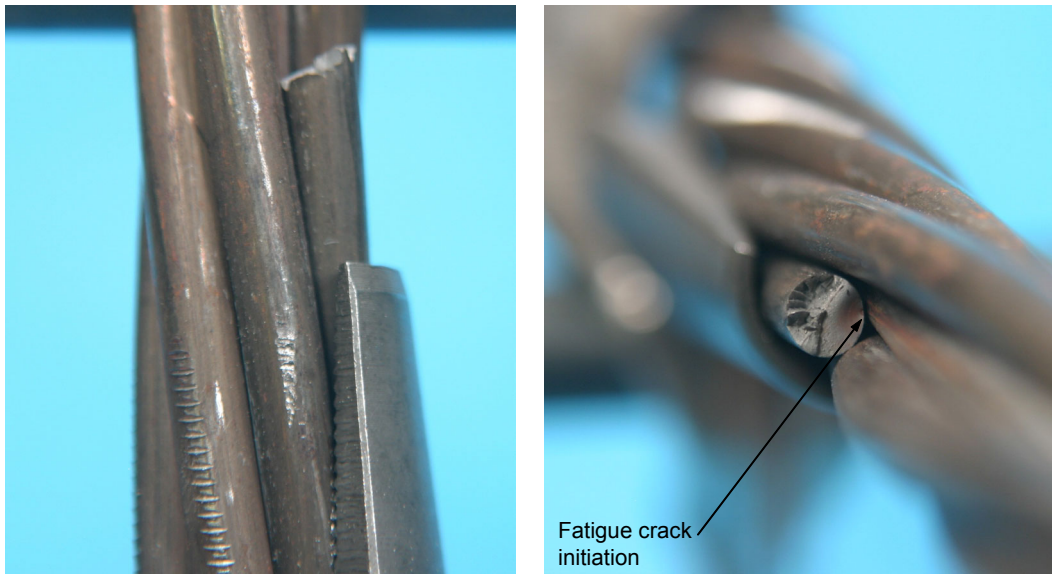


Figure 4-65: Wire break on strand 11 near wedge on the deck end - Specimen 8

At the tower end, which was the end from which the cable was stressed, both wire breaks were initiated by the first wedge tooth (Figure 4-66). Scraping was evident on the strand which is caused by the teeth as the strand is pulled through the wedge during stressing. This is typical at the stressing end of all specimens.

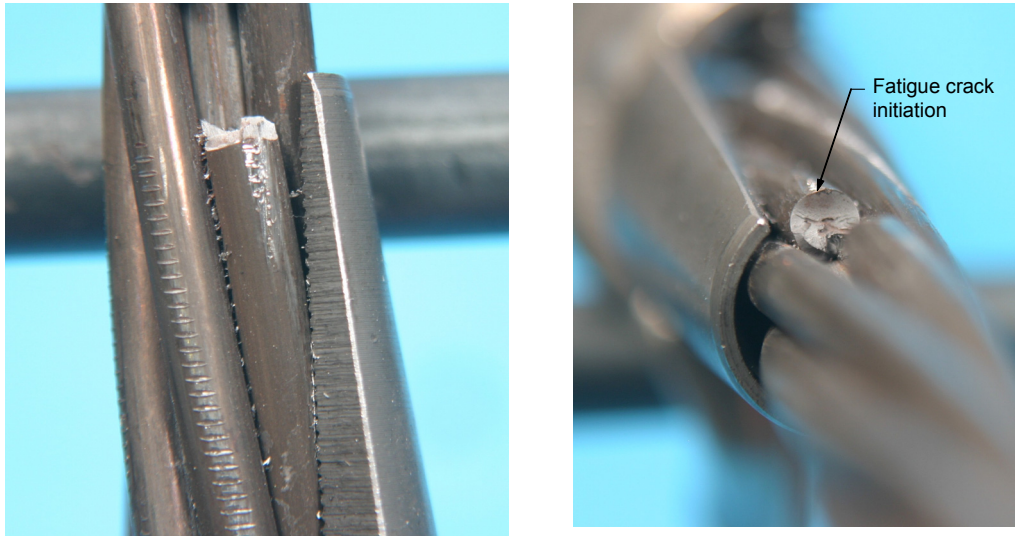


Figure 4-66: Wire breaks on strand 9 at wedge on tower end - Specimen 8

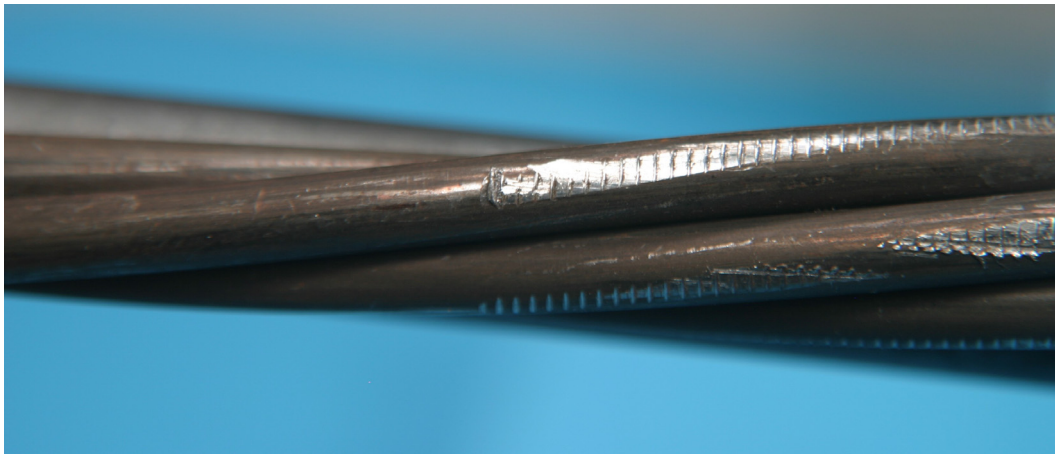


Figure 4-67: Scraping of strand due to stressing at tower end

A summary of wire break characteristics of Specimen 8 is shown in Figure 4-68.

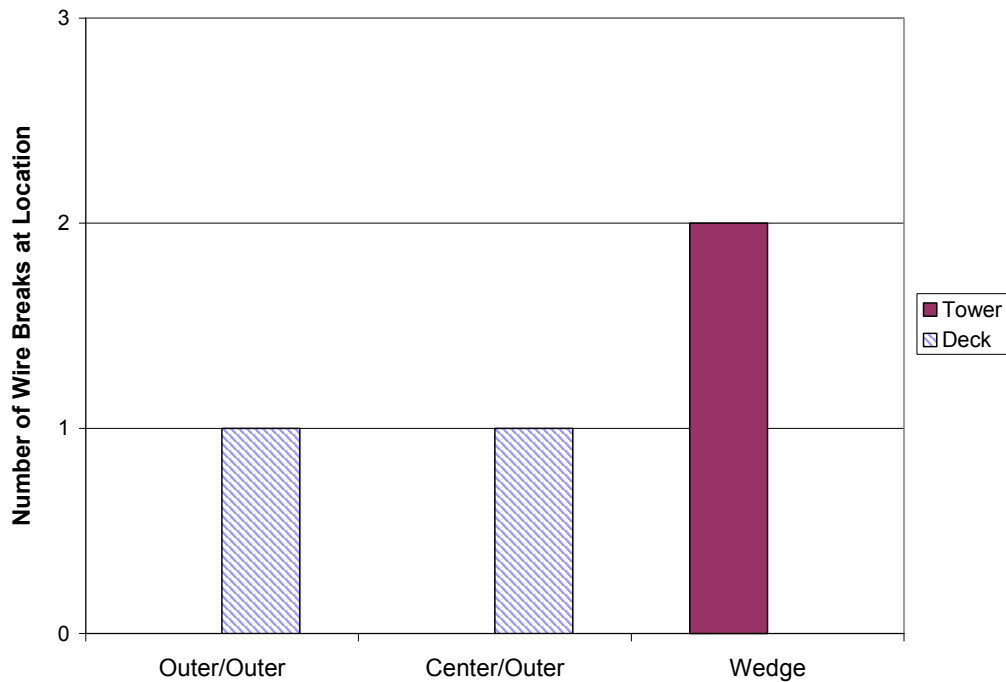


Figure 4-68: Observed fretting fatigue mechanisms - Specimen 8

4.2.4.5 Lateral Stiffness

The lateral stiffness of Specimen 8 was monitored throughout the fatigue test by recording the load required to reach the desired displacement of ± 1.6 in. on a daily basis. Figure 4-69 shows the peak loads to reach the maximum upward and downward displacement during the fatigue test of the specimen. The vertical lines on this plot represent each wire break reported by Soundprint. A decrease in load is observed after each wire break. The load stays relatively constant after the last wire break occurs.

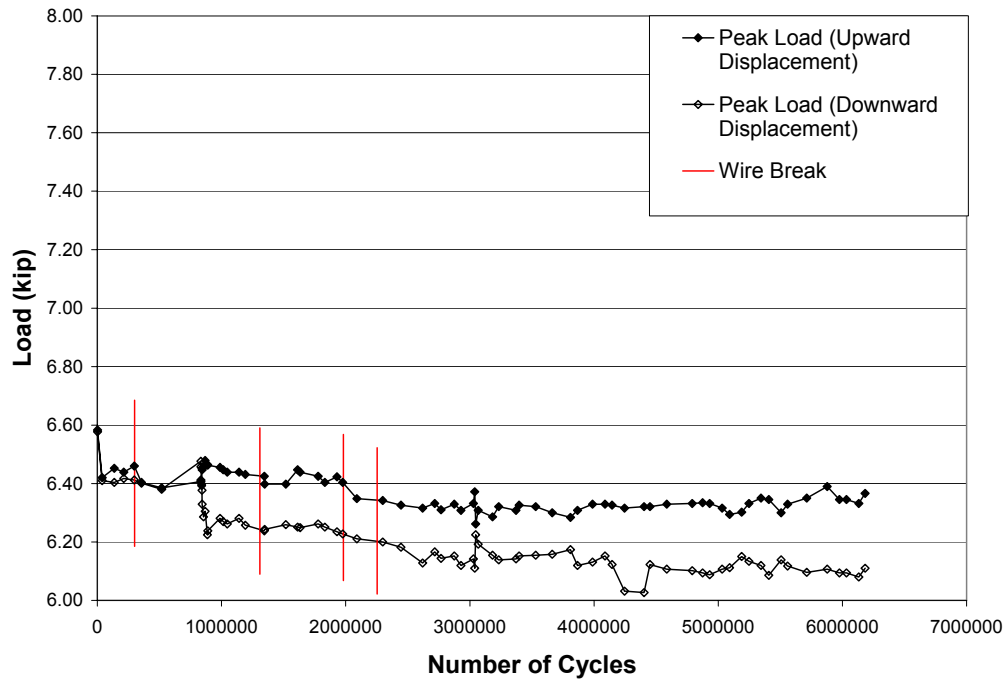


Figure 4-69: Peak load during the fatigue tests - Specimen 8

Figure 4-70 shows the measured load-displacement response from the initial and final static tests. The stiffness changed by 5%, from 4.1 k/in. initially to 3.9 k/in. after the fatigue tests.

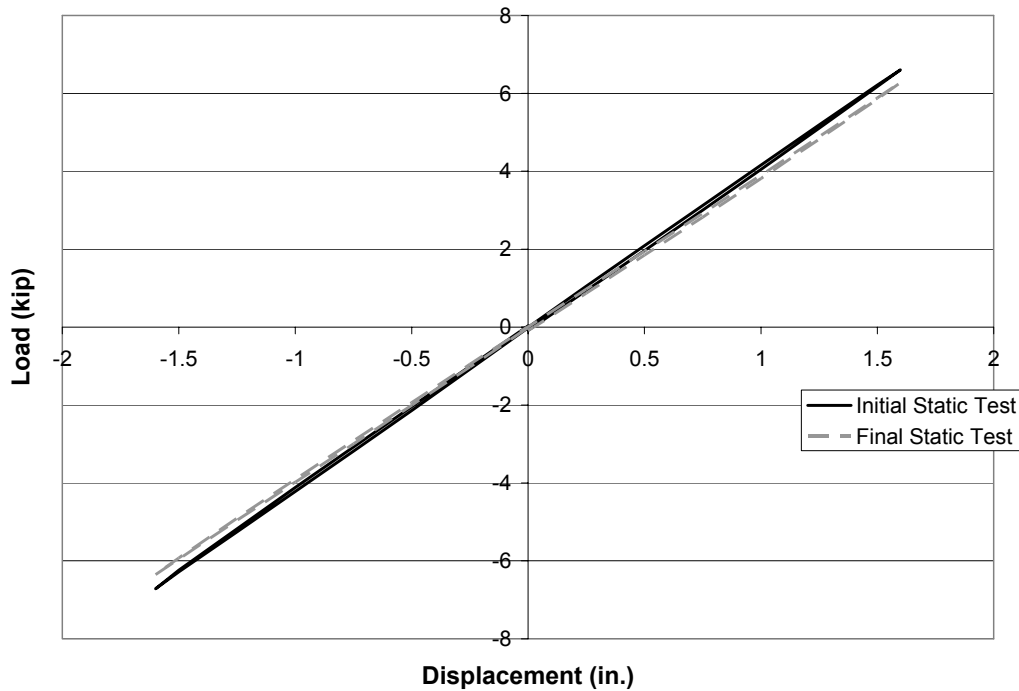


Figure 4-70: Load – displacement response from static tests - Specimen 8

Another measure of the change in stiffness is the natural frequency as determined by the free-vibration tests performed before and after cycling. As wires break the tension in the cable is reduced, thus reducing the natural frequency of the specimen. For Specimen 8, the initial natural frequency was 13.9 Hz and the final natural frequency was 13.4 Hz (Table 4-1), a difference of 3.5%.

4.2.5 Specimen 9

Specimen 9 sustained 2,566,126 loading cycles and 76 wire breaks were found. Twelve wire breaks were found at the tower end, 61 wire breaks were found at the center under the load point, and three breaks were found at the deck end. The cross-section consisted of 19 strands and the specimen was stressed from the tower end. The cable displacement was ± 1.6 in. at midspan during the

fatigue test. The specimen was grouted from the deck end, with a void left at the tower end which was filled with SikaGrout 300 PT grout compound before the fatigue test.

4.2.5.1 Grout Condition

An intentional grout void was left at the tower anchorage and filled with SikaGrout 300 PT one week after the primary grouting of the cable to investigate the effects of filling a grout void as found on the Fred Hartman Bridge. The SikaGrout, identified by its darker color, formed a lens on the surface of the original grout approximately 11 in. long starting 4 in. from the anchor head (Figure 4-71) and ending at the ring formed by the weld in the polyethylene transition pipe. This lens ranged from 1/16 in. thick near the anchor head to 1/32 in. thick at the far end of the lens.

Apart from the grout lens, no evidence of the grout void was found on the exterior of the cable at the face of the anchor head. However, the grout void was found around the grout inlet holes in the anchor heads under the surface of the original grout (Figure 4-72). The grout void is identified by the darker SikaGrout with which it was filled. The volume of the grout void was estimated to be 6 in.³ No strands intersected the grout void, thus no strand had contact with the SikaGrout.

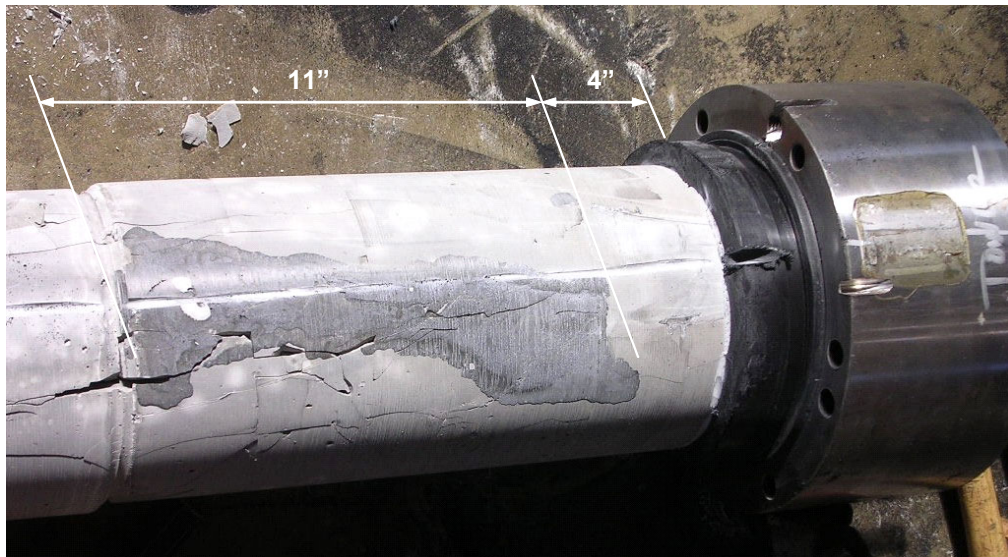


Figure 4-71: Grout lens at tower anchorage - Specimen 9



Figure 4-72: Grout void at tower anchorage - Specimen 9

The grout at the deck end of the stay was homogeneous and relatively uncracked, consistent with finding no wire breaks outside the anchor head. The grout in the center section, under the load point, was extremely damaged (Figure 4-73). This is similar to the results found for Specimen 7 and indicates a large number of wire breaks in the region.



Figure 4-73: Grout condition under the load point - Specimen 9

4.2.5.2 Corrosion

Specimen 9 was cured for 37 days after the main grouting of the stay and was then tested for 16 days.

Near the anchorages, corrosion was generally mild and found only near wire breaks. Several spots of heavy corrosion that were unaccompanied by wire breaks were found near the tower anchorage as seen in Figure 4-74. These areas were all located under the region of the lens of SikaGrout from the grout void.



Figure 4-74: Corrosion near the tower anchorage - Specimen 9

Severe corrosion was found in the region near the center of the stay. Heavy, red-orange corroded fretting product observed near wire breaks (Figure 4-75) was accompanied by black and red pitting corrosion in several places. Several breaks appeared to initiate at these points of pitting corrosion. White powder and grout coated many of the strands and obscured some fracture surfaces in this region. The amount of fretting residue tended to be more severe when all (or nearly all) the wires of a strand had fractured, which may indicate that such corrosion forms after wire breaks occur.



Figure 4-75: Corrosion under the load point - Specimen 9

4.2.5.3 Location of Wire Breaks

A total of 76 wire breaks occurred during the fatigue testing of Specimen 9. Table 4-5 shows the distribution of wire breaks found along the cable during the autopsy as well as the wire breaks reported by Soundprint.

Table 4-5: Wire break distribution on Specimen 9

	Tower	Center	Deck	Total
Autopsy	12	61	3	76
Soundprint	12	62	3	77

Figure 4-76 shows the cycle at which each wire break occurred based on Soundprint data. The first wire break occurred after 386,000 cycles at the tower anchorage, the first wire break at the deck anchorage occurred after 1,244,100 cycles, and the first break under the load point occurred after 746,700 cycles.

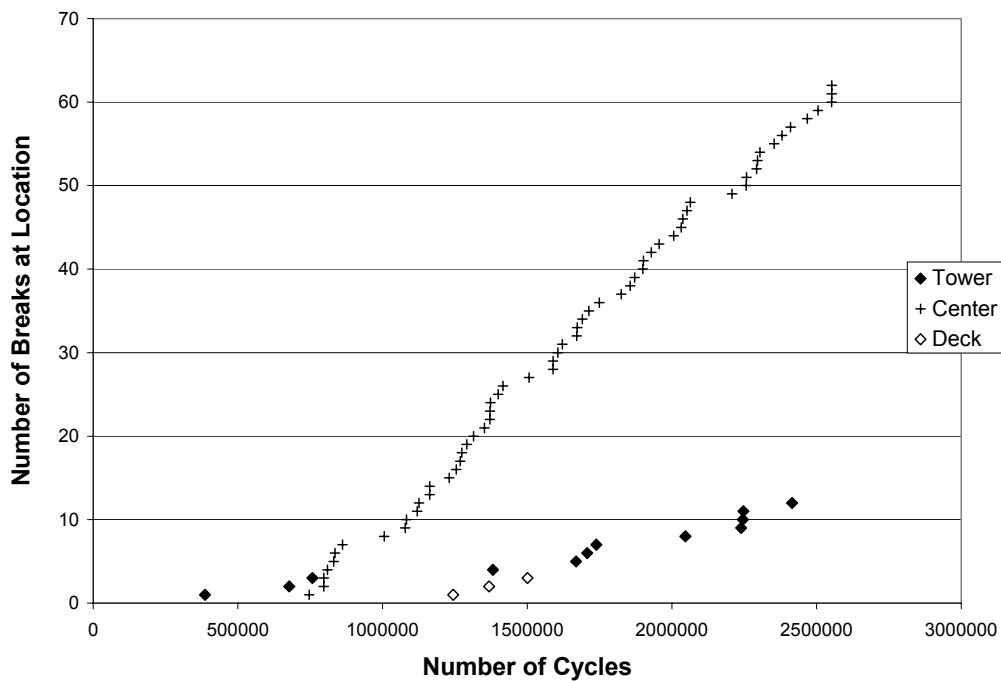
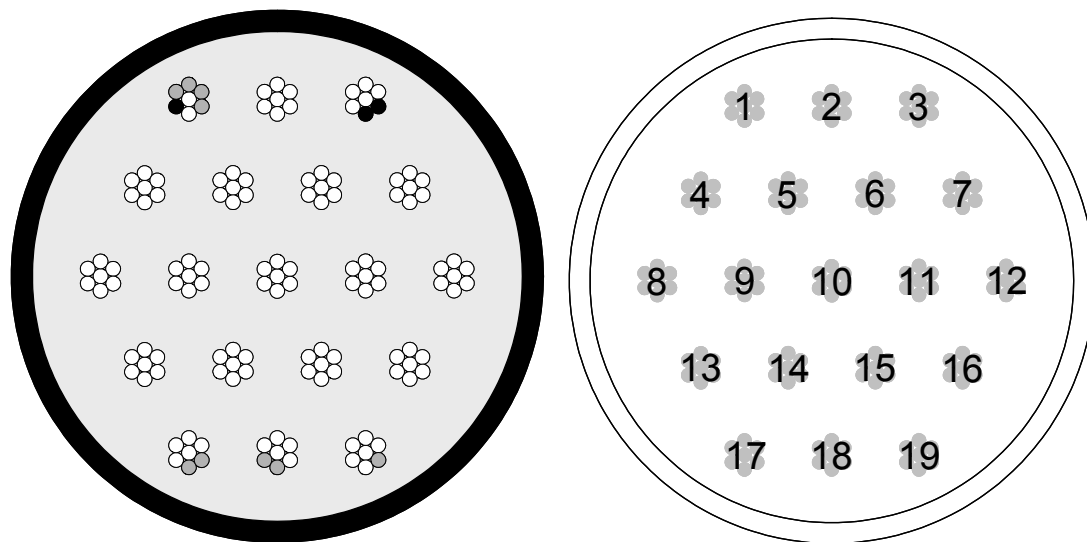


Figure 4-76: Wire breaks reported by Soundprint - Specimen 9

Figure 4-77 shows the location in the cross-section of each wire break near the tower anchorage. The 12 breaks occur on 5 strands (1, 3, 17, and 19) and are typically at the extreme fiber of the cross-section. Figure 4-78 shows the location

of each wire break near the tower anchorage. Three wires broke inside the anchor head at the contact point between the wedge and the strand. One wire break occurred 15 in. from the anchor head, where there is a weld in the polyethylene transition pipe.

An unintentional grout void was found in Specimen 1, which was built and tested by Poser (2001). The void in Specimen 1 was not filled before testing and was approximately four times larger than the void left in Specimen 9, which was filled with SikaGrout before testing as described in Chapter 2. 43% of the wire breaks at the tower anchorage of Specimen 1 were found on strands which were exposed in the grout void. On Specimen 9, no strands were in contact with the (filled) grout void or the subsequent lens which formed on the surface of the grout as described in Section 4.2.5.1. However, excluding three wires which failed at the wedge, the breaks which occurred at the tower end of Specimen 9 were located under the region of this grout lens, 4 in. to 15 in. in front of the anchor head. These breaks may be linked to irregular grout properties in this region of the cable.



- Unbroken wire
- Broken wire
- Wire broken at wedge

Figure 4-77: Wire breaks at tower anchorage - Specimen 9

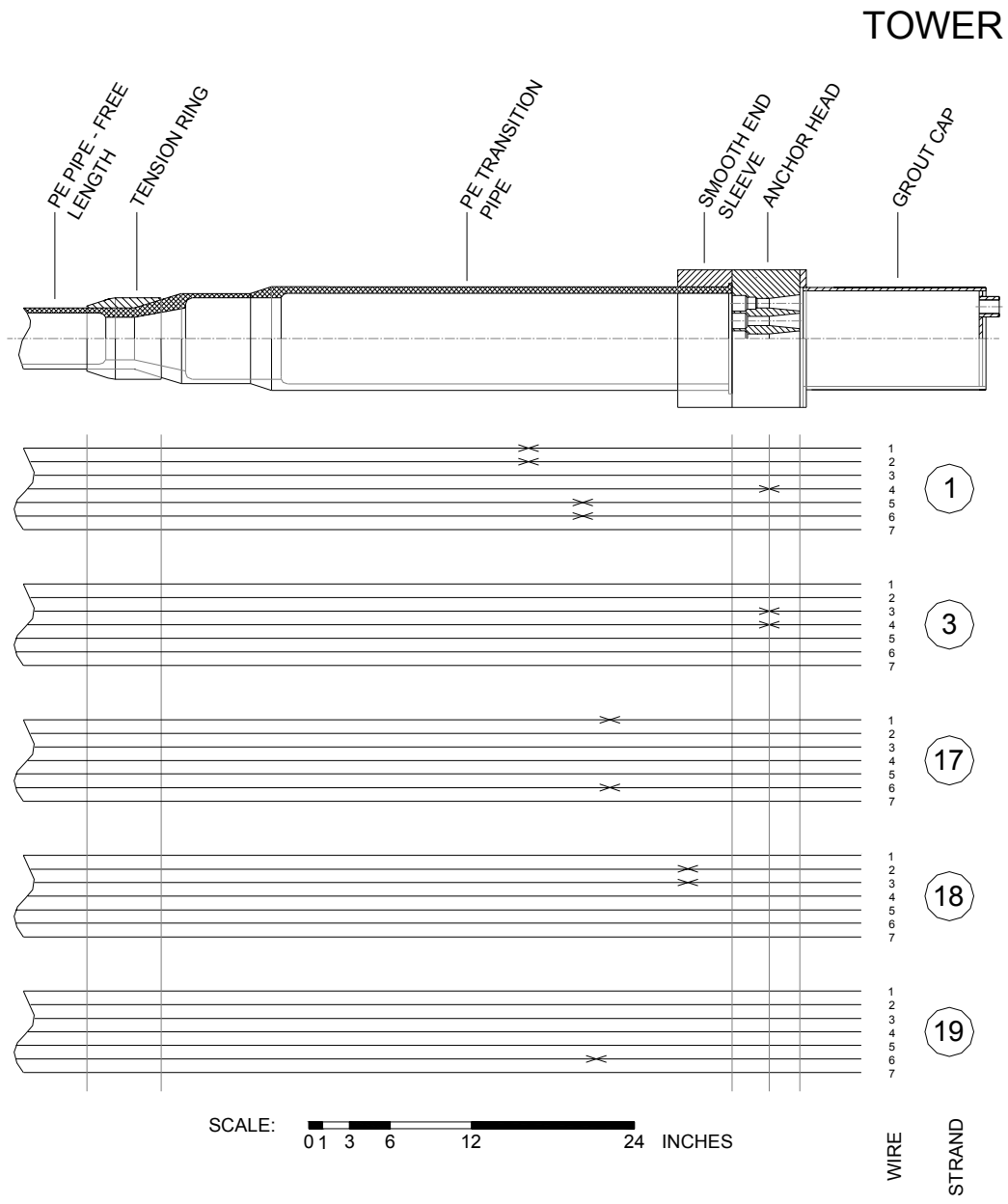


Figure 4-78: Location of wire breaks near tower anchorage - Specimen 9

Figure 4-79 shows the location in the cross-section of each wire break that occurred in the center of the stay under the load point. The 61 breaks occurred on

12 strands, mainly at the top and bottom of the specimen. Figure 4-80 and Figure 4-81 show the location of each wire break relative to the load point. 98% of the breaks occurred within the clamping region of the stay and tended to occur near points of stiffness transition (either the edge of the clamp or the edge of the load plate). Specimen 9 was the only stay to experience wire breaks within the middle layer of strands under the load point.

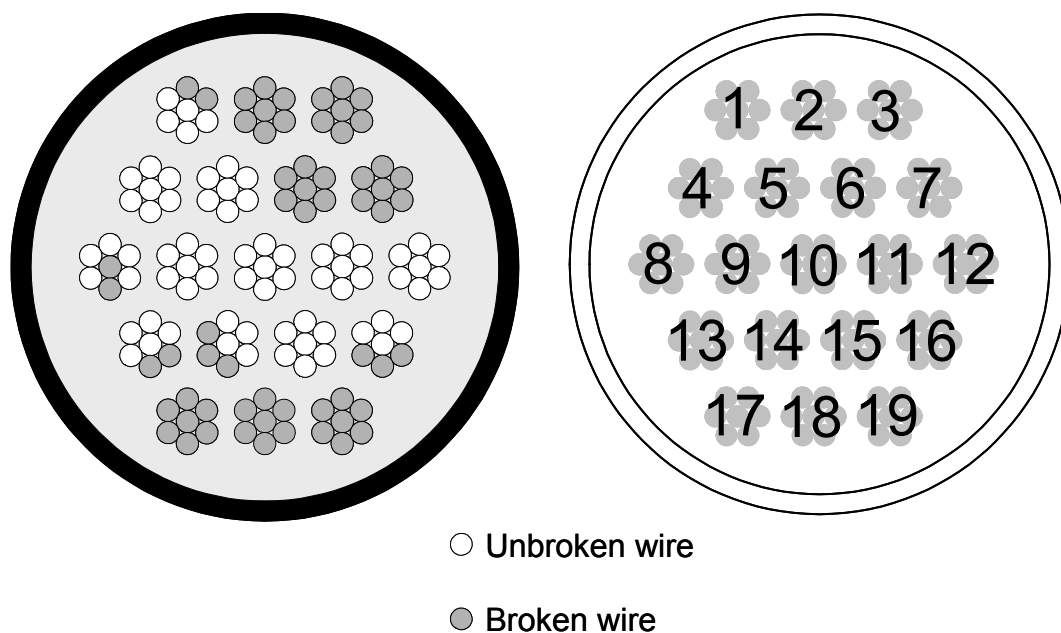


Figure 4-79: Wire breaks under the load point - Specimen 9

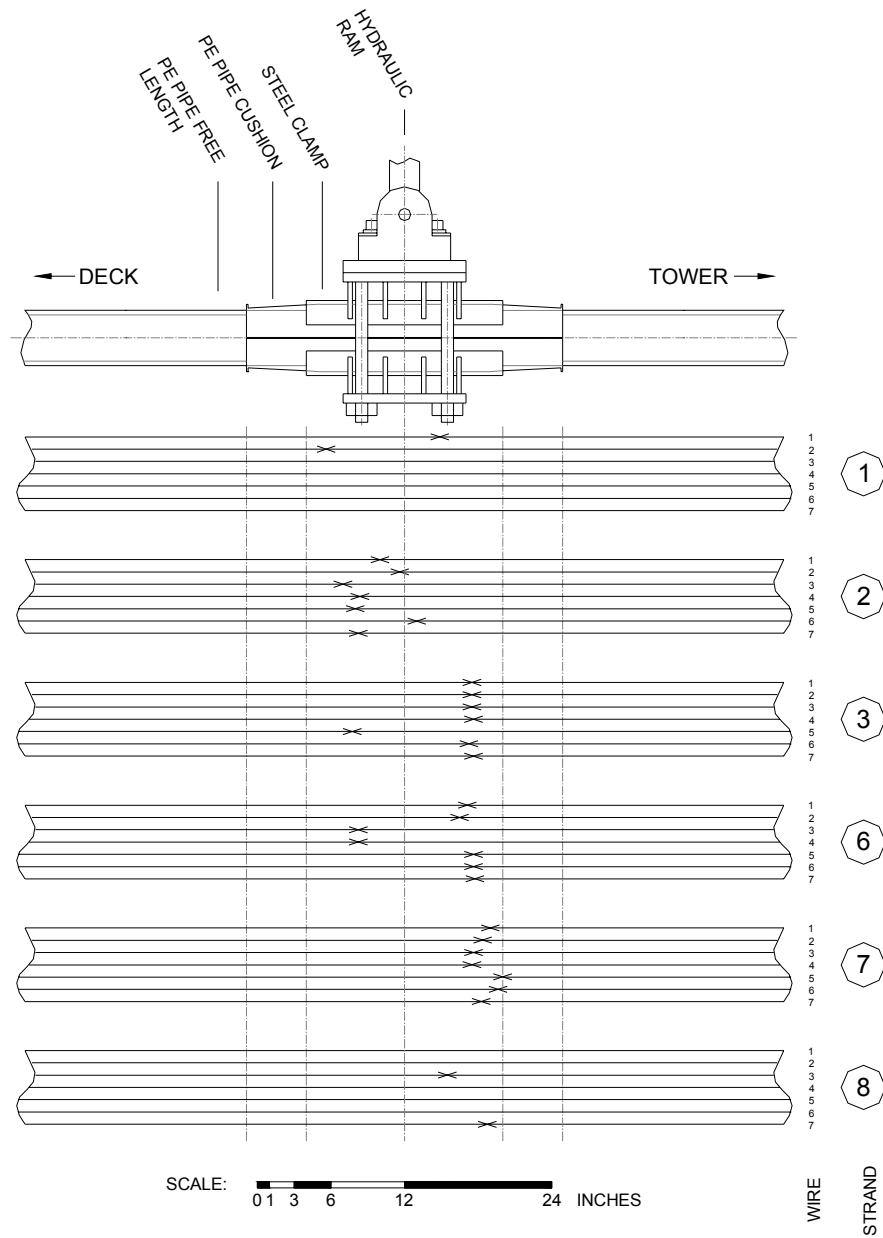


Figure 4-80: Location of wire breaks under the load point - Specimen 9

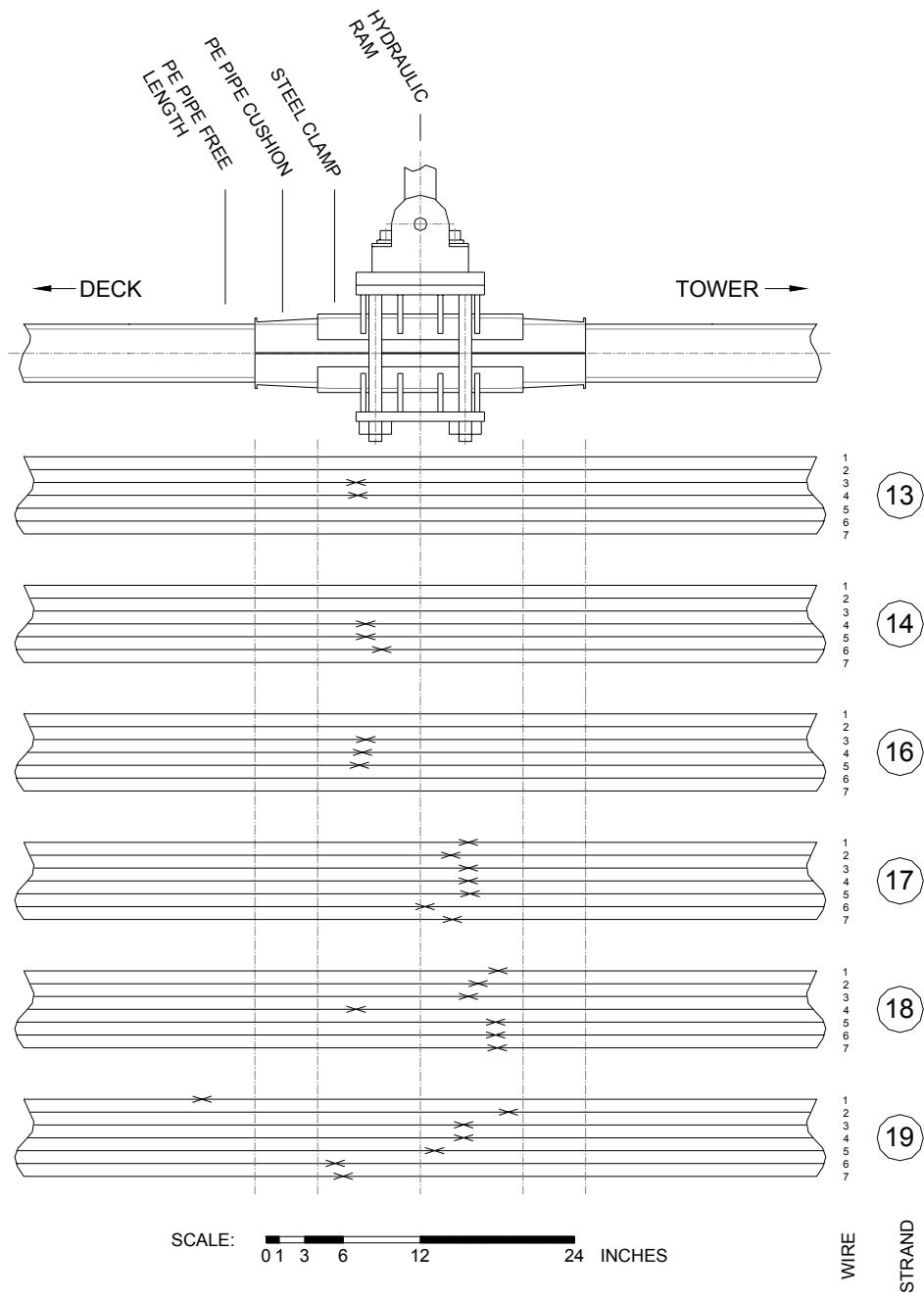


Figure 4-81: Location of wire breaks under the load point - Specimen 9

Figure 4-82 shows the location in the cross-section of each wire break near the deck anchorage and Figure 4-83 shows the longitudinal location of each break. All three breaks occurred on strand 1, and all breaks occurred inside the anchor head. Two breaks occurred at the wedges and were initiated by the first wedge tooth and one break occurred at the front of the polyethylene bushing at the face of the anchor head.

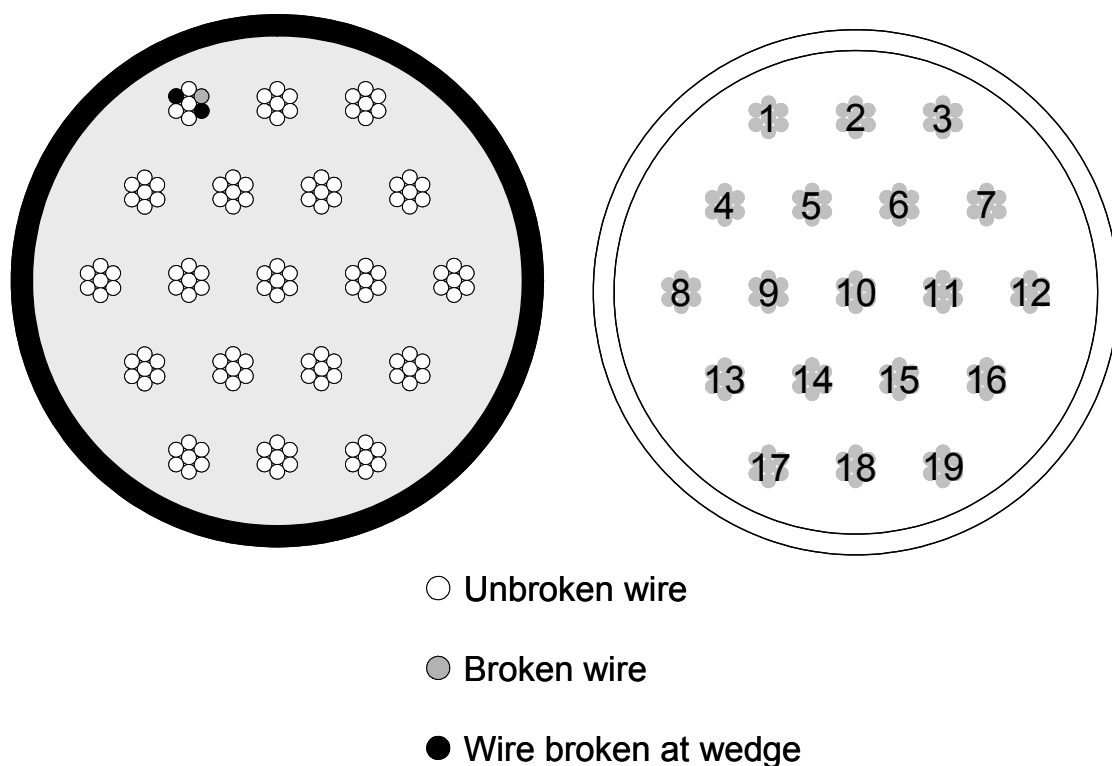


Figure 4-82: Wire breaks at deck anchorage - Specimen 9

DECK

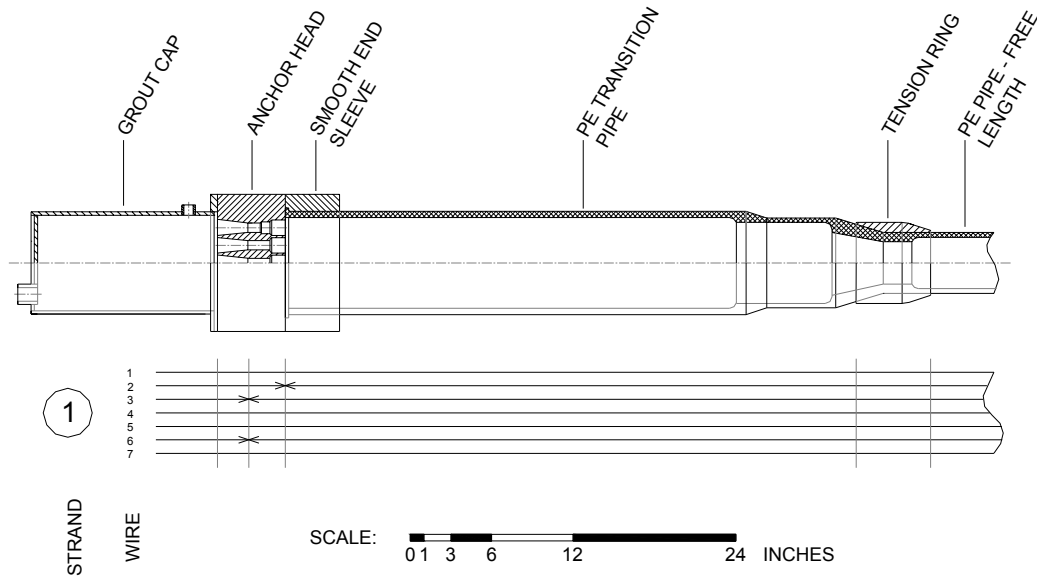


Figure 4-83: Location of wire breaks near the deck anchorage - Specimen 9

4.2.5.4 Wire Break Characteristics

The wire breaks on Specimen 9 were classified as shown in Figure 4-84. Figure 4-85 shows that fretting between adjacent outer wires was the primary mode of failure in the cable. As opposed to the other specimens, several fatigue failures initiated at points of pitting corrosion. It is unknown if this corrosion originated before or after grouting of the stay. This type of failure contributed significantly to the overall number of wire breaks under the load point. This type of failure was not observed near either anchorage.

While the percentage of breaks occurring at the wedges was comparable to the other grouted specimens, the characteristic of the breaks at the wedges varied slightly. On previous specimens, wedge breaks at the deck (non-stressing) end occurred slightly away from the wedges and were the result of fretting with other

wires of the strand and wedge breaks at the tower (stressing) end were initiated by the first wedge tooth. On Specimen 9, all breaks at wedges on both the stressing and non-stressing ends were initiated at the first wedge tooth.

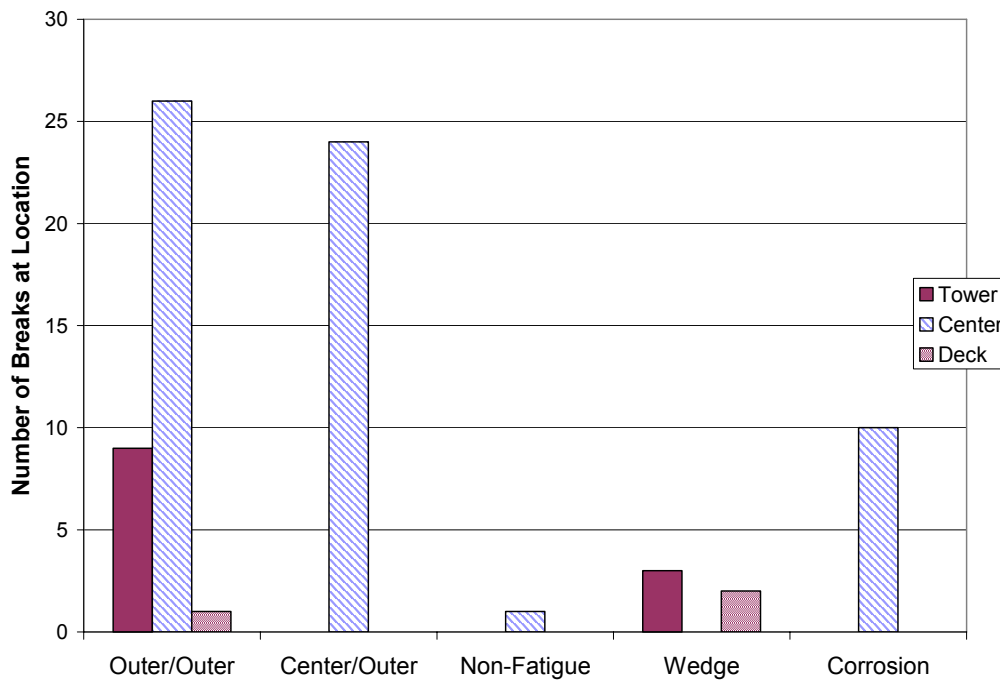


Figure 4-84: Observed failure mechanisms - Specimen 9

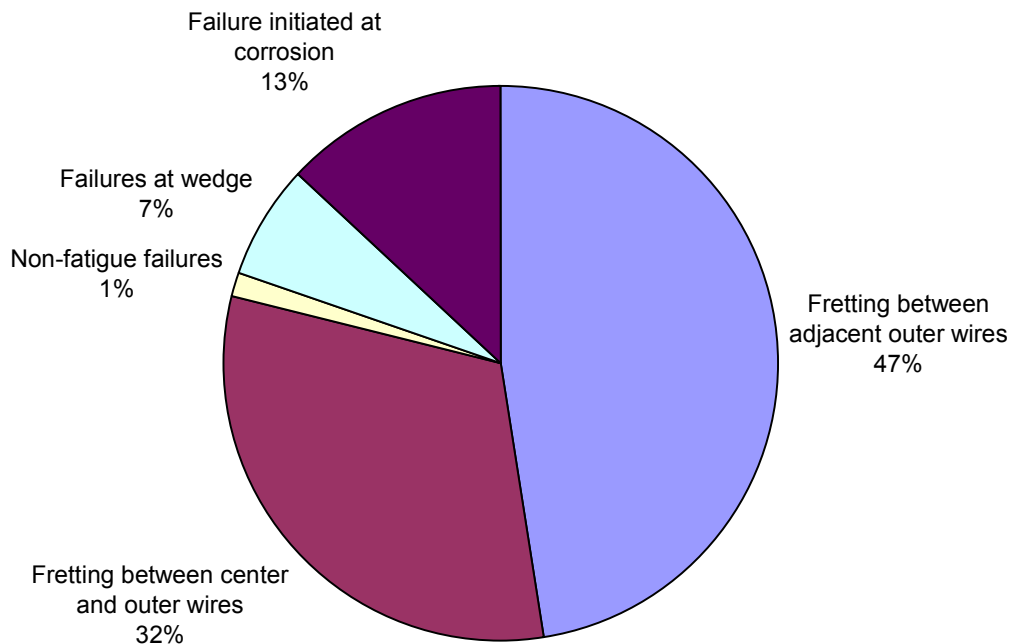


Figure 4-85: Distribution of failure mechanisms - Specimen 9

4.2.5.5 Lateral Stiffness

The lateral stiffness of Specimen 9 was monitored throughout the fatigue test by recording the load required to reach the desired displacement of ± 1.6 in. on a daily basis. Figure 4-86 shows the peak load required to reach the maximum upward and downward displacement during the fatigue test. The vertical lines on this plot represent each wire break reported by Soundprint.

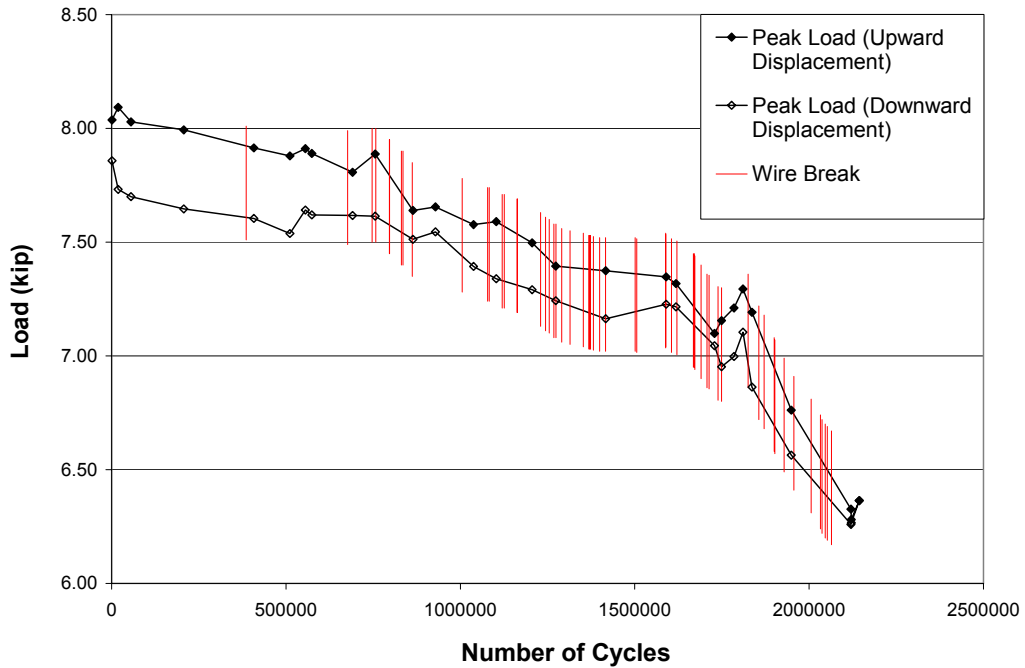


Figure 4-86: Peak load during fatigue tests - Specimen 9

Figure 4-87 presents the static test data from Specimen 9. The initial static test was performed before beginning the fatigue tests. The intermediate static test was performed after 1,748,800 cycles, approximately 70% of the way through the fatigue test. Soundprint reported 45 wire breaks at the time of this static test, 60% of the final number of wire breaks found in the specimen. A final static test was not performed due to mechanical failure of the hydraulic ram.

The load required to displace the cable in the upward direction changed very little (less than 0.25%) over the course of fatigue testing. However, the load required to displace the cable in the downward direction decreased by 11.9%. The difference in these two stiffnesses may be due to the uneven distribution of wire breaks across the cross-section as presented in Section 4.2.5.3; however, this result was not seen in other specimens with uneven wire break distributions.

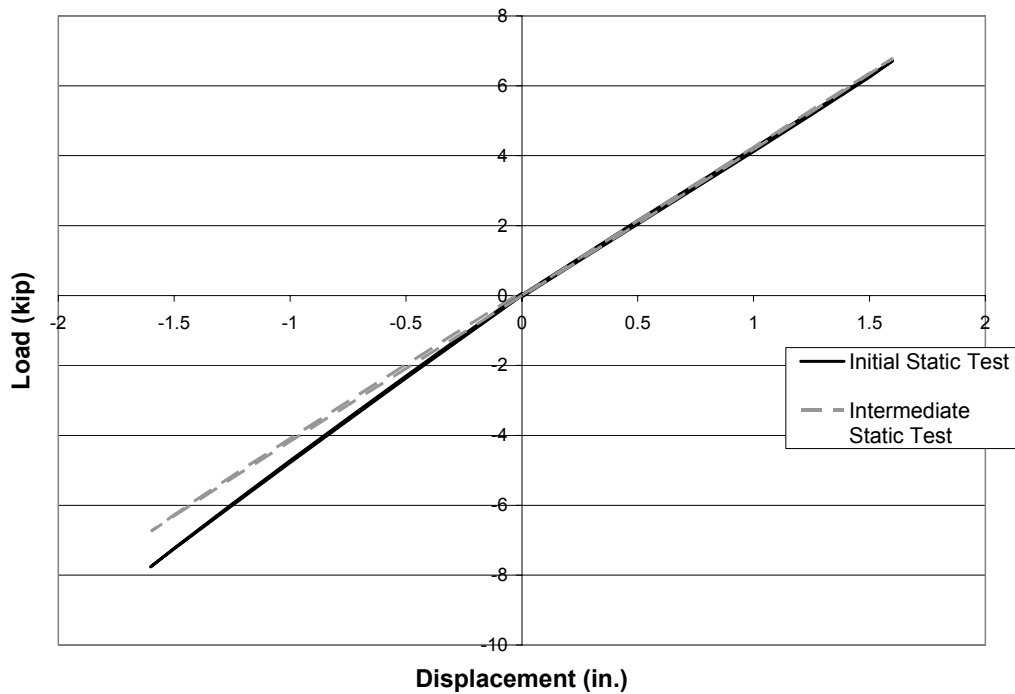


Figure 4-87: Load–displacement response from static tests - Specimen 9

A free-vibration test was performed on Specimen 9 before and after the fatigue tests. The initial natural frequency was 12.5 Hz and the final natural frequency was 10.5 Hz (Table 4-1), a difference of 15.6%.

4.2.6 Specimen 10

Specimen 10 sustained 5,614,211 loading cycles and 52 wire breaks were found. Twenty-three breaks were found at the tower anchorage, 21 breaks were found at the center under the load point, and 8 breaks were found at the deck anchorage. The cross-section consisted of 19 strands, the specimen was grouted from the deck end, and the specimen was stressed from the tower end. The cable displacement was ± 2.1 in. at midspan for the first 2,220 cycles and then ± 1.1 in. for the rest of the fatigue test. The maximum midspan displacement was decreased due to excessive lateral movement of the loading apparatus.

4.2.6.1 Grout Condition

Figure 4-88 shows the grout condition at the tower end immediately after removing the polyethylene transition pipe. Severe longitudinal cracks were observed, which indicate wire breaks in the region. Apart from the cracking, no other visual imperfections in the grout were observed.



Figure 4-88: Grout at tower end immediately after opening - Specimen 10

Figure 4-89 shows the grout condition under the load point of Specimen 10. The grout in this region was severely cracked, although the damage was not as severe as that found on Specimens 7 and 9. This is consistent with the Soundprint data, which predicted only 20 breaks in the region compared with over 60 breaks each on Specimens 7 and 9.



Figure 4-89: Grout at midspan immediately after opening - Specimen 10

Figure 4-90 depicts the grout condition at the deck end. Large longitudinal cracks were observed, despite the fact that no wire breaks were found outside of the anchor head. The cracking in the region is most likely due to the large displacement the stay experienced during the first 2,220 cycles of the fatigue test.

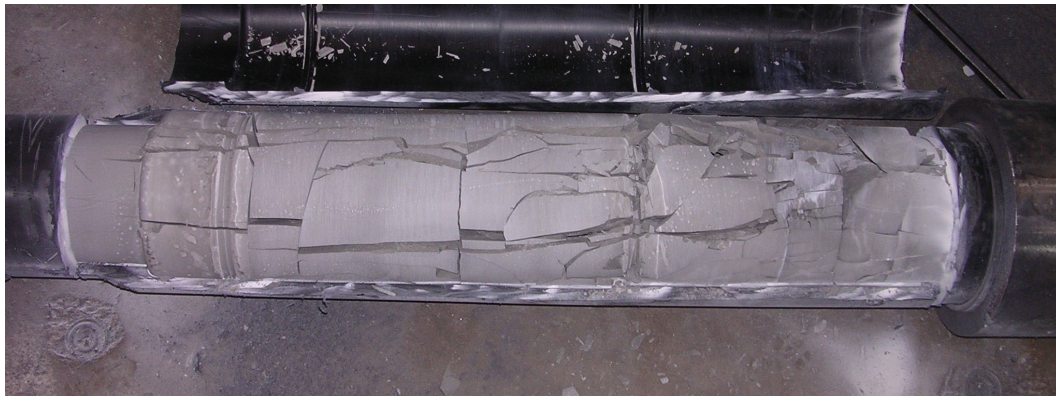


Figure 4-90: Grout at deck end immediately after opening - Specimen 10

4.2.6.2 Corrosion

Corroded fretting residue was found near the breaks on the tower end and under the load point (Figure 4-91). The amount of fretting residue observed was less than on Specimens 7 and 9. At the tower end (Figure 4-92), the amount of

corroded fretting residue was similar to that found on other specimens. Traces of corroded residue were found in the grout at the tower end.



Figure 4-91: Corroded fretting product under the load point – Specimen 10



Figure 4-92: Corroded fretting product at the tower end - Specimen 10

4.2.6.3 Location of Wire Breaks

A total of 52 wire breaks occurred during the fatigue test of Specimen 10. Table 4-6 shows the distribution of wire breaks found along the cable during the autopsy as well as the wire breaks reported by Soundprint.

Table 4-6: Wire break distribution on Specimen 10

	Tower	Center	Deck	Total
Autopsy	23	21	8	52
Soundprint	23	20	9	52

Figure 4-93 shows the cycle at which each wire break occurred based on Soundprint data. The first wire break occurred after 926,871 cycles at the tower anchorage.

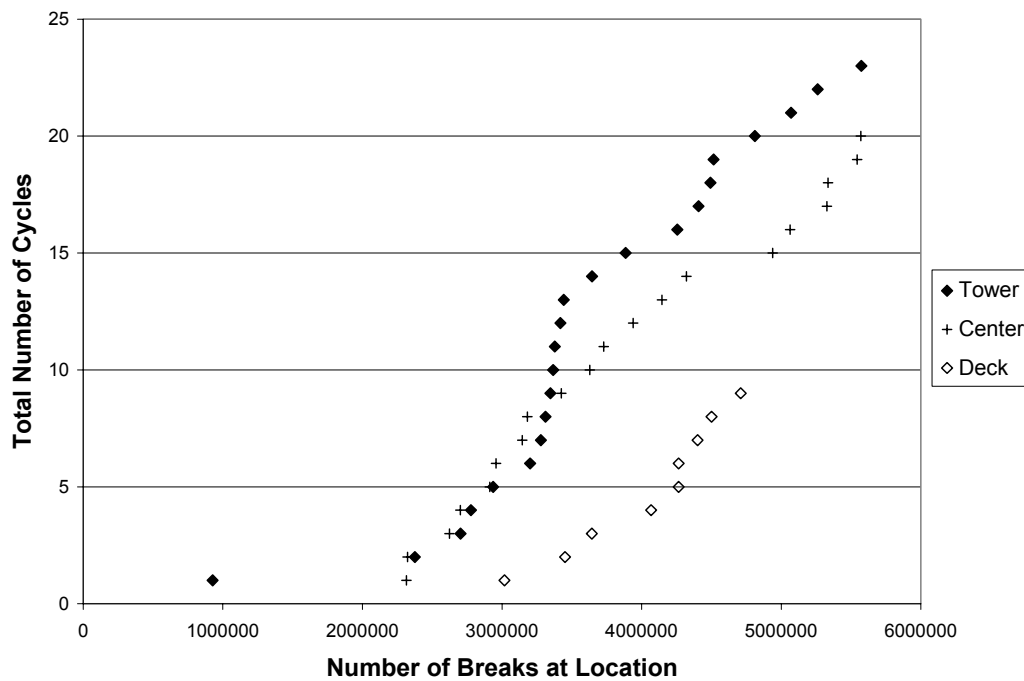


Figure 4-93: Wire breaks reported by Soundprint - Specimen 10

Figure 4-94 shows the location in the cross-section of each wire break near the tower anchorage. The 23 breaks occur on 4 strands (2, 17, 18, and 19). Over 90% of the breaks at the tower end occurred on the bottom layer of strands. Only one break occurred at the wedge. In addition to the 23 breaks, a fatigue crack was found 3 ¾” from the anchor head on wire 4 of Strand 18. The wire was not fractured at this point, although it was fractured 4 ¾” away. Because the wire had already fractured in one place, there was not enough tension to cause the second crack to fracture before the fatigue test was stopped.

Figure 4-95 shows the longitudinal location of each wire break relative to the tower anchorage. Thirteen percent of the wire breaks occurred inside the anchor head, including the wire break which occurred at the wedge. Over 52% of the wire breaks occurred in the region of the smooth end sleeve, and nearly 35% of the wire breaks occurred beyond the smooth end sleeve.

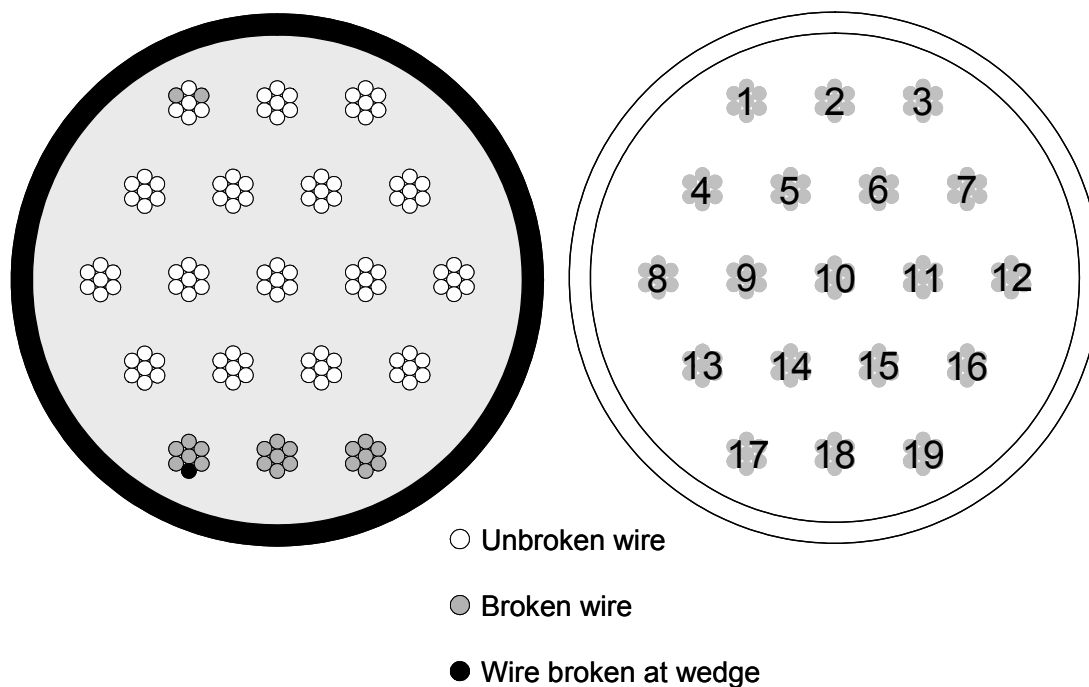


Figure 4-94: Wire breaks at the tower anchorage - Specimen 10

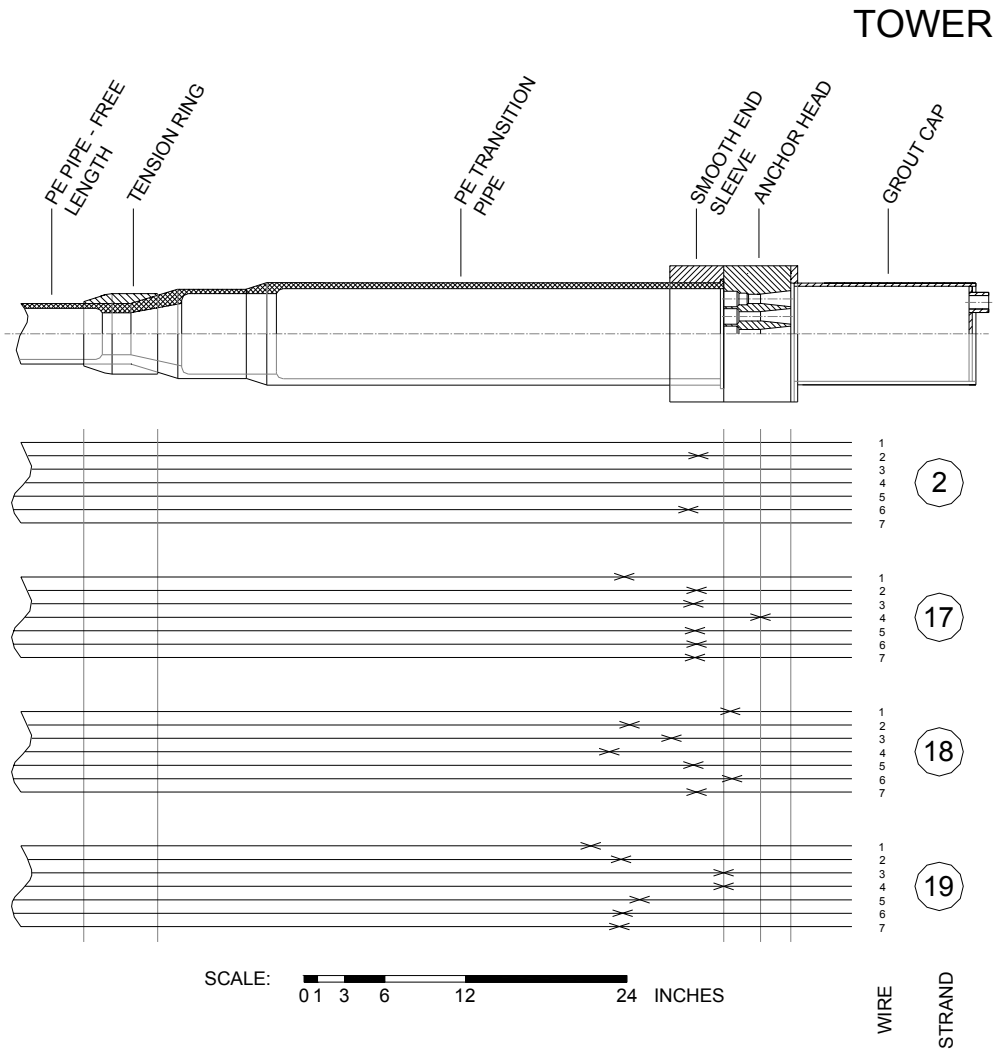


Figure 4-95: Location of wire breaks near tower anchorage - Specimen 10

Figure 4-96 shows the location in the cross-section of each wire break under the load point. The 21 breaks occurred on 4 strands (2, 3, 18, and 19). The wire breaks tended to occur below the neutral axis of the specimen, with 67% of the breaks occurring on the bottom layer of strands. Figure 4-97 shows the location of each wire break relative to the load point. The breaks all occurred

within the clamp region, and tended to occur between the edge of the load plate and the end of the steel clamp. Seventy-one percent of the breaks occurred on the deck side of the loading apparatus.

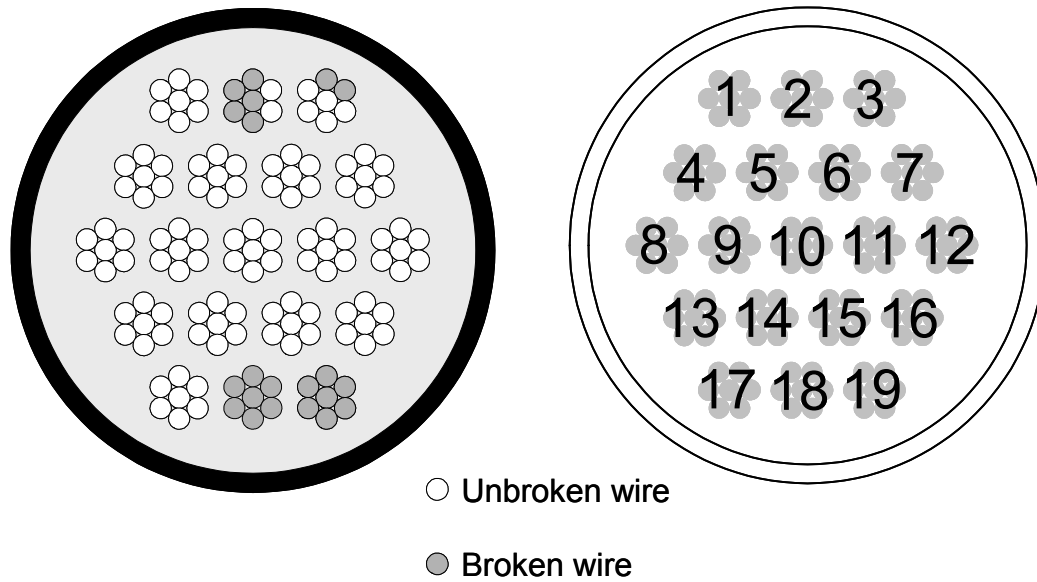


Figure 4-96: Wire breaks under the load point - Specimen 10

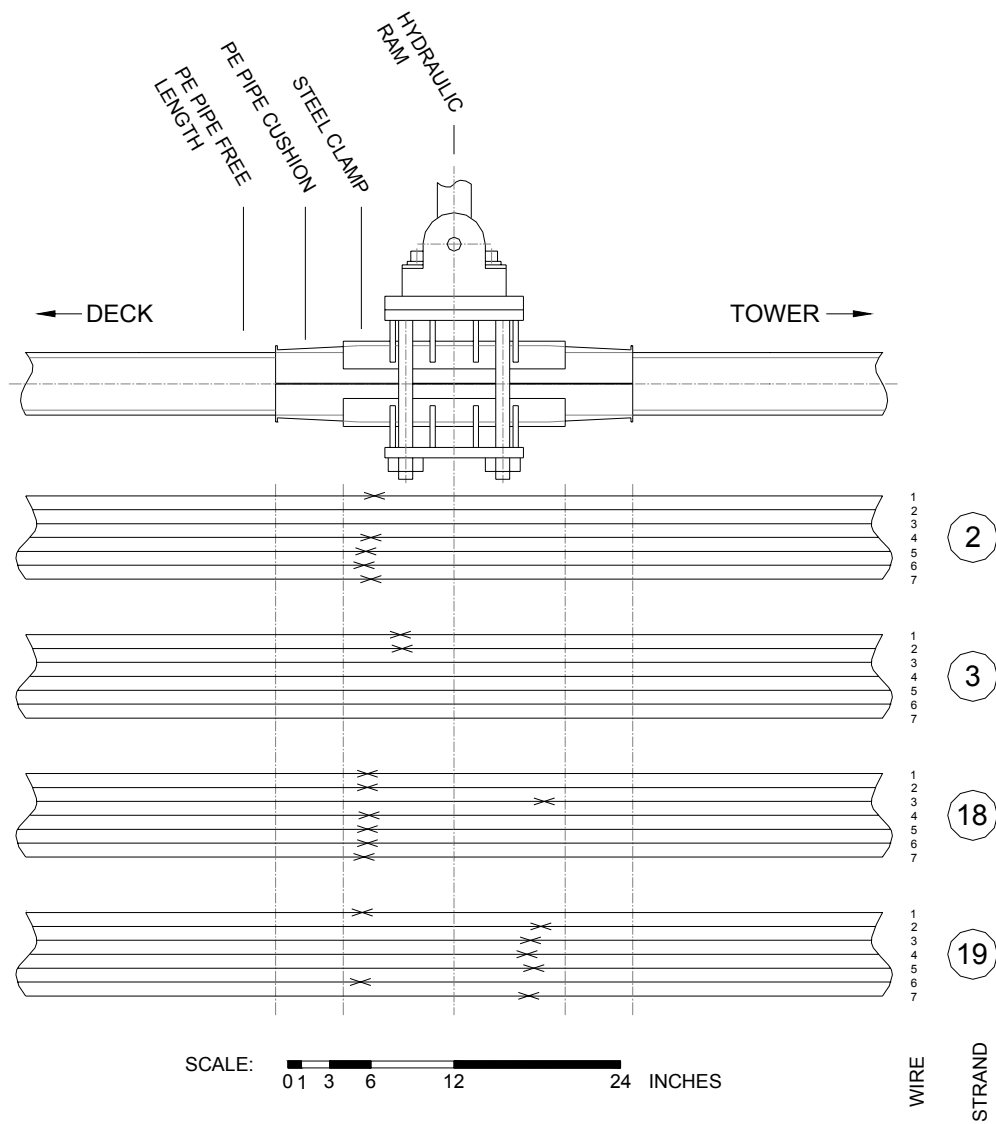


Figure 4-97: Location of wire breaks relative to the load point - Specimen 10

Figure 4-98 shows the location in the cross-section of each wire break near the deck anchorage. The 8 breaks occurred on two strands (18 and 19). All of the breaks occurred on the bottom layer of strands. Figure 4-99 shows the location of each wire break relative to the deck anchorage. All of the breaks occurred

either within or at the face of the anchor head, but no wires fractured at the wedge.

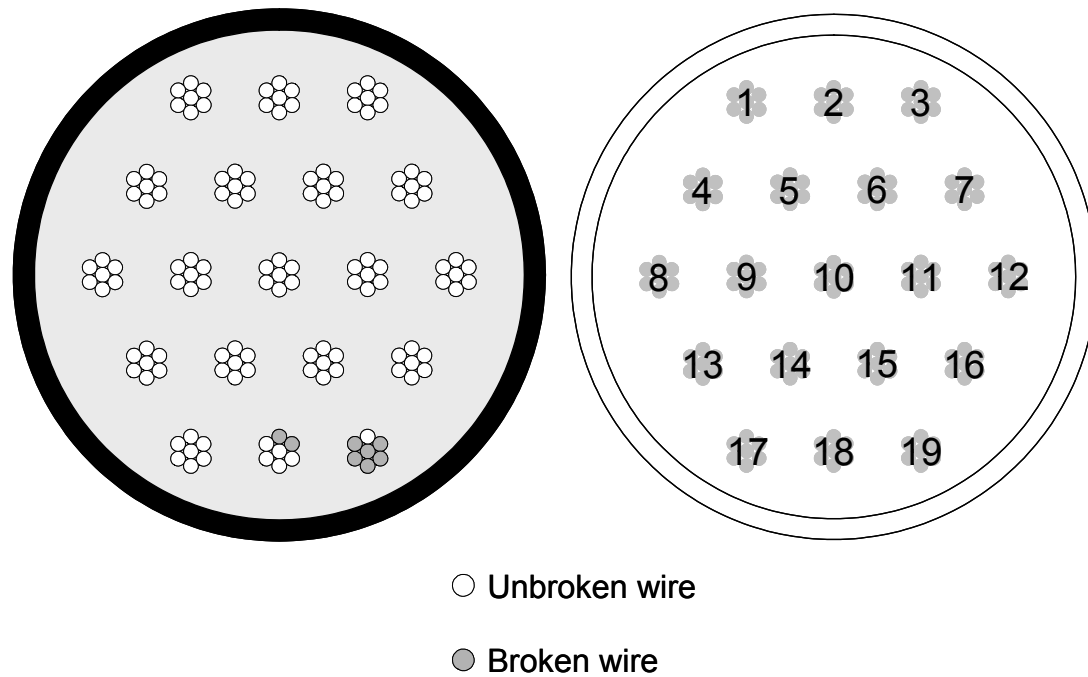


Figure 4-98: Wire breaks near the deck anchorage - Specimen 10

DECK

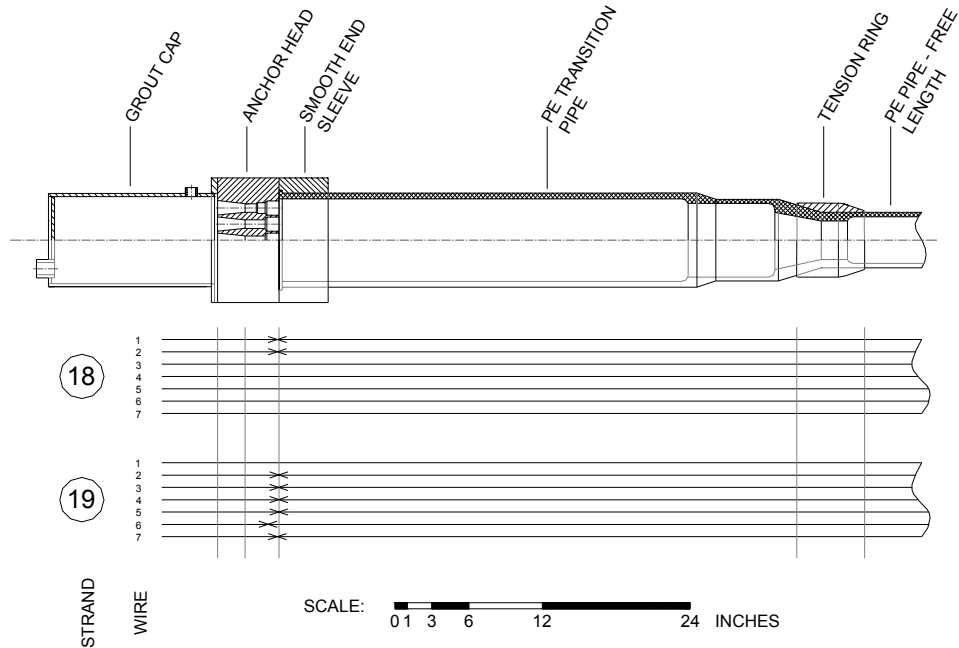


Figure 4-99: Location of wire breaks relative to deck anchorage - Specimen 10

4.2.6.4 Wire Break Characteristics

The wire breaks on Specimen 10 were classified as shown in Figure 4-100. Fretting between adjacent outer wires was the dominant failure mechanism at the deck end as well as at midspan. At the tower end, an equal number of failures were attributed to fretting between adjacent outer wires and fretting between the center wire and an outer wire. Only one wire broke due to fretting fatigue at the wedge. Figure 4-101 shows that fretting between adjacent outer wires was the dominant failure mechanism for the specimen as a whole.

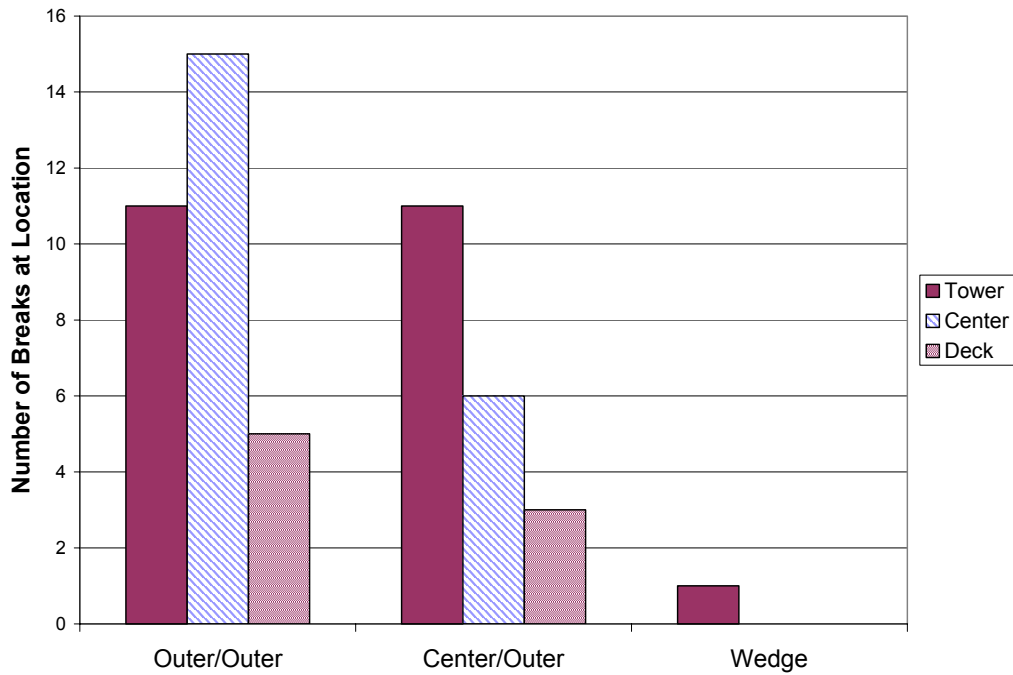


Figure 4-100: Observed fretting fatigue mechanisms - Specimen 10

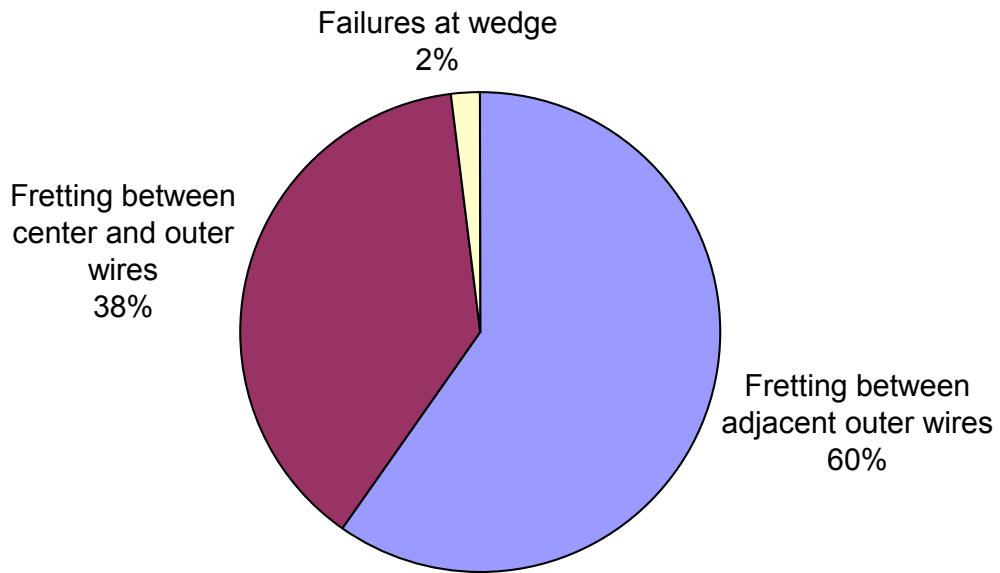


Figure 4-101: Distribution of failure mechanisms - Specimen 10

4.2.6.5 Lateral Stiffness

The lateral stiffness of Specimen 10 was monitored throughout the fatigue test by recording the load required to reach the desired displacement of ± 1.1 in. on a daily basis. Figure 4-102 shows the peak load required to reach the maximum upward and downward displacement during the fatigue test of the specimen. The vertical lines on this plot represent each wire break reported by Soundprint. The data presented represents only that portion of the test where the maximum midspan displacement was ± 1.1 in. For the first 2,220 cycles the maximum displacement was ± 2.1 in. but no wire breaks occurred during this portion of the test.

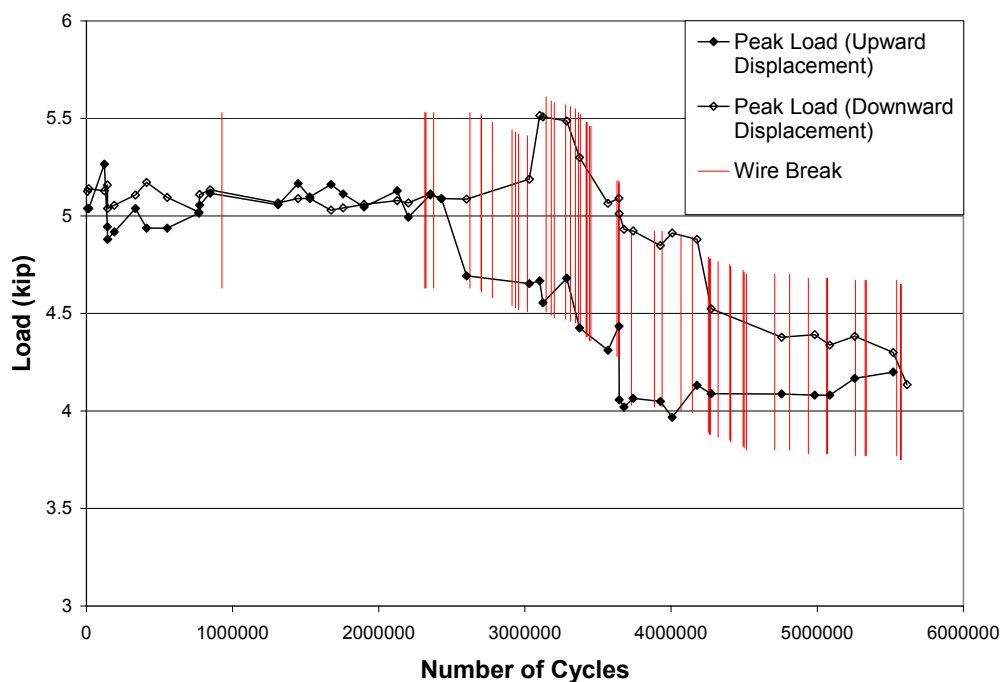


Figure 4-102: Average load during the fatigue test - Specimen 10

Figure 4-103 presents the static test data from Specimen 10. The initial static test was performed with a maximum midspan displacement of ± 2.1 in. The

final static test was performed with a maximum midspan displacement of ± 1.1 in. The stiffness decreased by 17% from 4.8 kip/in. to 4.0 kip/in.

A free-vibration test was performed on Specimen 10 before and after cycling to determine the natural frequency of the stay. The initial natural frequency was 13.0 Hz and the final natural frequency was 11.8 Hz (Table 4-1), a decrease of 9%.

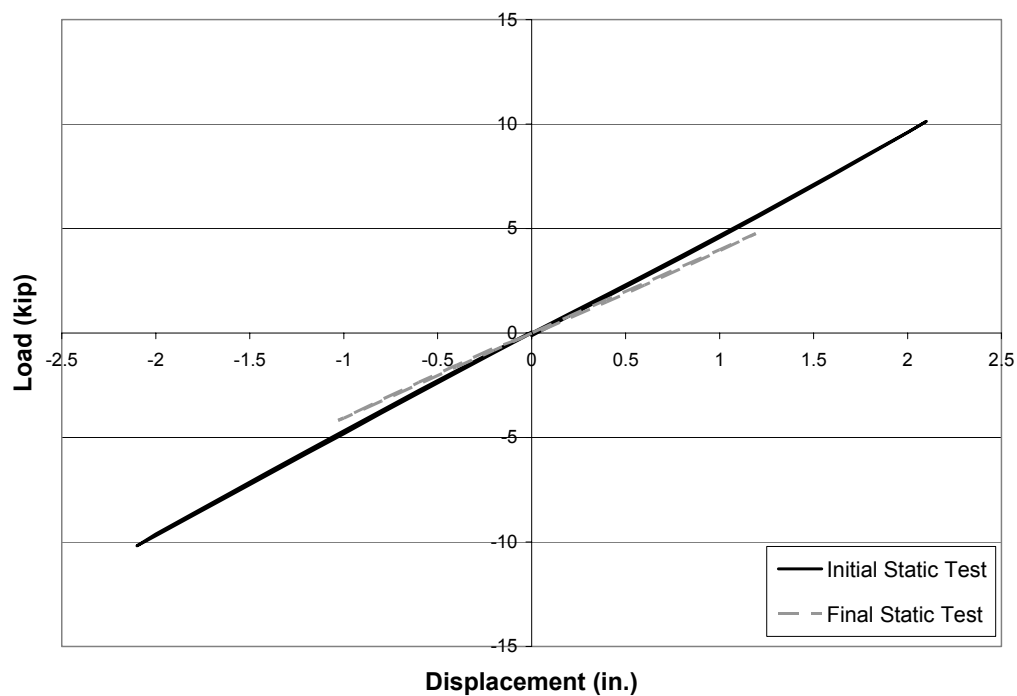


Figure 4-103: Load - displacement response from static test data - Specimen 10

CHAPTER 5

Analysis of Results

The results of ten full-scale, cable-stay fatigue tests were documented in Chapter 4. Combined, the specimens withstood more than 47,000,000 loading cycles and sustained nearly 500 wire breaks. This chapter compares the response of the specimens and investigates the reliability of the acoustic monitoring system used to identify wire breaks during the fatigue tests.

5.1 EFFECT OF TESTING VARIABLES

The influence of five parameters was evaluated experimentally during the fatigue tests (Table 2-1). The primary parameters were the type of strand, presence of grout, amplitude of the imposed midspan displacements, number of strands, and orientation of the stressing end. While not all these parameters represent realistic conditions for cable stays, they provided valuable information about the parameters that influence fatigue performance.

The first six specimens were constructed using Strand A, and the final four specimens were constructed using Strand B. The two types of strand were manufactured by different producers. Strand B was specifically designed for cable-stay applications, while Strand A was not. The influence of the strand on the fatigue response of the specimens is described in Section 5.1.1.

Eight of the ten specimens were grouted along their entire length using a portland cement grout, while the remaining two specimens were ungrouted, except for a short section near midspan. The influence of the grout on the fatigue response is discussed in Section 5.1.2.

Eight of the specimens were subjected to midspan displacements of ± 1.6 in. A displacement range of ± 1.1 in. was used for the other two specimens. The

influence of the displacement amplitude on the fatigue response is discussed in Section 5.1.3.

Among the grouted specimens, grout was always pumped from the deck end toward the tower end. In most cases, the strands were stressed at the tower end; however, two of the specimens were stressed at the deck end. The influence of the orientation of the stressing end on the fatigue response is discussed in Section 5.1.4.

Nine of the specimens were constructed with 19 strands. This configuration represents the smallest diameter cable in the Fred Hartman Bridge. One specimen was constructed with 13 strands to provide information on the influence of strand and grout on the stiffness of the stay cable. These results are presented in Section 5.1.5.

The behavior of nominally identical specimens is compared in Sections 5.1.1 through 5.1.5. Because the duration of the fatigue tests varied for each specimen, the condition of the specimens is evaluated after the same number of cycles.

5.1.1 Type of Strand

Two types of strand were used to construct the full-scale test specimens. Both types were 0.6-in. diameter, seven-wire prestressing strand, but type B was specifically manufactured for cable-stay applications. The condition of Specimens 2, 7, and 9 is presented in Table 5-1 after 2,250,000 loading cycles. The only intended difference among the specimens was the type of prestressing strand. Specimen 2 was constructed with Strand A, and Specimens 7 and 9 were constructed with Strand B.

Table 5-1: Comparison of strand type

Stay	Strand Type	Number of Cycles	Number of Wire Breaks		
			Tower	Center	Deck
2	A	2,250,000	33	8	1
7	B	2,250,000	33	59	16
9	B	2,250,000	11	49	3

The two specimens constructed with Strand B tended to experience more wire breaks than the specimen constructed with Strand A after a comparable number of cycles. This result was not expected, because the in-air fatigue behavior of Strand B was superior to that of Strand A (Figure 3-8).

The data in Table 5-1 also suggest that specimens built with Strand B have a higher tendency for wire breaks to occur in the center. However, this observation may be more representative of geometry of the attachment used to connect the loading apparatus to the specimen than the type of strand. For example, Specimen 3 also experienced a large number of wire breaks near midspan. Because three different configurations of the attachment were used during the series of ten fatigue tests, the number of wire breaks at the center is not considered to depend only on the type of strand.

5.1.2 Presence of Grout

The grout appears to reduce the fatigue life of the specimens. Specimens 5 and 8 were nominally identical to Specimens 2 and 7, respectively. Specimen 5 sustained more than 5 million cycles without a single wire break, while Specimen 2 experienced 52 wire breaks near the anchor heads after only 2.8 million cycles (Table 5-2). Similarly, Specimen 8 experienced 4 wire breaks near the anchor heads after 6.2 million cycles, while Specimen 7 experienced 54 wire breaks near the anchor heads after 2.2 million cycles (Table 5-3). Although the mechanism

by which the grout influences the fatigue performance of the strand is not known, the trend is clear and was reproduced with both types of strand.

Table 5-2: Comparison between Specimen 2 and Specimen 5

Stay	Grout	Number of Cycles	Number of Wire Breaks		
			Tower	Center	Deck
2	Grouted	2,865,000	51	16	1
5	Ungouted	5,211,000	0	0	0

Table 5-3: Comparison between Specimen 7 and Specimen 8

Stay	Grout	Number of Cycles	Number of Wire Breaks		
			Tower	Center	Deck
7	Grouted	2,247,000	37	65	17
8	Ungouted	6,201,000	2	0	2

5.1.3 Amplitude of Imposed Displacements

The amplitude of the displacements imposed at midspan during the fatigue tests influenced the number of wire breaks at the ends of the specimens. As indicated in Table 5-4, reducing the displacement amplitude by approximately 30% led to a dramatic reduction in the number of wire breaks.

Table 5-4: Comparison of displacement amplitude

Stay	Displacement Amplitude	Strand Type	Number of Cycles	Number of Wire Breaks		
				Tower	Center	Deck
2	1.6 in.	A	2,600,000	40	11	1
4	1.1 in.	A	2,600,000	0	0	0
9	1.6 in.	B	2,600,000	12	61	3
10	1.1 in.	B	2,600,000	2	2	0

In addition, the number of cycles sustained before first wire break occurred was also affected (Table 5-5). Specimen 4, tested at the lower displacement amplitude, sustained over six times as many cycles as Specimen 2 before the first wire fractured. Specimen 10 sustained over twice as many cycles as Specimen 9 before the first wire break. However, Specimen 10 was tested at a

displacement of ± 2.1 in. for the first 2,100 cycles of the fatigue test, which may have accelerated fatigue cracking. Thus, wire breaks may have occurred earlier in Stay 10 than if the entire test had been run at the amplitude of ± 1.1 in. The response at the tower ends of Specimens 2 and 4 is compared in Figure 5-1.

Table 5-5: Number of cycles to first wire break

Stay	Displacement Amplitude	Number of Cycles to First Break
2	1.6 in.	422,466
4	1.1 in.	2,831,873
9	1.6 in.	385,970
10	1.1 in.	926,871

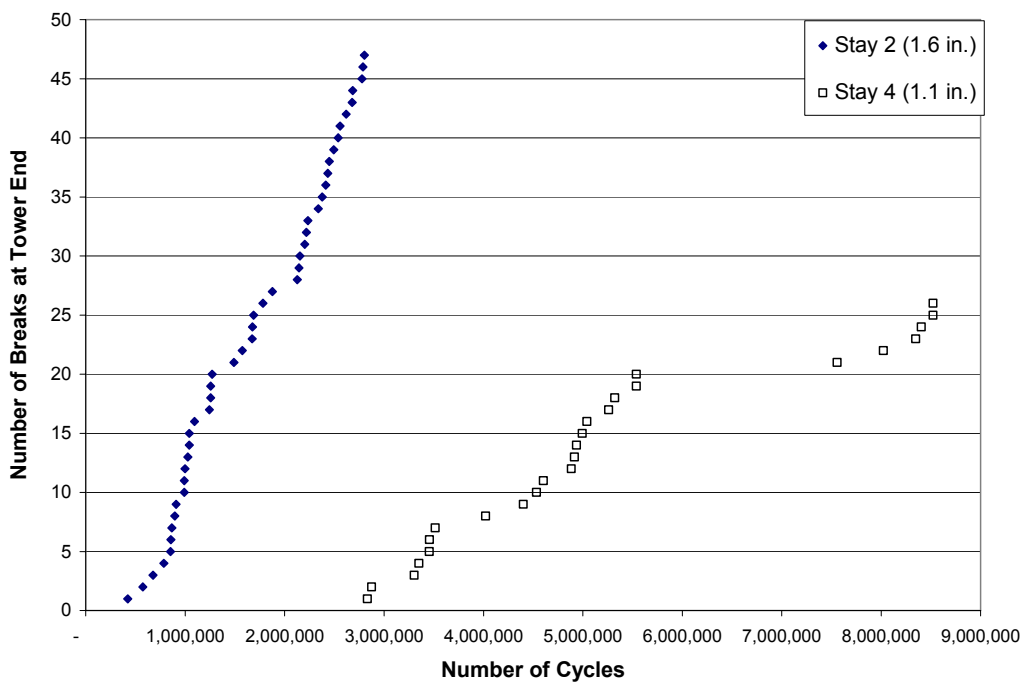


Figure 5-1: Comparison of specimens with different displacement amplitudes

5.1.4 Orientation of Stressing End

Based on the data presented in Chapter 4, more wire breaks are typically found at the tower end than at the deck end. However, for a majority of the specimens, the tower end is not only the end elevated during grouting but also the end from which the cable was stressed. This was done because stressing from the tower end more closely resembles the construction process in the field. Specimens 3 and 4 were stressed from the deck end to attempt to separate the influence of the grouting from the stressing.

Table 5-6 compares Specimens 4 and 10, which both consisted of 19 strands and were both fully grouted. Both specimens were tested at the same amplitude. At the deck end and at the center, Specimen 4 experienced fewer breaks than Specimen 10. No appreciable difference was seen in the overall number of breaks at the tower ends of the specimens. However, the other specimen that was stressed from the deck end (Specimen 3) was the only specimen that experienced more wire breaks at the deck end than the tower end. These results are not conclusive. Based on the available data, it is not possible to determine the influence of the stressing end.

Table 5-6: Comparison of stressing end

Stay	Stressing End	Number of Cycles	Number of Wire Breaks		
			Tower	Center	Deck
4	Deck	5,600,000	19	0	0
10	Tower	5,600,000	23	21	8

5.1.5 Number of Strands in the Cross-Section

Specimen 6 was constructed with only 13 strands to investigate the effect of changing the section modulus of the cable stays. Table 5-7 presents the number of wire breaks after 2,250,000 cycles for three specimens.

Table 5-7: Comparison of number of strands

Stay	No. of Strands	Strand Type	Number of Cycles	Number of Wire Breaks		
				Tower	Center	Deck
6	13	A	2,250,000	7	0	0
2	19	A	2,250,000	32	8	1
7	19	B	2,250,000	37	65	17

Nearly all of the wire breaks in grouted specimens occurred in the outer layers of strands, and a few occur in the second layers of strands (Figure 5-2). Because Specimen 6 had two fewer strands in the outer layers and four fewer strands in the second layers, the number of wire breaks is expected to be less in Specimen 6. However, the number of wire breaks experienced by Specimen 6 was considerably less than would be anticipated by the decrease in the number of strands.

However, the number of strands does relate directly to the lateral stiffness of the specimen. Comparing Specimen 6 and Specimen 2, a 37% decrease in stiffness was observed. This correlates to approximately 13/19, which accounts for the decrease in the number of strands.

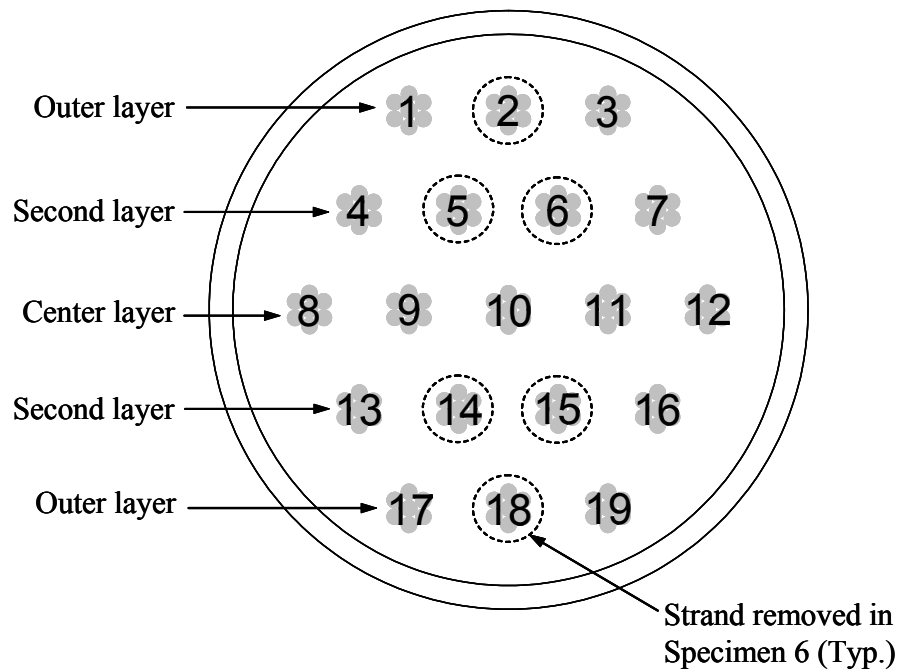


Figure 5-2: Cross-section of specimen

5.2 STIFFNESS COMPARISON

There are various means of determining the stiffness of a cable-stay specimen. One way to determine the stiffness is from a static load-displacement test. Another indication of stiffness is the measured natural frequency determined by a free-vibration test. Table 5-8 presents a comparison between static stiffness and natural frequency for the full-scale cable-stay test specimens. Not all test specimens are presented. Specimens 1 through 4 are not presented because of lack of sufficient data and Specimen 9 is not presented because the cable sustained over 800,000 loading cycles between the final static stiffness test and the final free-vibration test.

Table 5-8: Comparison of cable stiffness

Stay	Initial Static Stiffness	Final Static Stiffness	Difference in Static Stiffness	Initial Natural Frequency	Final Natural Frequency	Difference in Natural Frequency	Total Number of Wire Breaks
	(kip/in)	(kip/in)	(%)	(Hz)	(Hz)	(%)	
5	4.1	3.9	4.9	13.8	13.5	2.0	0
6	3.3	3.0	8.4	11.5	11.0	4.5	28
7	5.0	3.4	31.6	13.3	11.1	16.4	119
8	4.1	3.9	4.9	13.9	13.4	3.4	4
10	4.8	4.0	16.7	13.0	11.8	9.2	52

Assuming that the cable behaves like a string, the natural frequency can be calculated by Equation 5.1, where T is the tension on the cable, ρ is the mass per unit length of the specimen, and L is the length. Theoretically, as the tension decreases, the natural frequency of the specimen decreases by the square root of the change in tension. For a perfect string, the loss in tension is proportional to the decrease in static stiffness.

$$\omega = \sqrt{\frac{T}{\rho L^2}} \quad (5.1)$$

However, the cable stay specimens can not be modeled as a simple string, because the ends of the specimen are restrained against rotation. Therefore, the flexural response of the test specimens must also be considered.

In an ideal beam, the natural frequency is related to the bending stiffness of the specimen as shown in Equation 5.2, where E is the modulus of elasticity and I is the moment of inertia.

$$\omega = \frac{\pi}{L^2} \sqrt{\frac{EI}{\rho}} \quad (5.2)$$

As wires break during a fatigue test, the natural frequency is influenced by both the loss in tension and the loss in moment of inertia of the cross-section. These effects are not proportional to one another, as the moment of inertia is

affected by both the loss in area as well as the distance from the neutral axis to the broken wire. In contrast, the loss in tension does not depend on the position of the broken wire.

The two ungrouted specimens experienced only a modest number of wire breaks and the corresponding decrease in tension was minimal. For these specimens, the change in natural frequency was approximately equal to the square root of the change in the static stiffness. This observation suggests that the ungrouted specimens behaved primarily as strings.

In contrast, the grouted specimens were expected to experience a combination of beam and string response. The change in frequency for the grouted specimens was larger than the square root of the change in static stiffness. Because these specimens experienced a larger number of wire breaks than the ungrouted specimens, they also experienced a larger decrease in tension. However, the corresponding loss in tension was not proportional to the decrease in static stiffness. No clear relationship is evident between the change in natural frequency and the change in static stiffness for the grouted specimens.

5.3 LOCATION OF WIRE BREAKS

The location of wire breaks along the length of the test specimen provided valuable information about the fatigue behavior of stay cables. As discussed in Section 5.3.1, the wire breaks from all ten fatigue tests were concentrated near the ends of the stay and directly under the loading apparatus. Wire breaks that occurred inside the anchor head as a result of a stress concentration at the wedge are discussed in Section 5.3.2.

Acoustic sensors provided by Soundprint were used to monitor the number and location of wire breaks during the fatigue tests. The reliability of this real-time monitoring system is discussed in Section 5.3.3.

5.3.1 Location of Wire Breaks

All the wire breaks in the full-scale fatigue tests occurred within two feet of the anchor heads or at midspan near the loading apparatus. The wire breaks at midspan may be attributed to the loading apparatus and are not considered to be representative of conditions in the field. No wire breaks were found along the free length of the specimens. The distribution of wire breaks and the geometry at the ends of the specimens are presented in Figure 5-3 and Figure 5-4. The wire break distribution and geometry at midspan is presented in Figure 5-5 and Figure 5-6.

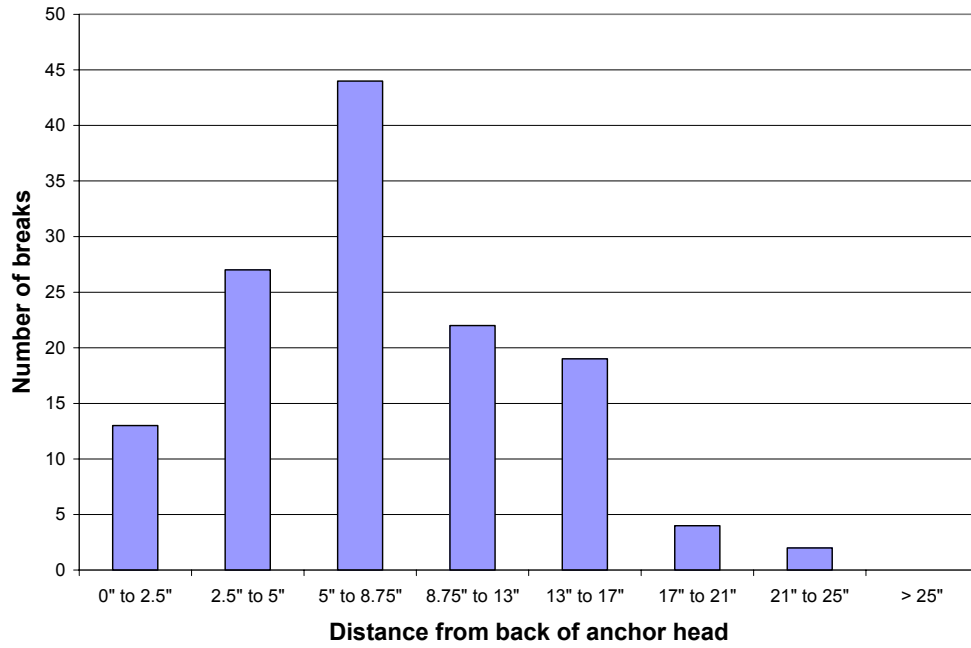


Figure 5-3: Location of wire breaks at ends of stay

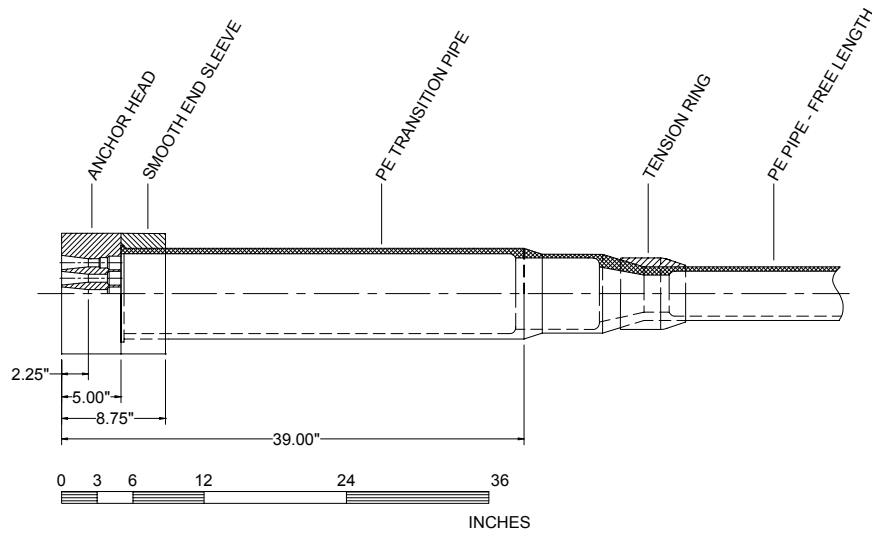


Figure 5-4: Geometry at end of stay

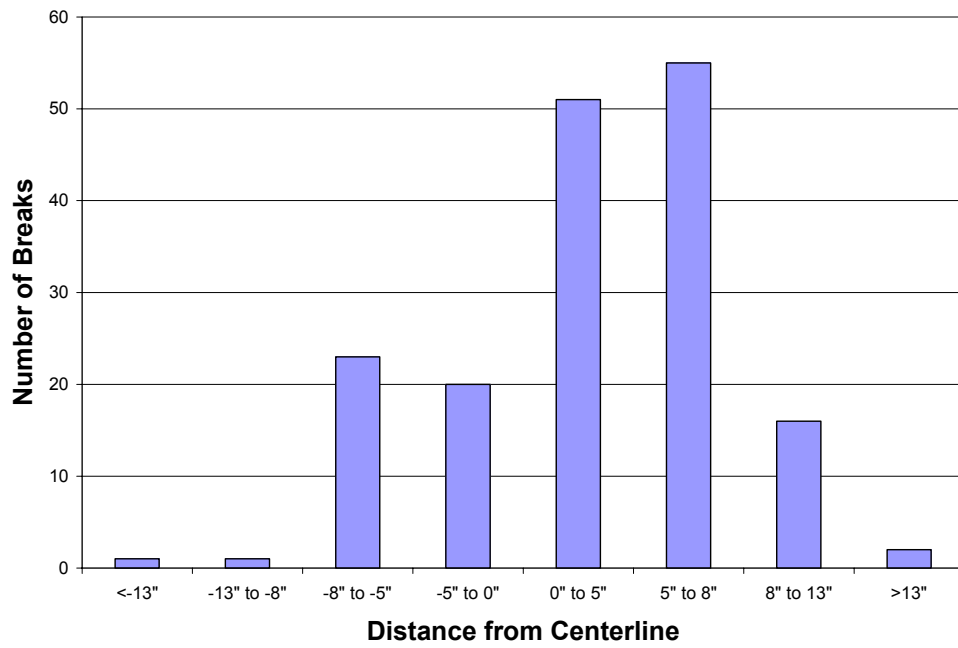


Figure 5-5: Location of wire breaks at center of stay

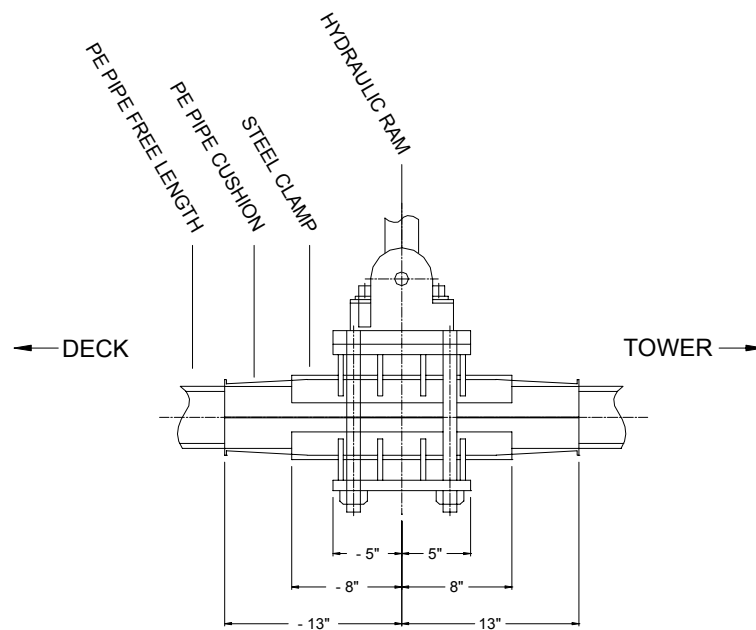


Figure 5-6: Geometry at center of stay

Despite the severe fretting between strands at the tension ring, no wire breaks were observed in this region. This indicates that fretting between wires, which was the source of nearly all the wire breaks both near the ends and at midspan, is more detrimental to the cable than fretting between the strands.

Overall, more wire breaks occurred at the tower end of stays than at the deck end. This was true for all specimens and experimental parameters. As the breaks at midspan were not representative of field conditions, the condition of the cable at the tower end should be used to determine the fatigue life of the specimens.

5.3.2 Wire Breaks at Wedges

Wire breaks at the wedges are more likely to occur at the end from which the cable was stressed. Throughout the full-scale tests, 19 wire breaks were caused by the wedges; only five wire breaks were found at the wedges on the dead end of the specimen. Wire breaks which occur near the wedges on the dead end are typically caused by inter-wire fretting rather than the stress concentration of the wedge tooth.

5.3.3 Soundprint Comparison

The Soundprint system is considered to provide an accurate estimate of the number of wire breaks in the large-scale fatigue specimens. Soundprint reported the correct number of breaks for Specimens 5, 6, 8, and 10. For Specimen 7, five wire breaks were found that were not reported by Soundprint. Soundprint reported one wire break that was not found on Specimen 9. Even with these slight discrepancies, the system is considered to be accurate.

When Soundprint detects a wire break along the specimen, the distance between the break and the three nearest sensors is reported. In the case of the ungrouted specimens, the distance between the break and each of the two sensors

is reported. Because the order in which wires breaks occur is not evident during the autopsy investigation, a wire-by-wire location comparison is not possible. However, general accuracy can be determined by considering the range over which wire breaks occurred.

The system tends to be more accurate at locating wire breaks when they do not occur near sensors. Along the free length (near the center of the test specimen) the Soundprint distance was generally accurate within 6 in. Near the ends of the cable, the system was generally accurate within 18 in. Breaks occurring in the anchor head (wedge breaks) directly beneath sensors were not accurately located.

Figure 5-7 and Figure 5-8 present a graphical comparison of the Soundprint data with the data recording during the autopsy. Specimens 1, 6, 7, 9, and 10 are included. The ungrouted specimens were not included. At the ends of the stay, Soundprint tends to overestimate the distance of the wire breaks from the anchorage. Under the load point, Soundprint generally places the breaks in the correct region.

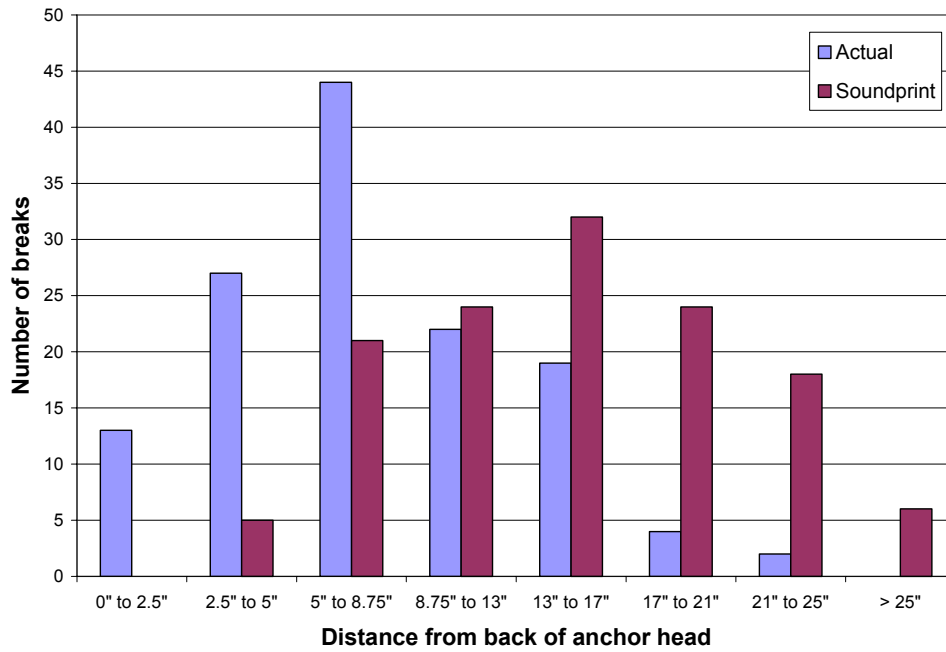


Figure 5-7: Soundprint comparison at ends of stay specimens

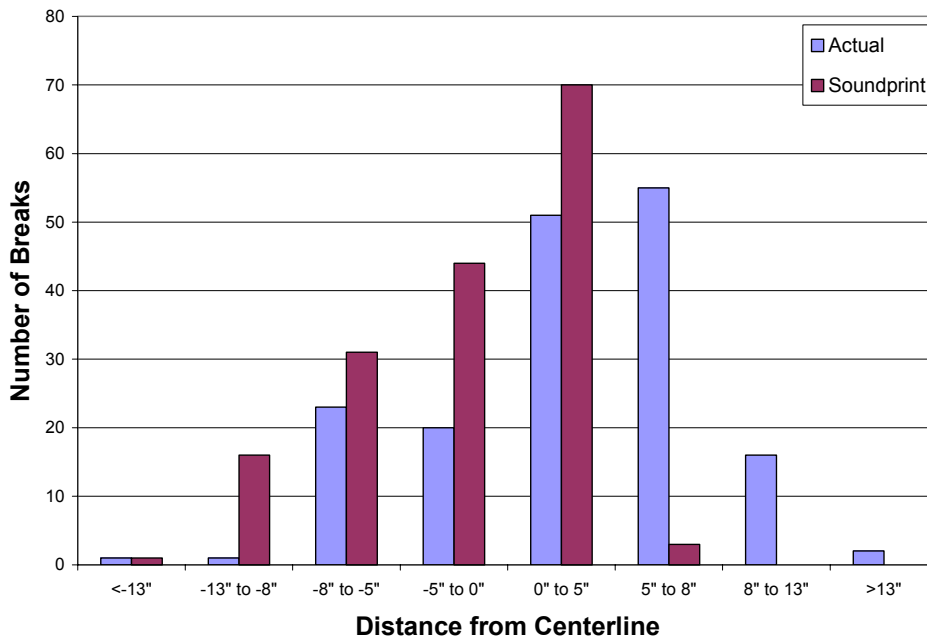


Figure 5-8: Soundprint comparison at midspan of stay specimens

CHAPTER 6

Conclusions

This chapter presents conclusions drawn from the observation of ten full-scale cable-stay test specimens.

6.1 SUMMARY

Large-amplitude vibrations of the stay cables on the Fred Hartman Bridge were first observed during construction and have continued since the bridge opened to traffic in 1995. Evidence of the damage caused by these vibrations includes fatigue failures of the original cable restrainers and numerous weld fractures at the connections between the anchorage boxes and guide pipes at the deck level. The Texas Department of Transportation was concerned that these vibrations had caused fatigue damage within the stays; however, methods do not exist to evaluate this damage in situ. Nondestructive tests to identify wire breaks are still under development and visual inspection is not possible. Therefore, TxDOT funded a series of large-scale laboratory fatigue tests to study the response of stay cables subjected to transverse loading. TxDOT also installed an acoustic monitoring system on the Fred Hartman Bridge in order to identify damage as it occurs.

A total of ten, large-scale fatigue test of stay cables have been performed in the Ferguson Structural Engineering Laboratory. The geometry of the anchorage zone for the specimens was modeled after the shortest stays on the Fred Hartman Bridge. Eight of the specimens were grouted along their entire length using a portland-cement grout to reproduce the configuration in the field. Two of the specimens were not grouted. This configuration was originally selected to obtain experimental data on the influence of the grout on the

transverse stiffness of the stay cables. However, the ungrouted specimens provided evidence that the grout also influences the fatigue life of the stay cables.

The conclusions from the large-scale fatigue tests are summarized below. Ongoing research is aimed at developing analytical models to relate the results from these laboratory tests to the condition of the stays in the field.

- The wire breaks in the large-scale fatigue specimens occurred in two locations: within two feet of the anchor head and at midspan near the attachment to the hydraulic actuator. No wire breaks were observed along the free length of the specimens. Wire breaks located near the load point are a direct consequence of the test setup and are not representative of the conditions to which the actual stay cables are subjected. Therefore, wire breaks in the field are expected to be concentrated near the anchor heads. Although the contact stresses among strands are highest at the tension ring, no wire breaks were observed at this location. Severe fretting between wires has been observed near the tension ring, but the fretting did not lead to wire breaks.
- The grout appears to have a negative influence on the fatigue performance of the stay cables. Specimens 5 and 8 were ungrouted and were otherwise nominally identical to Specimens 2 and 7, respectively. Specimen 5 experienced no wire breaks after over 5 million cycles and Specimen 8 experienced only 4 wire breaks after over 6 million cycles. All grouted specimens tested at the same amplitude experienced more wire breaks than did the ungrouted specimens. Although the mechanism by which the grout influences the fatigue performance of the strand is not known, the trend is clear.

- Among the eight grouted specimens, 191 wire breaks were observed at the tower end of the specimens (end that is elevated during grouting), while only 46 wire breaks were observed at the deck end of the specimens. Again, the mechanism that explains this observation is not known. It has been observed, however, that wires often break near the wedges on the tower (stressing) end of the test specimens, while wire breaks are rarely found near the wedges on the deck (dead) end of the specimens.
- Within the grouted specimens, wire breaks tend to occur near the top and bottom of the cross section. These regions experience the highest bending stresses if strains are assumed to vary linearly with depth. Only three wire breaks were observed within the middle layer of strands, and all occurred in Specimen 8, which was ungrouted.
- Large amounts of corroded fretting product were observed in the vicinity of the tension ring and wearing of the strands was observed. However, these phenomena did not generate wire breaks. Very little corrosion product was observed along the length of the ungrouted specimens.
- The observed corrosion was much more severe on the grouted specimens compared with the ungrouted specimens. Corrosion tended to be concentrated in the vicinity of wire breaks. On a strand that experienced only one or two wire breaks, corrosion tended to be mild and was due to fretting. Most of the corroded fretting product was limited to the voids between the wires within the strand. However, on a strand that experienced five or more wire breaks at the same location, the corrosion was more severe. In at least one case, pitting corrosion was observed on the exterior of the strand. It is not known if the corrosion forms before the wire breaks and serves as the initiator for the wire break or if the corrosion

forms after the wire breaks and is caused by fretting among the wires. The high pH environment of the portland cement grout does not appear to suppress this type of corrosion.

- The axial fatigue properties of the prestressing strand do not appear to be representative of the bending fatigue response of the stay cables. Strand B nearly satisfied the PTI requirements for stay cables, while Strand A clearly failed the tests. However, the specimens constructed using Strand A experienced fewer wire breaks than the specimens constructed using Strand B.
- The presence of grout influences the stiffness of the stay cable. Based on static tests, the average initial stiffness of 4.7 kip/in. for the grouted, 19-strand specimens is approximately 15% higher than the average initial stiffness of 4.1 kip/in. for the ungrouted, 19-strand specimens.
- The amplitude of vibration has an influence on both the number and location of wire breaks found in the stay cables. Specimens 4 and 10, which experienced a midspan displacement of only ± 1.1 in. during the fatigue tests, experienced fewer wire breaks under the load point than specimens tested with a midspan displacement of ± 1.6 in. although the number of breaks at the ends was comparable. Specimen 4, which was nominally identical to Specimen 2 but was tested at the lower amplitude, experienced 51 wire breaks at the tower end and 16 wire breaks at midspan compared with only 28 wire breaks at the tower anchorage and no breaks at midspan on Specimen 4. Similarly, Specimen 10, nominally identical to Specimen 7, experienced only 23 wire breaks at the tower end and 21 breaks at midspan compared with 37 breaks at the tower end and 65 breaks under the load point on Specimen 7. The vibration amplitude

also influences the fatigue life of the stay cables. A wire break did not occur during the first 2,850,000 cycles of the fatigue test on Specimen 4, which experienced a midspan displacement of ± 1.1 in. A wire break did not occur during the first 927,000 cycles of the fatigue test on Specimen 10, which experienced a midspan displacement of ± 2.1 in. for approximately 2,000 cycles and then a displacement of ± 1.1 in for the remainder of the fatigue test. The specimens that were tested with a displacement amplitude of ± 1.6 in. experienced the first wire break between 300,000 cycles and 667,000 cycles with an average of 460,000 cycles when the first break occurred.

APPENDIX A

Modulus and Tensile Testing of Strand

This appendix presents the details of the material property testing used to determine the elastic modulus and breaking strength of Strand A, used to construct Specimens 1 through 6, and Strand B, used to construct Specimens 7, 8, 9, and 10.

A.1 MODULUS TESTING

The goal of the strand modulus tests was to verify the value of the modulus of elasticity as reported on the mill certificate for the prestressing strand used in the full-scale, cable-stay test specimens. The modulus of elasticity is important in calculating the cross-sectional properties of the test specimens.

The strand modulus is measured by dividing the change in load by the change in average longitudinal strain of the overall specimen. As a seven-wire strand is loaded in tension, the helix of the wires tightens around the center strand before the individual wires experience strain, thus the strain along the axes of the wires is less than the longitudinal strain at the same load. Therefore the overall elongation of the strand during loading must be measured. The extensometer designed and used by Heller (2003) for similar tests was modified for the tests on Strand B presented in this appendix.

A.1.1 Test Program

Strand modulus testing was performed on a total of three specimens of each strand type. The calculated modulus presented in Section 2.2.1 is the average modulus of the three tests for each type.

Each specimen was tested by measuring the load vs. elongation in the range where the strand response remained elastic. Some residual curvature remains in the strand after being removed from the spool, so each specimen was loaded to 10 kips to ensure straightness before load-elongation testing was started. The test involved linearly loading the specimen to 35.5 kip (approximately 60% of GUTS for the strand) and unloading back to 10 kip. These values are well within the elastic range for the strand as shown by the direct tension tests presented in Section A.2. This loading procedure was cycled three times for each specimen.

Due to the limited range over which the LVDTs attached to the extensometer were accurate, only a portion of the load range was used to evaluate the modulus of the strand.

A.1.1.1 Test Setup

Modulus testing was performed in the MTS 220-kip load frame used to perform the axial fatigue tests (Section 3.2.1). Each test was run under load control, with input provided by PC-based software (MTS TestStar II) which was connected to the MTS system. Load and elongation data were taken using LabVIEW data acquisition software, which was programmed to capture the desired data.

Each test was set up in a similar manner to the axial fatigue tests. The extensometer was placed over the specimen before wrapping the ends with 8-gauge solid copper wire and attaching the aluminum grips described in Section 3.2.2. The specimen was centered in the hydraulically-controlled MTS clamps to ensure concentric loading. The setup of a specimen in the MTS load frame is shown in Figure A-1.

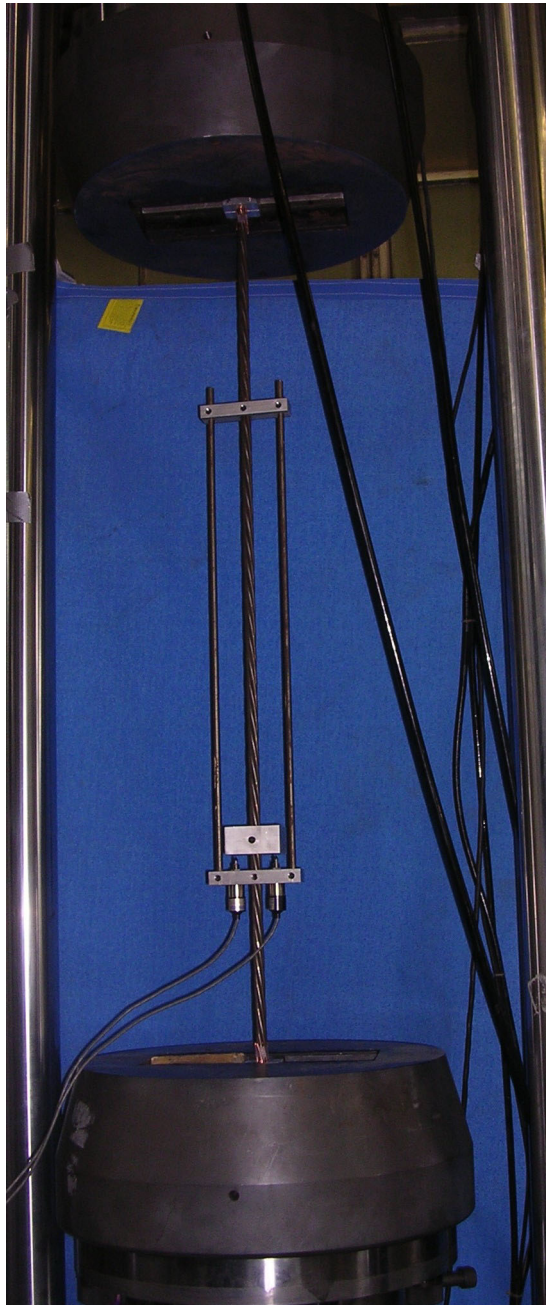


Figure A-1: Setup for modulus testing

A.1.1.2 Extensometer Details

The extensometer used was designed and built by Heller (2003) to test 0.5-in. diameter strand. This extensometer consisted of three aluminum blocks, two steel rods, and two linear variable differential transformers (LVDTs) as shown in Figure A-2. Set screws were used to hold the pieces of the extensometer together. The center hole through which the strand passes on each block was enlarged for the 0.6-in. diameter strand; this was the only modification made to Heller's extensometer for the tests presented in this thesis.

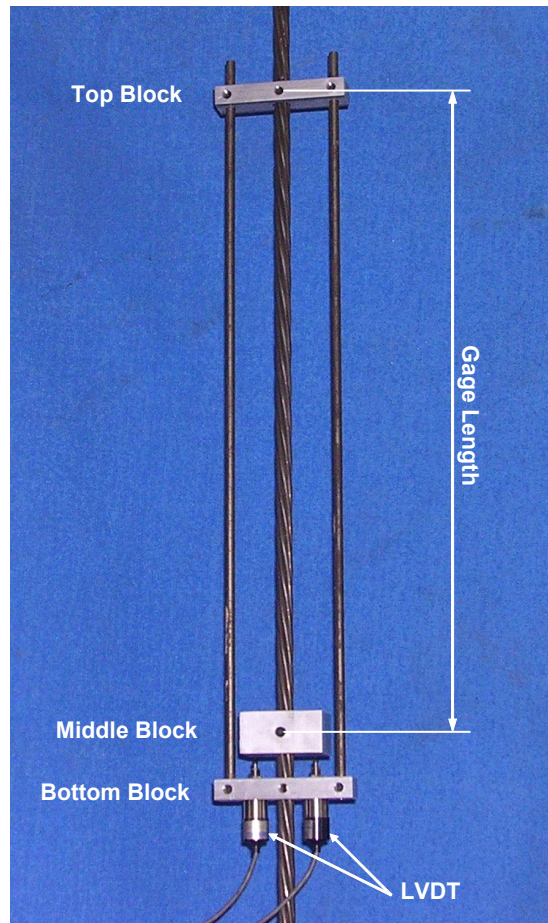


Figure A-2: Full view of extensometer

The function of the extensometer was to measure the longitudinal displacement of the strand over the gage length of 24 in. The top and bottom blocks are fixed in position relative to each other by the two steel rods. As the strand elongates under axial tension, the middle block moves relative to the rest of the extensometer and the displacement is measured and recorded by the LVDTs, which are attached to the bottom block (Figure A-3). Two LVDTs are used to minimize errors caused by block position and rotation. Each LVDT is equidistant from the strand and the values from the two are averaged.

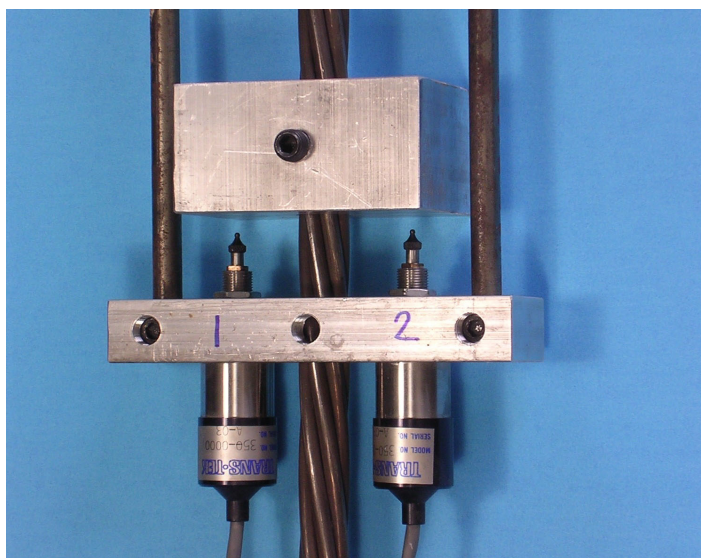


Figure A-3: Bottom portion of extensometer with LVDTs

The two displacement transducers were TRANS-TEK Series 350 General Purpose DC Gaging LVDTs, model number 0350-0000, with a working range of 0.050 in. and an overall travel of 0.16 in. The non-linearity rating was less than 0.50% full scale over the total working range.

Because the accuracy of the modulus test is only as accurate as the LVDTs, each transformer was calibrated with gage blocks before testing. From the calibration curve, the range over which LVDT was accurate was obtained.

The calibration curves for each LVDT are shown in Figure A-4 and Figure A-5. The LVDT reads a voltage, which is then converted to a displacement by the data acquisition software using the slope of the calibration curve, thus the calibration curves show actual displacement due to the gage blocks vs. voltage as reported by the LVDT. The LVDT is considered accurate over the region where slope is constant. The accurate range for each LVDT is shown by vertical lines on Figure A-4 and Figure A-5. From the data presented, LVDT 1 was determined to be accurate in the range of -3V to 3V and LVDT 2 was determined to be accurate over the range of -2V to 4V. When examining the test data, only data points which fell into these ranges were considered in calculating the modulus of the specimen. The 24-in. gage length of the specimen was chosen because it was long enough to provide accurate results but short enough that most of the test data would fall within the accurate range for the LVDTs.

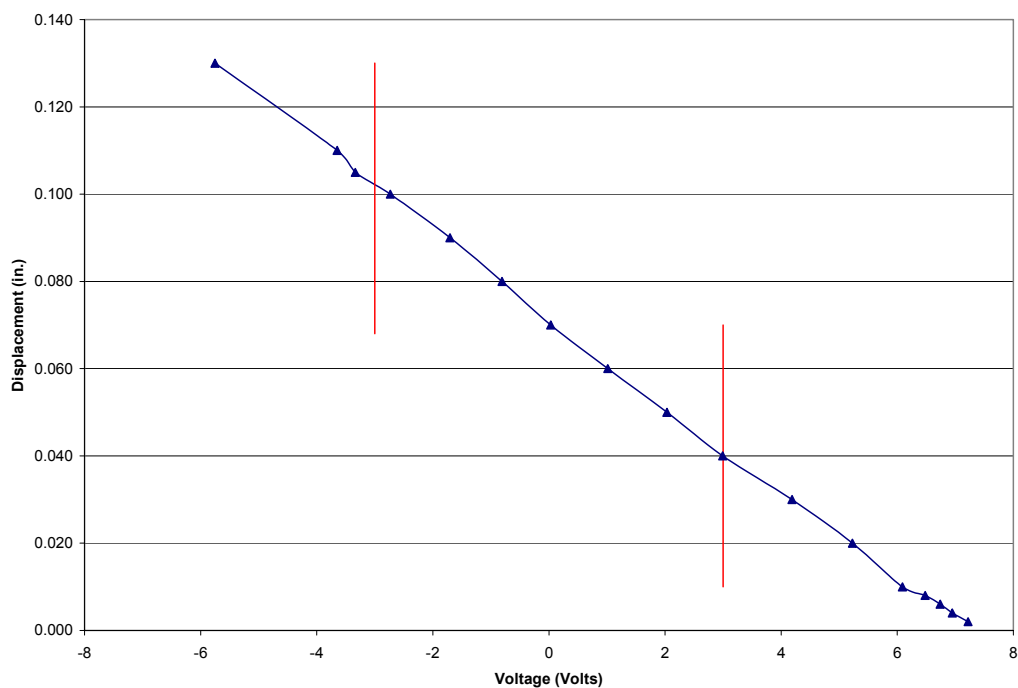


Figure A-4: Calibration curve for LVDT 1

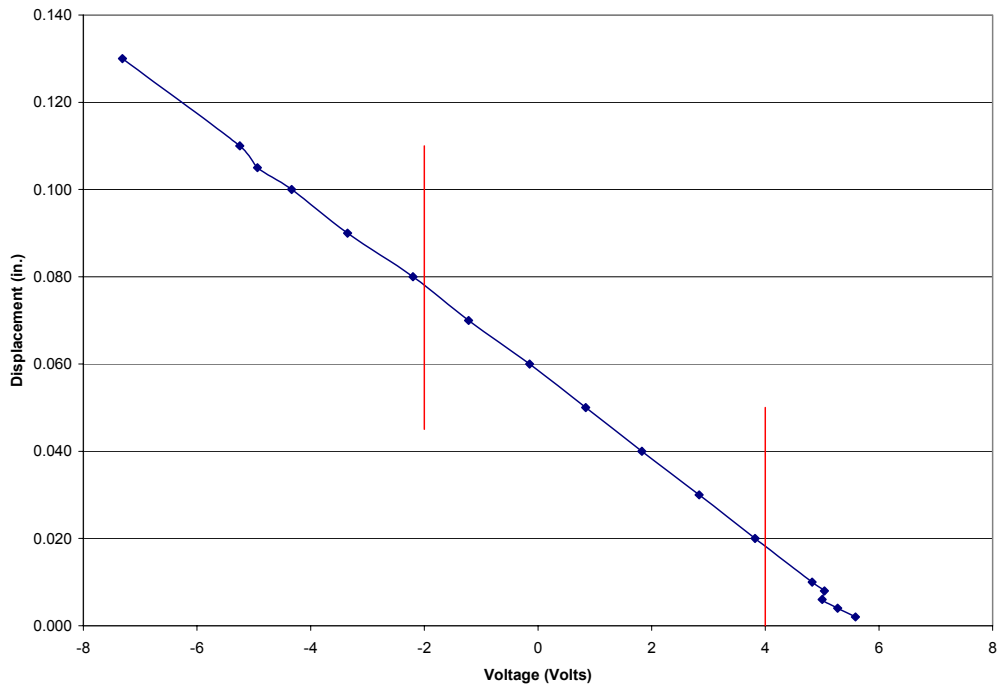


Figure A-5: Calibration curve for LVDT 2

A.1.2 Test Results

After performing a test as described in Section A.1.1 the load vs. displacement data were plotted for each of the two LVDTs, as shown in Figure A-6 for Strand B, Specimen 1. A linear trendline was fit through each set of data and the resulting slope indicated the linear stiffness of the specimen in kip/in. The stiffnesses of the two individual LVDTs were averaged to obtain the overall average stiffness of the specimen. The modulus of elasticity was then calculated by taking the average stiffness of the specimen, k , as determined from the two LVDTs, and multiplying by the gage length, L , divided by the strand area, A , as shown in Equation A.1. The resulting calculated modulus for each test is presented in Table A-1. The average modulus of 28,880 ksi for Strand A varied by 3% from the mill certificate value of 28,000 ksi. The average modulus of

28,630 ksi for Strand B varied by only 1% from the mill certificate value of 28,300 ksi. Both values satisfy the ASTM A 416 minimum of 27,500 ksi.

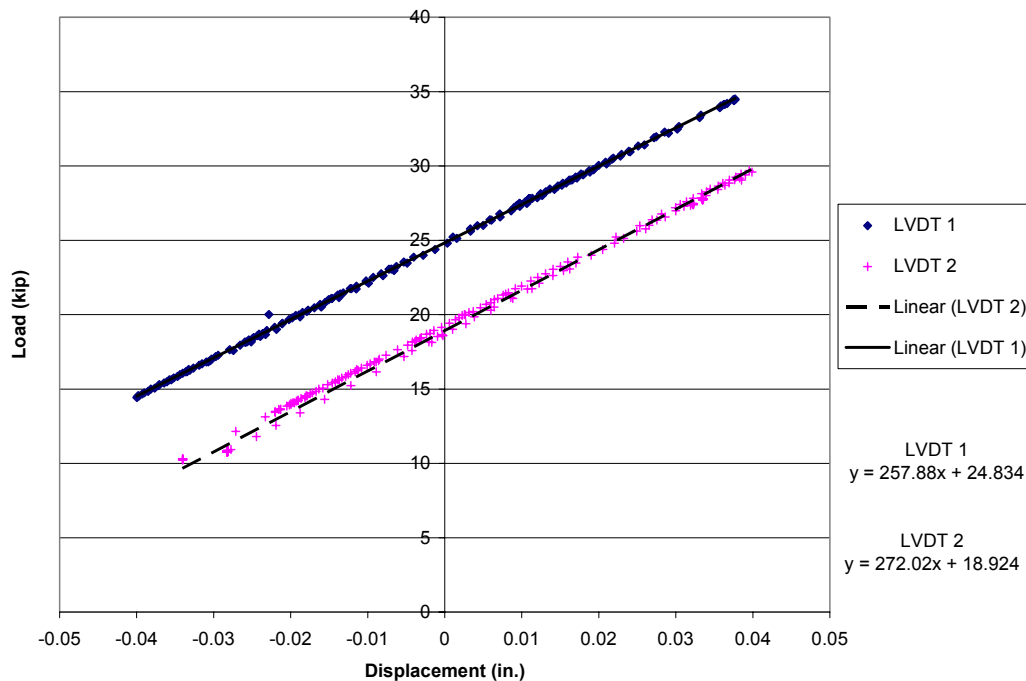


Figure A-6: Load vs. Displacement for Strand B, Specimen 1 modulus test

$$E = \frac{kL}{A} \tag{A.1}$$

Table A-1: Measured modulus of elasticity for prestressing strand

	Elastic Modulus (ksi)	
	Strand A	Strand B
Test 1	29130	28530
Test 2	29090	28650
Test 3	28430	28720
Average	28880	28630

A.2 DIRECT TENSION TESTS

The goal of the direct tension tests was to verify that the strand used to build the full-scale, cable-stay specimens satisfied the provision of ASTM A 416, as well as to verify the value of minimum breaking strength as reported on the mill certificate for the strand. Tensile testing was performed based on the provisions of ASTM E 8.

A.2.1 Test Setup

Three direct tension tests were performed on 48-in long specimens and the results were averaged to determine the breaking strength of the strand. The tensile tests were performed in the same MTS 220-kip load frame used to perform the axial fatigue and strand modulus tests. The strand was gripped and clamped into the load frame at zero load using the same procedure described in Section 3.2.

The test was run under displacement control using MTS TestStar II software with a displacement rate of 0.04 in./sec. This value corresponds to the minimum strain rate prescribed by ASTM E 8 for this type of test. Each specimen was loaded until one or more wires fractured.

A.2.2 Test Results

Table A-2 presents the results of the direct tension tests on each strand.

Table A-2: Results of direct tension tests

	Minimum Breaking Strength (kip)	
	Strand A	Strand B
Test 1	59.2	60.4
Test 2	59.5	60.3
Test 3	59.4	60.5
Average	59.4	60.4

A.2.2.1 Strand A

The load-displacement curves for each of the three tensile tests on Strand A are shown in Figure A-7 through Figure A-9. Part of the linear-elastic response is not shown for Test 2 because the graphical tracking of the load-displacement test was not started at the beginning of the test. The peak load is still visible. During Test 2, the strand experienced some slippage through the aluminum grips during testing which is indicated by several slight load decreases in Figure A-8. The slipping did not affect the resulting failure load.

Table A-2 shows the resulting failure loads of each specimen. The average failure load of 59.4 kip is less than 0.7% different from the value of 59.0 kip as reported on the mill certificate for the strand. Both values satisfy the ASTM minimum of 58.6 kip.

A.2.2.2 Strand B

The load-displacement curves for each of the three tensile tests on Strand B are shown in Figure A-10 through Figure A-12. Part of the linear-elastic response is not shown for Test 3 because the graphical tracking of the load-

displacement test was not started at the beginning of the test. The peak load is still visible.

Table A-2 shows the resulting failure loads of each specimen. The average failure load of 60.4 kip is less than 0.25% different from the value of 60.3 kip as reported on the mill certificate for the strand. Both values satisfy the ASTM minimum of 58.6 kip.

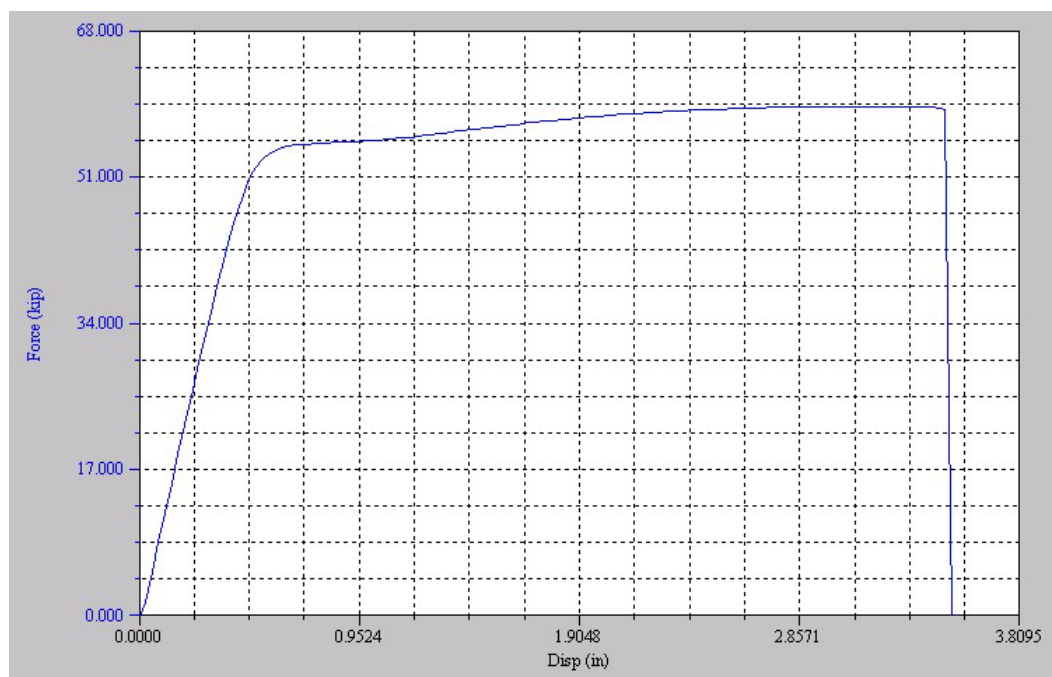


Figure A-7: Load vs. Displacement for Strand A Tensile Test 1

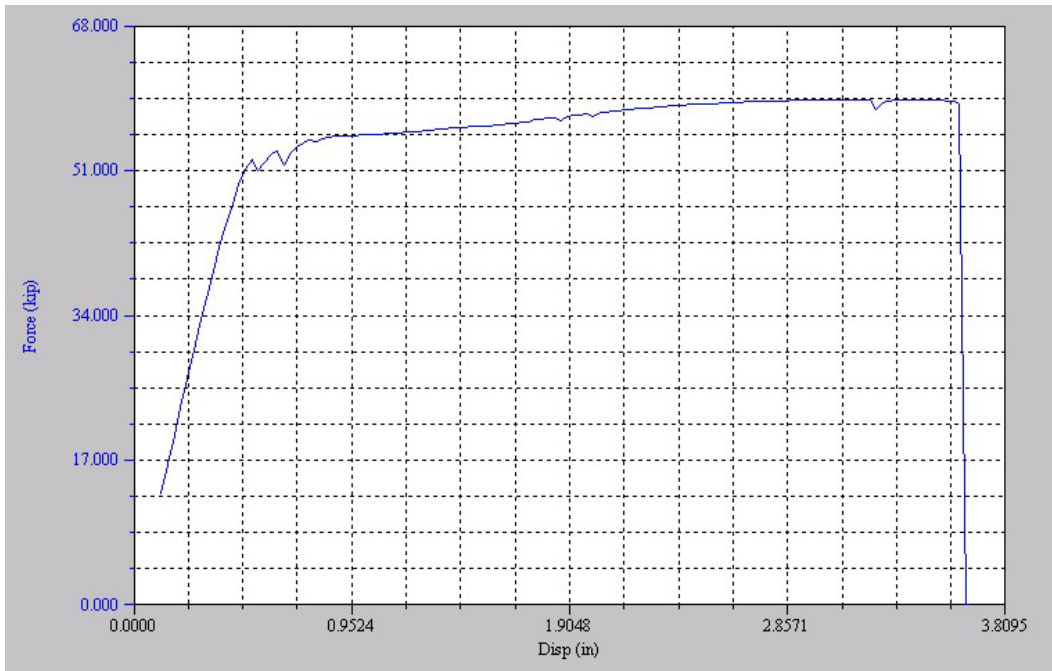


Figure A-8: Load vs. Displacement for Strand A Tensile Test 2

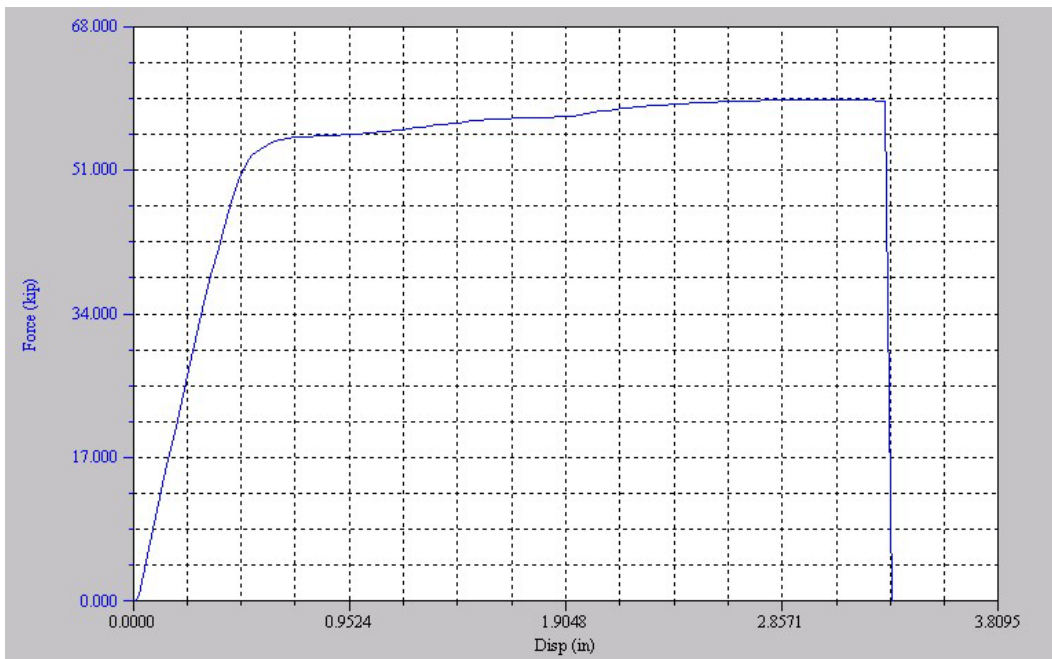


Figure A-9: Load vs. Displacement for Strand A Tensile Test 3

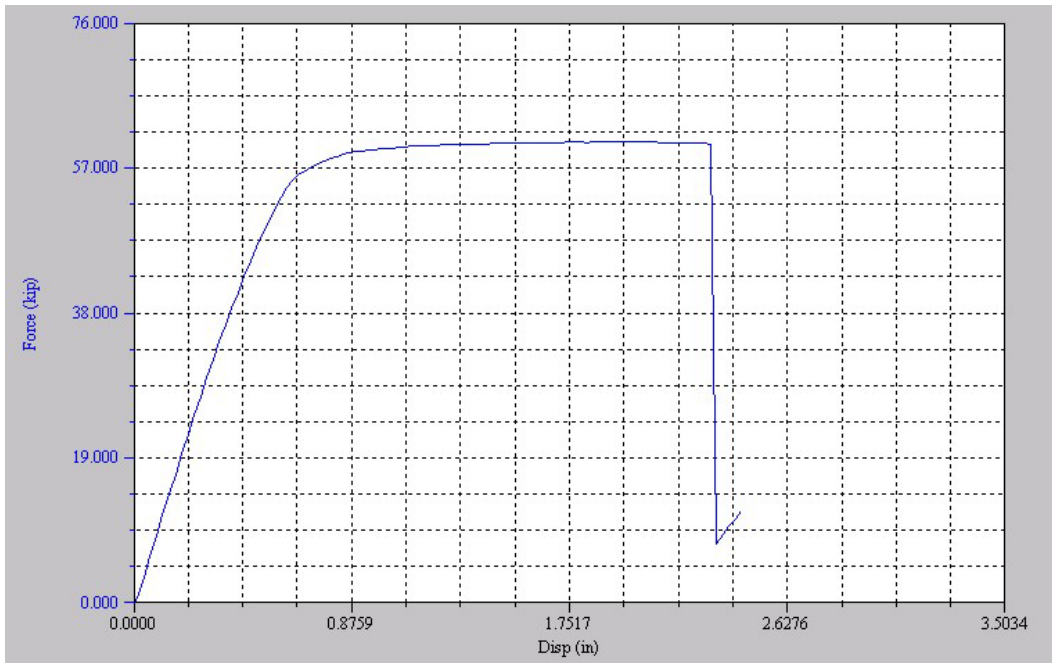


Figure A-10: Load vs. Displacement for Strand B Tensile Test 1

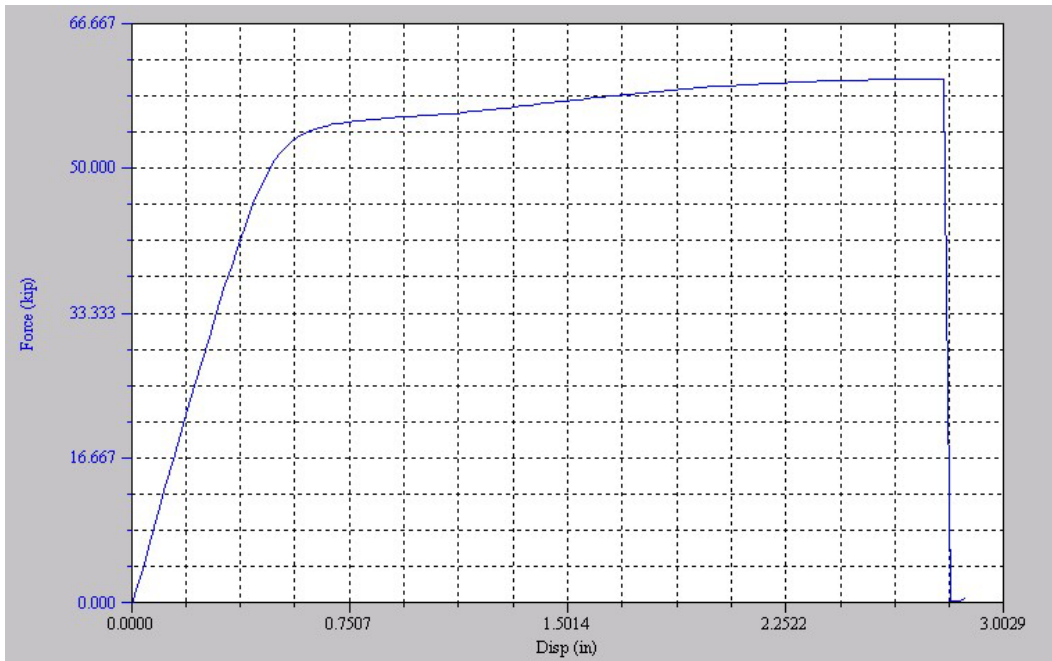


Figure A-11: Load vs. Displacement for Strand B Tensile Test 2

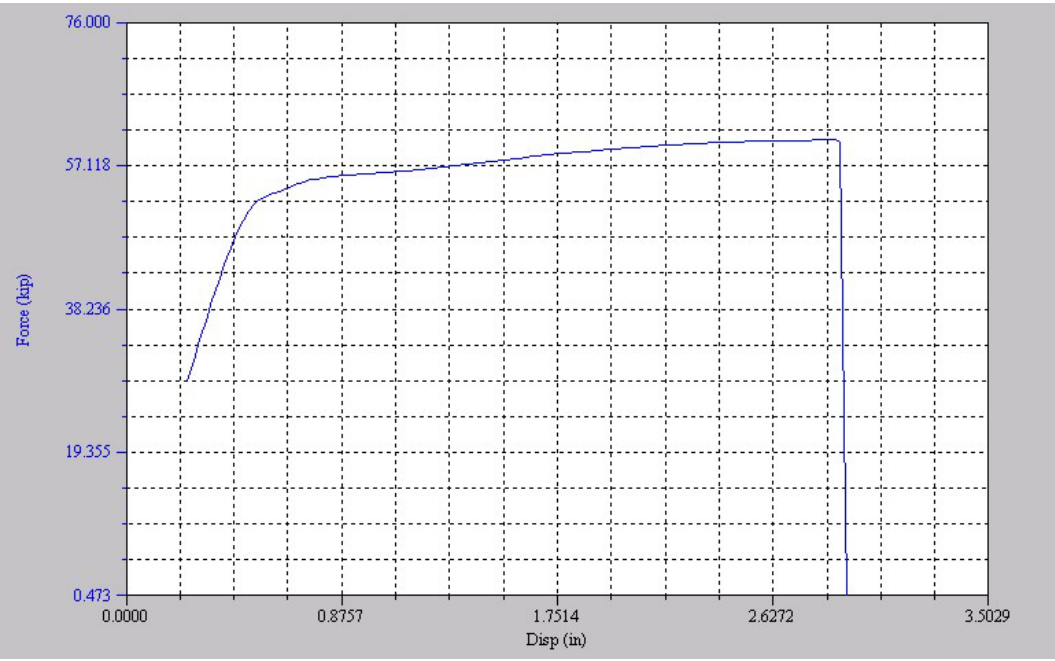


Figure A-12: Load vs. Displacement for Strand B Tensile Test 3

APPENDIX B

Grout Strength

B.1 SUMMARY

Two-inch grout cube samples were taken from the excess grout of some of the full-scale specimens to evaluate the strength of the grout.

For Specimens 5 and 6, which were grouted on the same day, cubes were covered with moist burlap and tested after 28 days. For Specimens 7 and 8, the cubes were moist-cured for 28 days before testing

Table B-1 presents the breaking strength of each cube. Three cubes were made for Specimens 5 and 6. For Specimen 7, three separate samples were taken from the tower and deck end. Five cubes were tested for Specimen 8.

Table B-1: Grout cube breaking strength

Stay 5/6	Stay 7		Stay 8	
	Deck	Tower		
(ksi)	(ksi)	(ksi)	(ksi)	
8.15	7.00	4.15	7.12	7.47
7.91	7.56	9.22	8.17	7.78
6.11	7.97	9.67	8.16	N/A

References

ASTM E 8 (2003), "Standard Test Methods for Tension Testing of Metallic Materials," American Society for Testing and Materials, West Conshohocken, Pennsylvania.

ASTM A 416 (2002), "Standard Specification for Steel Strand, Uncoated Seven-Wire for Prestressed Concrete," American Society for Testing and Materials, West Conshohocken, Pennsylvania.

Eggers, John (2003), "Cable Stay Fatigue Analysis for the Fred Hartman Bridge", M.S. Thesis, Department of Civil Engineering, The University of Texas at Austin, Austin, Texas.

Frank, Karl H. (2004), "Durable Cable Stays: A Design Challenge", CE 397 Class Notes, The University of Texas at Austin, Austin, Texas.

Heller, Bryan (2003), "Fatigue Response of Pretensioned Concrete Beams", M.S. Thesis, Department of Civil Engineering, The University of Texas at Austin, Austin, Texas.

Paulson, C., Frank, K., and Breen, J. (1983), "A Fatigue Study of Prestressing Strand," Research Report 300-1, Center for Transportation Research, Bureau of Engineering Research, The University of Texas at Austin, Austin, Texas, April 1983.

Poser, Marcel (2001), "Full-Scale Bending Fatigue Tests on Stay Cables", M.S. Thesis, Department of Civil Engineering, The University of Texas at Austin, Austin, Texas.

Poston, R. W. and Kesner, Keith (1998), "Progress Report Number One, Evaluation and Repair of Stay-Cable Vibrations: Fred Hartman Bridge, Veterans Memorial Bridge", Whitlock, Dalrymple, Poston & Associates, Manassas, Virginia.

PTI Guide Specification (2001), "Recommendations for Stay Cable Design, Testing and Installation", Post-Tensioning Institute, Phoenix, Arizona.

Verwiebe, Constantin (1998), "Rain-Wind-Induced Vibrations of Cables and Bars," *Bridge Aerodynamics*, Proceedings of the International Symposium on Advances in Bridge Aerodynamics, Copenhagen, Denmark.

VITA

Jennifer E. Ridd was born in Dayton, Ohio on August 12, 1980 to W. John Ridd and Janie H. Ridd. After graduating from high school in Springboro, Ohio as valedictorian of her class in 1998, she attended Purdue University in West Lafayette, Indiana. She received her Bachelor of Science in Civil Engineering degree with highest honors in May, 2002. Jennifer began her graduate education as a graduate research assistant at the University of Texas at Austin in August, 2002 and completed her Master of Science in Engineering degree in 2004 under the supervision of Dr. Sharon L. Wood and Dr. Karl H. Frank.

Permanent Address: 440 Queensgate Rd.
Springboro, Ohio 45066

This thesis was typed by the author.